

Novel Syntheses, Functionalization, and Applications of Octa-, Deca-, and Dodecasilsesquioxanes

by

Michael Z. Asuncion

A dissertation submitted in partial fulfillment
of the requirements for the degree of
Doctor of Philosophy
(Macromolecular Science and Engineering)
in The University of Michigan
2009

Doctoral Committee:

Professor Richard M. Laine, Chair
Professor David C. Martin
Associate Professor Joerg Lahann
Assistant Professor Jinsang Kim

© Michael Z. Asuncion 2009
All Rights Reserved

**This thesis is dedicated to my loving parents
Zacarias G. and Conchita G. Asuncion.
All of my accomplishments are owed solely to them.**

Acknowledgements

First and foremost I would like to thank my family for their unwavering moral support with all of my endeavors. I simply could not have accomplished anything without them. I would also like to thank all of the professors, teachers, and instructors who have left an indelible influence on my life. I would especially like to thank my advisor, Professor Richard M. Laine, for his guidance and direction, and his compassion when it was needed. I am also grateful to the members of my doctoral committee: Professor David C. Martin, Professor Joerg Lahann, and Professor Jinsang Kim for their guidance in this work.

I would also like to acknowledge: Nonna Hamilton of the Macromolecular Science and Engineering Department for all of her day-to-day help; Marco Ronchi of Università degli Studi di Milano, for his contributions to Chapter 5; all of the former and current members of the UM Laine Group, especially Dr. Chad Brick, Mark Roll, and Santy Sulaiman for their collaboration and Dr. Jose Azurdia for his help in configuring the GC used in Chapter 3; Haya Abu-Seir for all of her help and enthusiasm when I could not muster it alone; Joyce Loh, my UROP student; my friends and loved ones for their encouragement. Finally, I would like to thank NSF-IGERT, Kuraray Co. Ltd., Mayaterials, Inc., Canon, Ltd., and the Department of Chemistry at the University of Michigan for financial support.

Table of Contents

Dedication	ii
Acknowledgements	iii
List of Figures	viii
List of Schemes	xi
List of Tables	xiii
List of Abbreviations	xiv
Chapter 1 - Introduction	1
1.1 Project Goals and Objectives.....	1
1.2 Introduction to Nanocomposite Materials.....	2
1.3 Introduction to Silsesquioxanes.....	4
1.3.1 Definitions, Structures, and Nomenclature.....	6
1.3.2 Mechanism of Formation of Silsesquioxane Cages and Networks.....	8
1.3.3 Silsesquioxanes as Nanoplatfoms.....	10
1.4 General Chemical Reactions.....	14
1.4.1 The Heck Reaction.....	14
1.4.2 The Sonogashira Reaction.....	16
1.4.3 Cross Metathesis Reaction.....	17
1.5 References.....	20
Chapter 2 - General Experimental Techniques	25
2.1 Analytical Procedures.....	25

2.2	General Synthetic Methods.....	27
2.2.1	Synthesis of Octaphenylsilsesquioxane (OPS).....	27
2.2.2	Synthesis of Octa(nitrophenyl)silsesquioxane (ONPS).....	28
2.2.3	Synthesis of Octa(aminophenyl)silsesquioxane (OAPS).....	28
2.2.4	Synthesis of Octa(Br _{5,3} phenyl)silsesquioxane (Br _{5,3} OPS).....	29
2.2.5	Synthesis of Octa(iodophenyl)silsesquioxane (I ₈ OPS).....	29
2.3	References.....	31
Chapter 3 - Silsesquioxane Barrier Materials.....		32
3.1	Introduction.....	33
3.2	Experimental.....	36
3.2.1	Materials.....	36
3.2.2	Curing and Pressing Studies.....	36
3.2.3	Oxygen Transmission Rate (OTR) Measurements.....	37
3.2.4	Synthetic Methods and Sample Curing Studies.....	38
3.3	Results and Discussion.....	41
3.3.1	Solution Cast Films.....	44
3.3.2	Warm-Pressed Films.....	47
3.3.3	Temperature Dependence.....	49
3.4	Conclusions.....	51
3.5	References.....	53
Chapter 4 - Octalykynylsilsesquioxanes, Nano Sea Urchin Molecular Building Blocks for 3-D Nanostructures.....		56
4.1	Introduction.....	57
4.2	Experimental.....	58
4.2.1	Materials.....	58
4.2.2	Synthetic Methods.....	58
4.3	Results and Discussion.....	64
4.3.1	Sonogashira Reactions from Br _{5,3} OPS.....	65
4.3.2	Sonogashira Reactions from I ₈ OPS.....	67
4.3.3	Thermal Studies.....	67
4.4	Conclusions.....	72

4.5	References.....	74
Chapter 5 - Synthesis, Characterization and Functionalization of Incompletely Condensed “Half Cube” [RSi(OH)O]₄ or [RSi(ONa)O]₄ Silsesquioxanes as a Potential Route to Nanoscale Janus Particles.....		
5.1	Introduction.....	77
5.2	Experimental.....	79
5.2.1	Materials.....	79
5.2.2	Synthetic Methods.....	80
5.3	Results and Discussion.....	84
5.3.1	Synthesis of Tetra(<i>p</i> -iodo)phenyl Tetrasilesquioxane (I ₄ Ph ₄) Sodium Salt.....	85
5.3.2	Synthesis of Tetramethyltetraphenyl (Me ₄ Ph ₄) silsesquioxane.....	86
5.3.3	Synthesis of Tetravinyltetraphenyl (vinyl ₄ Ph ₄) silsesquioxane.....	90
5.3.4	Tetracyclohexyltetraphenyl (Cyclohexyl ₄ Ph ₄) Dimethoxy Derivative.....	92
5.4	Conclusions.....	93
5.5	References.....	94
Chapter 6 - Fluoride Rearrangement Reactions of Polyphenyl- and Polyvinylsilsesquioxanes as a Facile Route to Fluorescent Oligomers.....		
6.1	Introduction.....	99
6.2	Experimental.....	107
6.2.1	Materials.....	107
6.2.2	Synthetic Methods.....	107
6.3	Results and Discussion.....	112
6.3.1	Synthesis of Vinyl _x Ph ₁ (x = 9, 11) T ₁₀ and T ₁₂ Silsesquioxanes.....	113
6.3.2	Synthesis of Vinyl ₂ Ph _x (x = 8, 10) T ₁₀ and T ₁₂ Silsesquioxanes.....	116
6.3.3	Metathesis Reaction of Vinyl ₂ Ph _x (x = 8, 10) T ₁₀ and T ₁₂ Silsesquioxanes and 4-Bromostyrene.....	121
6.3.4	Heck Reaction of BrStyr ₂ Ph _x (x = 8, 10) T ₁₀ and T ₁₂ Silsesquioxanes and Vinyl ₂ Ph _x (x = 8, 10) T ₁₀ and T ₁₂ Silsesquioxanes.....	125

6.3.5	Synthesis of Model Compounds by Heck Reaction of BrStyr ₂ Ph _x (x = 8, 10) T ₁₀ and T ₁₂ Silsesquioxanes and Vinyltriethoxysilane.....	131
6.3.6	Photoluminescence Studies.....	135
6.4	Conclusions.....	138
6.5	References.....	139
Chapter 7 – Future Work.....		143
7.1	Discussion.....	143
7.2	References.....	148

List of Figures

Figure

1.1	Some representative silsesquioxane structures.....	5
1.2	Idealized T ₁₀ and T ₁₂ silsesquioxane structures.....	7
1.3	Acid and base-catalyzed hydrolysis mechanisms of trialkoxysilane.....	9
1.4	Typical dimensions of cubic octameric silsesquioxanes.....	11
1.5	(a) Octaphenylsilsesquioxane (OPS), (b) octa(nitrophenyl)silsesquioxane (ONPS), and (c) octa(aminophenyl)silsesquioxane (OAPS).....	12
1.6	Proposed structure of polyphenylsilsesquioxane (PPS).....	12
1.7	Proposed mechanism of the Heck reaction.....	16
1.8	Proposed mechanism of the Sonogashira reaction.....	17
1.9	Proposed mechanism for olefin cross metathesis reaction.....	19
3.1	Typical (a) Q ₈ and (b) T ₈ Structures.....	34
3.2	Schematic of GC/permeation cell for determination of OTR.....	38
3.3	Sets of epoxies tested with various amine curing agents.....	43
3.4	Chemical structure of oxydianiline (ODA).....	46
3.5	OTR vs. Temperature.....	49
4.1	TGA of <i>p</i> -methoxydiphenylethyne derivative before/after 400 °C/4 h heat treatment.....	69
4.2	DRIFT spectra of [diphenylethyneSiO _{1.5}] ₈ (a) before, (b) after heating to 400 °C/4h.....	70
4.3	DSC thermogram of diphenylethyne derivative (N ₂).....	71
4.4	Possible structure of octa-acetylenes after thermal polymerization.....	72

5.1	Structure of a. $(\text{RSiO}_{1.5})_4(\text{H}_2\text{O})_2$ “half cube” b. $[\text{Ph}_4\text{SiO}(\text{ONa})]_4$ half cube salt c. $[p\text{-IPhSiO}(\text{ONa})]_4$ half cube salt.....	78
5.2	Target structure of a tetrastilbene Janus cube.....	79
5.3	Tetramethyltetraphenyl (Me_4Ph_4) silsesquioxane.....	87
5.4	TGA (air) of tetramethyltetraphenyl (Me_4Ph_4) cubic silsesquioxane.....	88
5.5	FTIR of tetramethyltetraphenyl (Me_4Ph_4) cubic silsesquioxane.....	89
5.6	^1H NMR of tetravinyltetraphenyl ($\text{vinyl}_4\text{Ph}_4$) dimethoxy derivative (CD_3OD).....	91
5.7	Tetravinyltetraphenyl ($\text{vinyl}_4\text{Ph}_4$) silsesquioxane.....	91
5.8	MALDI of tetravinyltetraphenyl ($\text{vinyl}_4\text{Ph}_4$) Janus cube (m/z Ag^+).....	92
6.1	Idealized structures of (a) T_8 octasilsesquioxane “cube”, (b) T_{10} decasilsesquioxane, and (c) T_{12} dodecasilsesquioxane.....	100
6.2	(a) HOMO and (b) LUMO of $[\text{XSiO}_{1.5}]_8$	102
6.3	(a) ^{29}Si NMR spectrum obtained from mixing $\text{F}^-@OPS$ and $\text{F}^-@OVS$ in THF and the (b) spectrum obtained from mixing TMAF with equivalent amounts of OPS and OVS in THF.....	103
6.4	ESI mass spectrum of fluoride species derived from reaction of $(i\text{-Bu})_7(\text{C}_6\text{H}_5\text{CH}=\text{CH}_2)_1 \text{T}_8$ and TMAF.....	104
6.5	Disilanol silsesquioxane monomer ($\mathbf{R} = c\text{-C}_6\text{H}_{11}$).....	105
6.6	MALDI-TOF spectrum of 10:1 PVS:PPS reaction with TBAF (RT/48 h).....	115
6.7	MALDI-TOF spectrum of 10:1 PPS:PVS reaction with TBAF (RT/48 h).....	116
6.8	MALDI-TOF spectrum of 4.4:1 PPS:PVS reaction with TBAF (RT/48 h) after purification by column chromatography.....	118
6.9	Progress of the reaction of a 4.4:1 mole ratio of PPS:PVS with 1 mol% TBAF as monitored by GPC.....	121
6.10	MALDI-TOF spectrum of metathesis reaction of $\text{vinyl}_2\text{Ph}_x$ ($x = 8, 10$) T_{10} and T_{12} silsesquioxanes and 4-bromostyrene after column chromatography.....	123
6.11	Schematic depiction of the proposed structure of the Heck coupling product.....	126
6.12	MALDI-TOF spectrum after Heck reaction of $\text{BrStyr}_2\text{Ph}_x$ ($x = 8, 10$) T_{10} and T_{12} silsesquioxanes and $\text{vinyl}_2\text{Ph}_x$ ($x = 8, 10$) T_{10} and T_{12} silsesquioxanes.....	126

6.13	GPC chromatogram of Heck, model and metathesis compounds, vinyl ₂ Ph ₈ T ₁₀ and vinyl ₂ Ph ₁₀ T ₁₂ , and OPS/OVS (for comparison).....	128
6.14	TGA of Heck, model and metathesis compounds, vinyl ₂ Ph ₈ T ₁₀ and vinyl ₂ Ph ₁₀ T ₁₂ silsesquioxanes (air, 10°C/min to 1000 °C).....	129
6.15	TGA of Heck, model and metathesis compounds, vinyl ₂ Ph ₈ T ₁₀ and vinyl ₂ Ph ₁₀ T ₁₂ silsesquioxanes (N ₂ , 10°C/min to 1000 °C).....	131
6.16	Structures of Heck model compounds from reaction of BrStyr ₂ Ph _x (x = 8, 10) T ₁₀ and T ₁₂ silsesquioxanes with vinyltriethoxysilane.....	132
6.17	MALDI-TOF spectrum after Heck reaction of BrStyr ₂ Ph _x (x = 8, 10) T ₁₀ and T ₁₂ silsesquioxanes and vinyltriethoxysilane.....	133
6.18	¹ H NMR spectrum (CDCl ₃) after Heck reaction of BrStyr ₂ Ph _x (x = 8, 10) T ₁₀ and T ₁₂ silsesquioxanes and vinyltriethoxysilane.....	134
6.19	¹³ C NMR spectrum (CDCl ₃) after Heck reaction of BrStyr ₂ Ph _x (x = 8, 10) T ₁₀ and T ₁₂ silsesquioxanes and vinyltriethoxysilane.....	135
6.20	Solution (THF) absorption and emission spectra ($\lambda_{\text{excitation}} = 265 \text{ nm}$) of Heck compounds and corresponding Heck model -Si(OEt) ₃ compounds....	137

List of Schemes

Scheme

1.1	Bromination of octaphenylsilsesquioxane.....	13
1.2	Iodination of octaphenylsilsesquioxane.....	14
1.3	General Heck reaction.....	15
1.4	General Sonogashira reaction.....	17
1.5	General olefin cross metathesis.....	18
3.1	Reaction of octaminophenylsilsesquioxane (OAPS) and tetraglycidyl- <i>m</i> -xylenediamine (TGMX) to form nanocomposite films.....	34
3.2	Reaction of OAPS with oxydiphthalic anhydride (ODPA) or pyromellitic dianhydride (PMDA) to form imide nanocomposite films.....	34
3.3	(1) Preparation of TCHS from OHS and 4-vinyl-1-cyclohexene and (2) self-curing of TCHS at 200 °C.....	42
4.1	Synthesis of octaalkyne silsesquioxane via Br _{5,3} OPS and I ₈ OPS.....	65
5.1	Hydrolysis of PhSiCl ₃ to form [PhSiO(OH)] ₄	84
5.2	Reaction of OPS with NaOH to form Ph ₄ sodium salt.....	85
5.3	Reaction of I ₈ OPS with NaOH to form I ₄ Ph ₄ sodium Salt.....	86
5.4	Reaction of Ph ₄ half cube sodium salt with MeSiCl ₃	87
5.5	Bromination of Me ₄ Ph ₄ Janus cube.....	89
5.6	Reaction of Ph ₄ half cube sodium salt with VinylSiCl ₃	90
5.7	Reaction of Ph ₄ half cube sodium salt with CyclohexylSiCl ₃	93
6.1	Synthesis and structure of F ⁻ @(PhSiO _{1.5}) ₈ from (a) reaction of phenyltriethoxysilane and TBAF and by (b) reaction of OPS and TMAF.....	101
6.2	F ⁻ -mediated reaction of OPS and OAPS with TBAF.....	106

6.3	Fluoride-mediated rearrangement of PPS and PVS to (a) vinyl _x Ph ₁ (x = 9, 11) T ₁₀ and T ₁₂ and (b) vinyl ₂ Ph _x (x = 8, 10) T ₁₀ and T ₁₂ silsesquioxanes	113
6.4	Olefin metathesis of vinyl ₂ Ph _x (x = 8, 10) T ₁₀ and T ₁₂ silsesquioxane with 4-bromostyrene.....	123
6.5	Attempted olefin self-metathesis of vinyl ₂ Ph _x (x = 8, 10) T ₁₀ and T ₁₂ silsesquioxanes.....	124
6.6	Heck coupling of vinyl ₂ Ph _x (x = 8, 10) T ₁₀ and T ₁₂ silsesquioxanes with BrStyr ₂ Ph _x (x = 8, 10) T ₁₀ and T ₁₂ silsesquioxanes.....	125
7.1	Synthesis of 3-D octagraphene silsesquioxane structures starting from I ₈ OPS	144
7.2	Reaction of diamino(phenyl) ₂ Ph ₈ T ₁₀ and T ₁₂ silsesquioxanes with oxydiphthalic anhydride (ODPA) to form imide oligomers.....	146

List of Tables

Table

1.1	Letter description of silicon structures.....	8
3.1	Oxygen Transmission Rates (OTR) of Cast Silsesquioxane Films.....	43
3.2	Oxygen Transmission Rates (OTR) of Heat-Pressed Silsesquioxane Films...	48
4.1	Alkyne Product Yields, Conversions, and GPC Data from Br _{5,3} OPS and I ₈ OPS.....	65
4.2	T _{d5%} for octa-alkynes from I ₈ OPS (in air).....	68
6.1	MALDI-TOF data (Ag ⁺ Adduct) for 10:1 PVS:PPS reaction with TBAF...	115
6.2	MALDI-TOF data (Ag ⁺ Adduct) for 10:1 PPS:PVS reaction with TBAF...	117
6.3	MALDI-TOF data (Ag ⁺ Adduct) for 4.4:1 PPS:PVS reaction with TBAF...	119
6.4	MALDI-TOF data (Ag ⁺ Adduct) for metathesis reaction of vinyl ₂ Ph _x (x = 8, 10) T ₁₀ and T ₁₂ and 4-bromostyrene.....	124
6.5	MALDI-TOF data (Ag ⁺ Adduct) for Heck reaction of BrStyr ₂ Ph _x (x = 8, 10) T ₁₀ and T ₁₂ and vinyl ₂ Ph _x (x = 8, 10) T ₁₀ and T ₁₂	127
6.6	GPC mass data for Heck, model and metathesis compounds, vinyl ₂ Ph ₈ T ₁₀ and vinyl ₂ Ph ₁₀ T ₁₂ , and OPS/OVS (for comparison).....	128
6.7	Decomposition temperatures (T _{d5%}) and ceramic yields for Heck, model and metathesis compounds, vinyl ₂ Ph ₈ T ₁₀ and vinyl ₂ Ph ₁₀ T ₁₂ (air, 10°C/min to 1000°C).....	130
6.8	MALDI-TOF data (Ag ⁺ Adduct) for Heck reaction of model compound.....	133

List of Abbreviations

Br _{5,3} OPS	octa(bromo _{5,3} -phenyl)silsesquioxane
CMC	ceramic matrix composite
CTE	coefficient of thermal expansion
Cyclohexyl ₄ Ph ₄	tetracyclohexyltetraphenyl silsesquioxane
DFT	density functional theory
DGEBA	diglycidyl ether of bisphenol A
DMA	dimethylacetamide
DMF	dimethylformamide
DMSO	dimethylsulfoxide
DRIFT	diffuse reflectance Fourier transform infrared spectroscopy
DSC	differential scanning calorimetry
ECHX	3,4-epoxy-cyclohexyl-methyl-3,4-epoxy-Cyclohexanecarboxylate
ESI MS	electrospray ionization mass spectrometry
F ⁻ @(RSiO _{1.5}) ₈	F ⁻ encapsulated octasilsesquioxane
F ⁻ @OPS	F ⁻ encapsulated octaphenylsilsesquioxane
FTIR	Fourier transform infrared spectroscopy
GC	gas chromatography
GPC	gel permeation chromatography
HOMO	highest occupied molecular orbital
I ₄ Ph ₄	tetra(<i>p</i> -iodo)phenyltetrasilsesquioxane
I ₈ OPS	octaiodo(phenyl)silsesquioxane
LUMO	lowest unoccupied molecular orbital

MALDI-TOF MS	matrix-assisted laser-desorption/time-of-flight mass spectrometry
Me ₄ Ph ₄	tetramethyltetraphenyl silsesquioxane
MMC	metal matrix composite
MW	molecular weight
NMP	N-methylpyrrolidinone
NMR	nuclear magnetic resonance
OAPS	octa(amino-phenyl)silsesquioxane
ODA	oxydianiline
ODPA	oxydiphthalic anhydride
OHS	octahydridosilsesquioxane
ONPS	octa(nitro-phenyl)silsesquioxane
OPS	octaphenylsilsesquioxane
OTR	oxygen transmission rate
OVS	octavinylsilsesquioxane
PDI	polydispersity index
PMC	polymer matrix composite
PMDA	pyromellitic dianhydride
PMS	polymethylsilsesquioxane
PPS	polyphenylsilsesquioxane
PTES	phenyltriethoxysilane
PVA	polyvinyl alcohol
PVS	polyvinylsilsesquioxane
RDGE	resorcinol diglycidyl ether
TBAF	tetrabutylammonium fluoride
TCHS	tetraethylcyclohexenyl silsesquioxane
TGA	thermal gravimetric analysis
T_g	glass transition temperature
TGMX	tetraglycidyl- <i>m</i> -xylenediamine
THF	tetrahydrofuran
T_m	melting point temperature

TMAF	tetramethylammoniumfluoride
t_R	retention time
UV-Vis	ultraviolet-visible
vinyl ₄ Ph ₄	tetravinyltetraphenyl silsesquioxane
XRD	x-ray diffraction

Chapter 1

Introduction

This dissertation is dedicated to the syntheses, characterization, and properties of both completely and incompletely condensed silsesquioxanes and their utility as nanoconstruction sites for a variety of applications. **Section 1.1** provides an overview of the primary research objectives and scientific motivation for this work. **Section 1.2** provides basic concepts regarding composites, in particular hybrid organic/inorganic nanocomposite materials. **Section 1.3** provides a brief overview of silsesquioxanes, including prior work pertinent to the studies described herein. **Section 1.4** describes the general synthetic routes and reaction mechanisms utilized throughout this work.

1.1 Project Goals and Objectives

Polyhedral silsesquioxanes represent a versatile class of highly symmetrical three-dimensional organosilicon compounds with well-defined nanometer structures. The combination of a rigid inorganic core and a more flexible and reactive organic shell makes these compounds extremely useful as potential platforms for nanoscale composite (“nanocomposite”) materials with hybrid properties intermediate of ceramics and organics.¹⁻¹²

The combination of high symmetry and nanometer size suggests that silsesquioxanes can be used as nanoscale building (“nanobuilding”) blocks for the assembly of larger

macroscale materials but with control of global properties extending through the finest length scales. Moreover, the inorganic core offers the rigidity and heat capacity of silica which can bolster both the mechanical and thermal properties of silsesquioxane-based nanocomposites beyond those typically found in organic-only frameworks.¹³

The objectives of this work were to develop simple, effective routes to nanocomposite precursors based on silsesquioxanes with tailorable properties for use in a variety of applications. These properties were readily achieved by simple chemical modification of the organic periphery. Our investigations have demonstrated that octameric silsesquioxane-based nanocomposites can be tailored to exhibit barrier properties with very low permeability to oxygen (**Chapter 3**) or as high temperature, thermal cross-linking agents (**Chapter 4**) and potential platforms to supramolecular structures. In **Chapter 5** we explore the use of incompletely condensed, cyclic silsesquioxane tetramers as possible precursors to fully condensed two-faced “Janus” octamers. Finally, in **Chapter 6** we investigate the fluoride rearrangement of high molecular weight silsesquioxane polymers to polyhedral silsesquioxanes with discrete structures and their subsequent chemical transformation to “string of bead” oligomeric materials with unique photoluminescent properties.

1.2 Introduction to Nanocomposite Materials

In the continuing quest to improve performance, currently-used materials frequently reach the limit of their usefulness. Thus materials scientists and engineers strive to improve traditional materials or develop completely new materials outright. A composite (a mixture of two or more physically and/or chemically distinct phases in intimate contact with one another) is generally grouped in the latter category. Modern composite materials are usually optimized to achieve a particular balance of properties for a given range of applications, with properties superior to either constituent material alone.^{2,3} Composites are either categorized as possessing a continuous phase (“matrix”) surrounding one or more discontinuous phases (“reinforcement”) or possessing two or more interpenetrating

continuous phases. Most composites are of the former type and are typically categorized by the nature of the matrix [i.e. polymer matrix composites (PMC's), metal matrix composites (MMC's), or ceramic matrix composites (CMC's)]. For traditional macroscale composites the components normally can be physically identified and exhibit an interface between one another.¹⁴

Properties for “traditional” (two-phase) macroscale composites are generally predicted based on the proportions and properties of the matrix and reinforcement. A generalized form of the “Law of Mixtures” for a multiphase system is

$$X_c = X_1v_1 + X_2v_2 + X_3v_3 + \dots,$$

where X_c is an appropriate property of the composite, v represents the volume fraction, and the numbered subscripts refer to the individual components. The interface between phases is particularly important in determining the properties of the composite because this is where property (load) transfer occurs. The volume fraction is generally regarded as the single most important parameter that influences a composite's properties.⁴ From a manufacturing standpoint, it is an easily controllable variable by which the properties of the composite may be altered to suit the application.¹⁵

The field of nanocomposite materials involves material phases where at least one dimension is less than 100 nm. Nanocomposites may be considered solid structures with nanometer-scale dimensional repeat distances between the different phases. Alternatively they can consist of two or more inorganic/organic phases in some combination with the proviso that at least one of the phases or features be nanosize.

Like conventional macroscale composites, the true potential of nanocomposite materials is realized in developing unique combinations of properties that are unachievable with traditional materials alone. However, because of the length scales involved, the interfacial interactions between phases (“interphase”) becomes very large with respect to the total volume of the composite as the sizes of the components shrinks to the nanometer scale. These interactions can lead to nonlinear changes in composite properties^{16,17} and can be so great that estimation according to the Law of Mixtures is insufficient, due to the fact that the properties and volume fraction of the interphase are

generally ignored when predicting the properties of macroscale composites. The unique properties of nanocomposites and the possibility to create novel materials consisting entirely of interphase¹⁸ represent a powerful motivation for the study of nanocomposite materials.

Hybrid organic-inorganic materials represent a subclass of nanocomposites that typically consist of an inorganic solid containing an organic component (or vice versa) with at least one component on the nanometer scale. These materials, poised at the interface of organic and inorganic realms, are highly versatile and offer a wide range of possibilities to elaborate and tailor the chemical and physical properties of materials as nanobuilding blocks.¹⁹ The useful size of these building blocks depends upon the desired property. For multifunctional applications, more than one property and one length scale must be considered. By altering the sizes of those building blocks and controlling their chemistry and assembly, it should be possible to engineer properties and functionalities in unprecedented ways.

As discussed above, the properties of hybrid organic-inorganic materials are not only the sum of the individual contributions of both phases but also highly dependent on interfacial interactions. Thus it has been suggested²⁰ that hybrid materials be divided into two broad classes where the organic and inorganic components are 1) simply embedded and held together by weak (hydrogen, van der Waals, or ionic) bonds or 2) linked together through strong (covalent/ionic-covalent) chemical bonds. Polyhedral silsesquioxanes, the focus of this dissertation, belong to the latter category.

1.3. Introduction to Silsesquioxanes

The term “silsesquioxane” refers to a very large family of silicon-oxygen compounds with the idealized empirical formula $(\text{RSiO}_{1.5})_n$, where R is hydrogen or any alkyl, alkylene, aryl, arylene, or derivatives of these groups.²¹ Silsesquioxanes have been synthesized with structures that are either polymeric or oligomeric (i.e. existing as discrete polyhedral structures) and generally exhibit different properties, hence their

research and applications are usually separated.²² Furthermore, silsesquioxanes can be further divided into two subgroups: completely condensed and incompletely condensed. For completely condensed species [Fig 1.1 (a-c)], oxygen acts only as a bridge between silicon atoms and there are no –OH functionalities. However, incompletely condensed silsesquioxanes contain silanol groups [Fig 1.1d] which make them ideal compounds for modeling the surfaces of silica²³⁻²⁶ and as ligands for metal coordinate complexes.²⁷⁻³⁰

Fully condensed silsesquioxanes (notably polyhedral oligomeric silsesquioxanes), because of their inherent thermal and oxidative stabilities, (pencil) hardness, relative ease of preparation, wide array of possible frameworks, and variety of pendant groups, have attracted much attention in recent years to model catalytic surfaces,^{23,31} generate new catalysts,³² novel porous media,³³ NMR standards,³⁴ and act as novel encapsulants.³⁵ Polyhedral silsesquioxanes have also been used as building blocks for nanocomposite materials³⁶⁻⁴⁰ (as discussed below) and serves as the central theme of this dissertation.

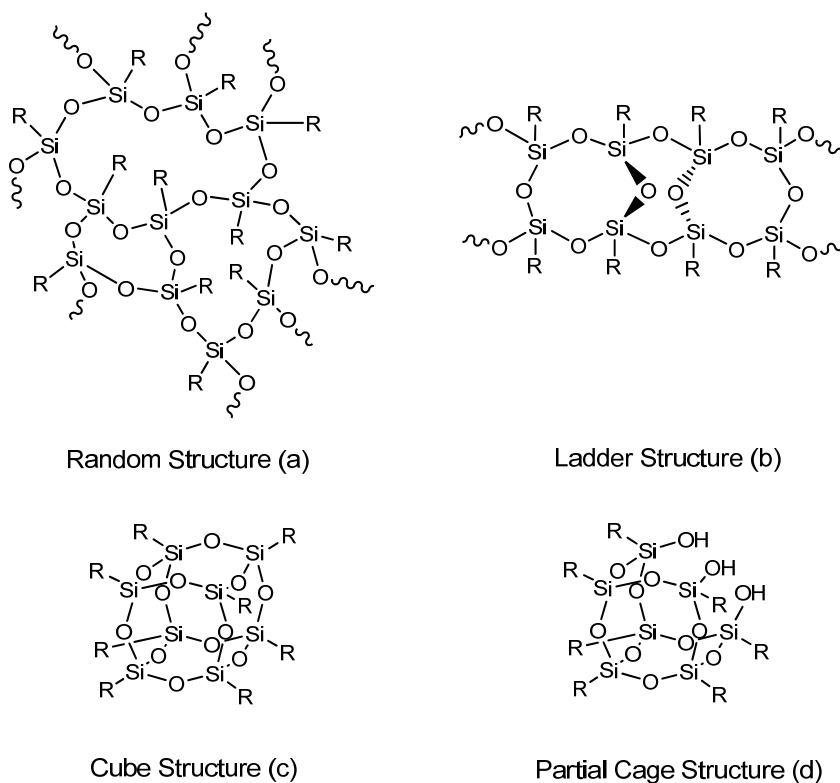


Figure 1.1. Some representative silsesquioxane structures

Many factors are known to influence the formation (and hence the structure) of silsesquioxanes from the hydrolytic condensation of trifunctional organosilanes (RSiX_3), from which they are typically formed. Such variables include: the nature of R group, nature of X group (usually $-\text{Cl}$, $-\text{OCH}_3$, or $-\text{OCH}_2\text{CH}_3$), solvent, concentration of starting materials, reaction time, rate of addition and quantity of H_2O , pH, solubility of product, etc.²² The structures of silsesquioxanes have been reported as cages, partial cages, ladder structures, or random structures as depicted in Figure 1.1.²¹

1.3.1 Definitions, Structures, and Nomenclature

The etymology of the term “silsesquioxane” [$(\text{RSiO}_{1.5})_n$] refers to the 1.5 ratio between silicon and oxygen atoms (from the Latin *semisque* – “and a half”). Structurally, silsesquioxanes consists of sp^3 hybridized Si atoms bound to three oxygen atoms and one R group, where R is typically an organic moiety as mentioned above. When $n = 4, 6, 8, 10,$ or 12 , the resulting compounds are called polyhedral oligomeric silsesquioxanes and possess three dimensional, symmetrical structures. In the specific instance where $n = 8$, the silsesquioxane octamers [Figure 1.1c] are referred to as cubic silsesquioxanes or simply “cubes.” Alternatively they are called “POSS” (trademarked by Hybrid Plastics, Inc., but here after referred to as cubes). Cubes have been the focus of many studies due to their nanometer size, high degree of symmetry, and numerous preparative routes to useful quantities as discussed further in this chapter.⁴¹⁻⁴³

In these studies, our composite precursors are built upon cubes as well as the $n = 10$ (“deca-”) and $n = 12$ (“dodeca-”) analogs (Figure 1.2). The decasilsesquioxane shape contains two distorted-pentagonal faces and four-distorted square faces. The dodeca-silsesquioxane consists of four distorted-pentagonal faces and four distorted square-triangular faces.²² The structures in Figure 1.2 are idealized representations of both structures.

When $n = \infty$ the compounds are polymeric and known simply as polysilsesquioxanes. While the actual structure of polysilsesquioxanes [typically referred to as “T Resins” (see below for nomenclature)] has been the subject of much debate,⁴⁴ it is believed that the

polymer chains contain a variety of structures including linear chain, open-caged, and ladder-like structures, depending on the reaction conditions employed.⁴⁵

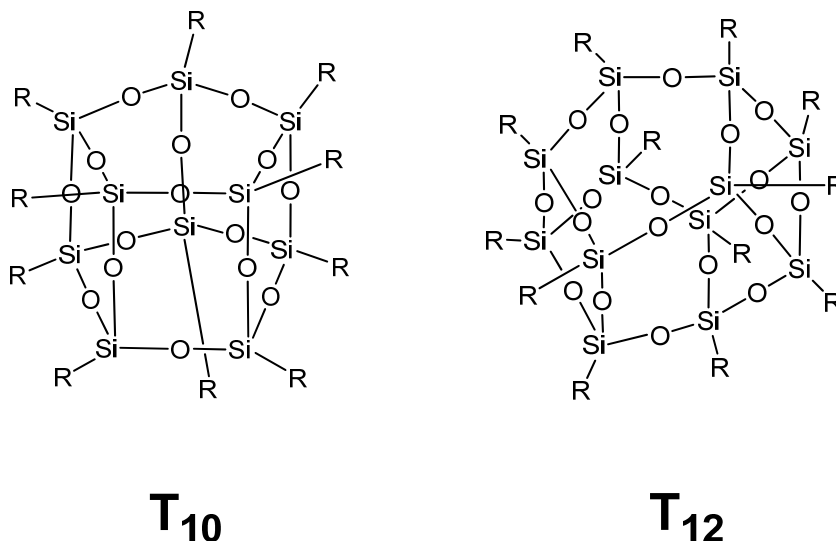


Figure 1.2. Idealized T₁₀ and T₁₂ silsesquioxane structures.

The shorthand notation for silicon atoms in a silicon-oxygen framework uses letters to denote the types of silicon and numerical subscripts and optional superscripts to denote the number and type of functional groups, respectively. Silicon bound to three oxygen atoms is commonly referred to as a “T” unit. Similarly, an “M” unit consists of silicon bound to one oxygen, a “D” unit has a silicon atom bound to two oxygens, and a “Q” unit is silicon bound to four oxygen atoms (**Table 1.1**).

The number of Si atoms is denoted by a subscript and the symbol for additional valences occupied by organic substituents is appended to the letter designation as a superscript. For example, T₈^H (H₈Si₈O₁₂) refers to a silsesquioxane cage structure containing eight silicon atoms, each connected to three oxygen atoms and one hydrido group. For simplicity, this is often shortened to “hydrido T₈” or “octahydrido” with understanding by those in the field.

Table 1.1. Letter description of silicon structures.

Silicon Species	General Formula	Valency	Nomenclature
Siloxy	$[R_3SiO_{1/2}]$	Mono	M
Siloxane	$[R_2SiO_{2/2}]$	Di	D
Silsesquioxane	$[RSiO_{3/2}]$	Tri	T
Silicate	$[SiO_{4/2}]$	Quarternary	Q

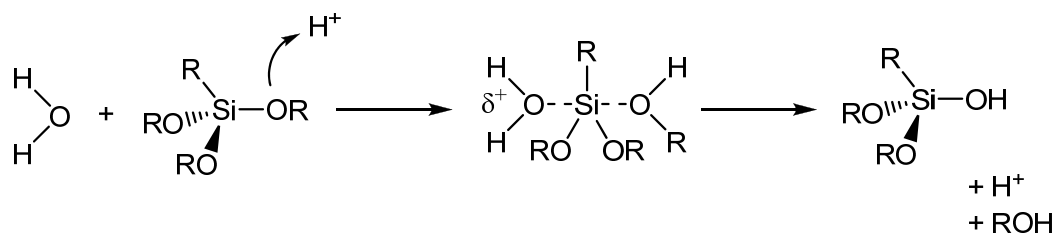
1.3.2 Mechanism of Formation of Silsesquioxane Cages and Networks

The preparation of silsesquioxane materials, usually prepared from the acid or base-catalyzed hydrolytic condensation of trifunctional organosilanes, is a multi-step and rather complicated process. The synthesis is very sensitive to a combination of experimental factors (as mentioned previously) due to a statistical distribution of intermediate components and usually produces a wide range of products, from small oligomers and polyhedral silsesquioxanes to mixtures of polymeric resins and gels. Sol-gel networks, polysilsesquioxanes, and polyhedral silsesquioxanes all form by the same general reaction mechanisms, however.

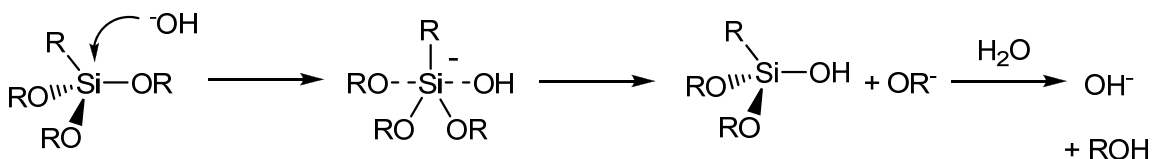
Since a suitable kinetic equation has yet to be determined for the synthesis of silsesquioxanes, no *universal* synthetic protocols have been established.²² However, control of reaction conditions can be made to favor the formation one structure (or mixture of structures) preferentially for certain silane monomers. Many procedures for the formation of *specific* silsesquioxanes have been developed recently and account for the increasing number of papers and patents published yearly on silsesquioxanes.²¹

While no universal preparative procedures have been established for the formation of silsesquioxanes, it is generally found that: (1) lower concentrations of silane monomers favor intermolecular condensation and thus polyhedral structures are favored while higher concentrations of monomers favor polymeric structures; (2) low pH favors

cyclization whereas higher pH favors polymerization; (3) water is essential to cyclization but excess water favors polymerization.²² While the rates of hydrolysis and condensation (as affected by the above factors) determine the final shape of the compound, the general hydrolysis mechanism is similar in any case. The general hydrolytic reaction mechanisms for trialkoxysilanes are shown below in Figure 1.3.



Acid Catalyzed Hydrolysis



Base Catalyzed Hydrolysis

Figure 1.3. Acid and base-catalyzed hydrolysis mechanisms of trialkoxysilane.

Under acidic conditions, an alkoxy group is protonated in a rapid first step. Electron density is withdrawn from the silicon atom, making it more electrophilic and thus more susceptible to attack from water. The rate of the first hydrolysis is the fastest because the penta-coordinate (S_N2) transition state (which is stabilized by electron-donating alkoxy groups⁴⁶) is at a maximum, while each ensuing hydrolysis occurs more slowly as alkoxy groups are displaced as alcohol. Similarly, condensation occurs most rapidly for singly-hydrolyzed species.

Under basic conditions, the alkoxy oxygens tend to repel the OH^- nucleophile. However, once initial hydrolysis has occurred, each subsequent alkoxy group becomes

more easily removed from the monomer than the previous one as the negatively-charged transition state is made relatively more stable by hydroxyl groups, which have lower electron density than alkoxy groups.⁴⁶ Therefore, highly hydrolyzed species are more prone to attack and condensation occurs most rapidly for fully-hydrolyzed species.

1.3.3. Silsesquioxanes as Nanoplatfoms

Since the ability to *precisely* tailor the macroscopic properties of a material requires manipulating component organization at the finest (nanometer) length scales, highly symmetrical nanobuilding blocks are required to minimize structural defects and maximize periodicity from the nanometer to the macroscopic length scales. These nanobuilding blocks should be easily prepared and modifiable (via chemical synthesis) to tailor to the property needs of the material. Clearly, nanocomponents that are easily made and whose properties and assembly can be closely controlled with high homogeneity could have a significant impact on the development of new nanomaterials.

The polyhedral octameric (T_8), decameric (T_{10}), and dodecameric (T_{12}) cages are shown above in Figures 1.1c and 1.2. The T_8 , T_{10} , and T_{12} silsesquioxanes have O_h , D_{5h} , and D_{2d} symmetry, respectively. The T_{10} and T_{12} cages are typically never found as the only products, but usually as by-products in the synthesis of T_8 cages.²²

Of particular interest to us are the highly symmetric cubic silsesquioxanes (Figure 1.4), which are unique spherical organic/inorganic molecules consisting of rigid silica cores with eight vertices (vertex body diagonal = 0.53 nm) each containing an organic moiety. They are 1-2 nm in diameter with volumes $< 2 \text{ nm}^3$ with each organic functional group located in a separate octant in Cartesian space, orthogonal or in opposition to each other. The positioning of the functional groups, the variety possible, and their size provide unique opportunities to build nanocomposites in 1-, 2- or 3-D, one nanometer at a time. In addition, the silica core makes these compounds thermally quite robust, adding to their utility in applications where typical organics fail.

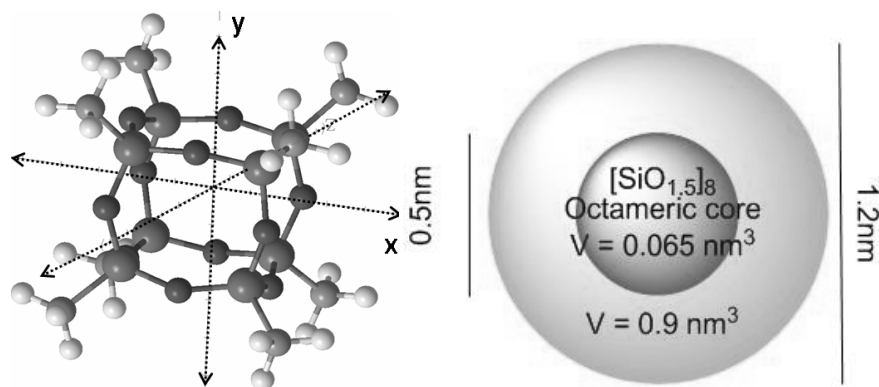


Figure 1.4. Typical dimensions of cubic octameric silsesquioxanes.

The construction of materials nanometer-by-nanometer should lead to the design of a variety of materials with well-defined nanoarchitectures and novel (for reasons mentioned previously) yet predictable behaviors. As “ideal” nanobuilding blocks, polyhedral silsesquioxanes allow for subsequent and selective chemical modification to provide a wide variety of derivatives, thus permitting specific assembly of these molecular components into larger, well-defined structures with tailorable properties. The synthesis, functionalization, and characterization of cubic silsesquioxanes and their T_{10} and T_{12} analogs, as well as incompletely condensed silsesquioxanes are the focus of this dissertation.

1.3.3.1 Octaphenylsilsesquioxane, Octa(nitrophenyl)silsesquioxane, and Octa(aminophenyl)silsesquioxane

Octaphenylsilsesquioxane (OPS, Figure 1.5a) has long been known in the literature⁴⁷⁻⁴⁹ but has rather limited usefulness, despite its nanometer size, 3-D symmetry, and high thermal stability (550 °C/air), because of its poor solubility in common organic solvents and decomposition before melting. Recent work⁵⁰ by our group has included the optimization of the synthesis of OPS (up to 90% yield) first reported by Brown.⁴⁹ The by-product of the synthesis is a phenyl(triethoxy)silsesquioxane polymer ($M_w \approx 3000$) which we refer to as polyphenylsilsesquioxane (PPS). The proposed structure of PPS (based on ^{29}Si NMR)⁵⁰ is shown below in Figure 1.6. PPS can be functionalized in

manners analogous to OPS and its derivatives have been shown to exhibit properties (reactivity, processibility, thermomechanical characteristics, etc.) comparable to OPS derivatives.⁵¹ PPS is used as a starting material for compounds synthesized in **Chapter 6**.

The utility (via increased solubility) of OPS was enhanced by nitration with fuming nitric acid to form octa(nitro-phenyl)silsesquioxane (ONPS, Figure **1.5b**) and subsequent reduction under mild conditions with formic acid and triethylamine (Pd/C catalyst 60 °C/N₂/5 h) to obtain octa(aminophenyl)silsesquioxane (OAPS, Figure **1.5c**).⁴¹ Nanocomposites synthesized from OAPS were studied as potential oxygen barrier materials and are described in **Chapter 3**.

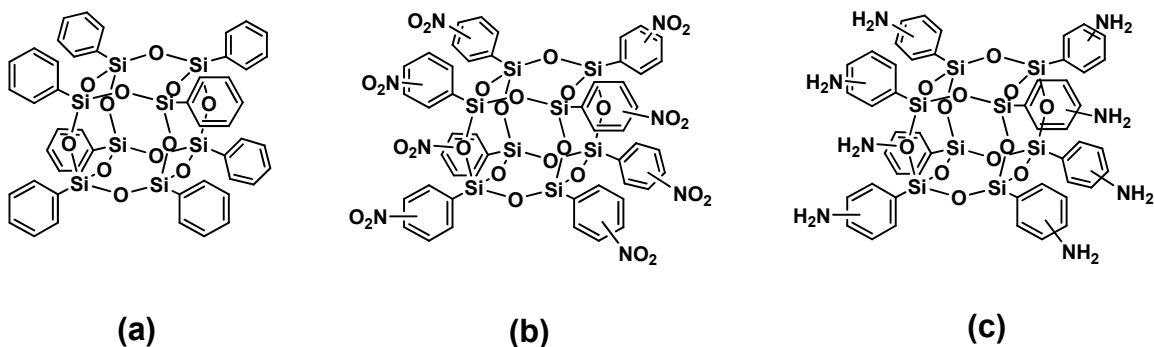


Figure 1.5. (a) Octaphenylsilsesquioxane (OPS), (b) octa(nitrophenyl)silsesquioxane (ONPS), and (c) octa(aminophenyl)silsesquioxane (OAPS).

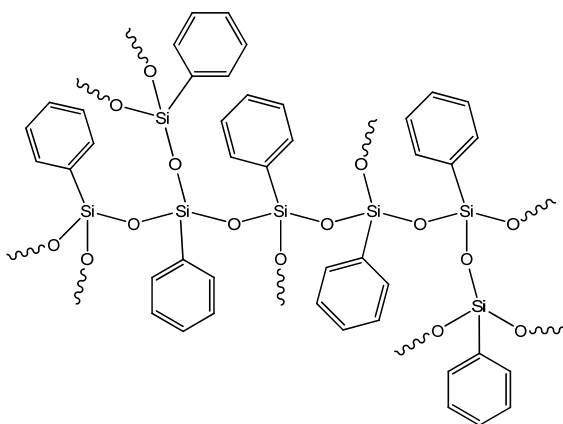
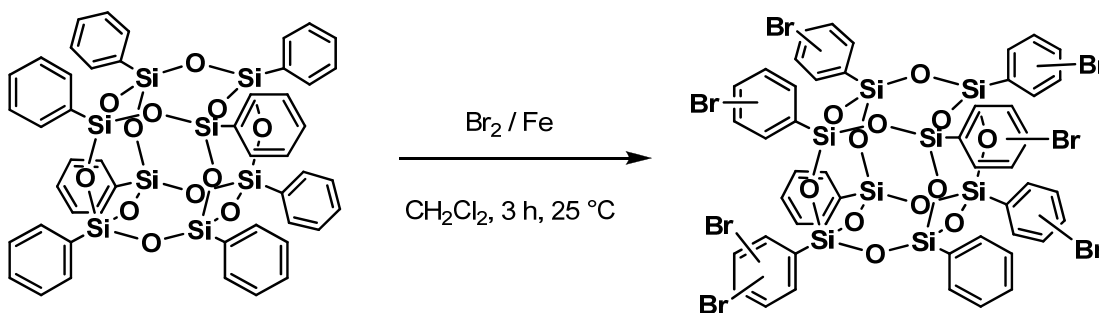


Figure 1.6. Proposed structure of polyphenylsilsesquioxane (PPS).

1.3.3.2 Octa(bromophenyl)- and octa(iodophenyl)silsesquioxanes

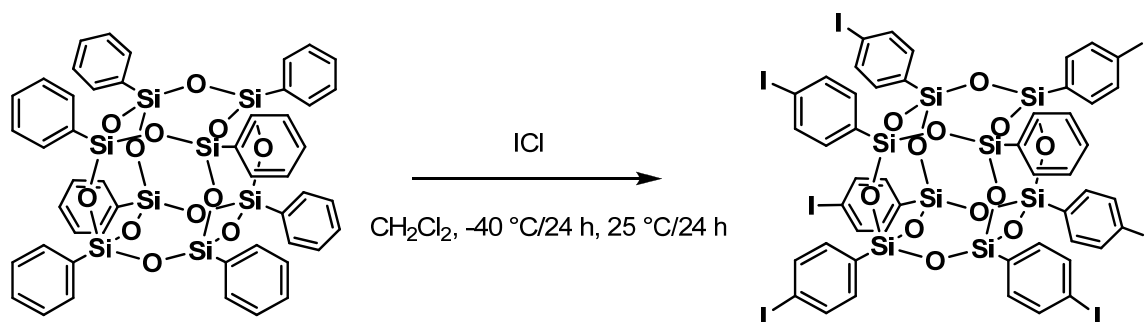
The utility of OPS was further extended via halogenation of the aromatic moieties. Preliminary efforts⁴² by our group focused on bromination of OPS with Br₂/Fe in dichloromethane (Scheme 1.1). For Br:OPS ratios less than 8:1, the products are singly brominated but are a mixture of (65:20:15 para:meta:ortho) isomers.⁴² At higher ratios of Br:OPS the products are primarily 2,5 bromo-substituted (meta and ortho to Si). Br_{5.3}OPS, with an average of 5.3 bromines per OPS molecule (as determined by ¹H NMR), was used in the studies discussed in **Chapter 4** to ensure that the products were primarily monobrominated and para-substituted to reduce unwanted disubstituted phenyl rings. While Br_{5.3}OPS has been shown to undergo further modification by chemical syntheses,⁴² the perfect cubic symmetry of the starting OPS is marginalized due to incomplete control of the substitution patterns via bromination.



Scheme 1.1. Bromination of octaphenylsilsesquioxane.

Since it is highly desirable to avoid the introduction of defects at the earliest stages of functionalization, a more “perfect” nanobuilding block was sought. Octaiodo(phenyl)silsesquioxane (I₈OPS) is afforded by the reaction of OPS with iodine monochloride at low temperature (Scheme 1.2).⁴³ Unlike the brominated OPS compounds, I₈OPS is achieved in high yield (90% - before recrystallization) with 99% conversion to the para isomer almost exclusively (93% - after recrystallization). Thus I₈OPS essentially preserves the cubic symmetry of the starting OPS compound and serves as a potential

scaffold to build higher-ordered nanostructures, as I₈OPS is completely soluble in most organic solvents and contains a facile iodo- moiety susceptible to a host of palladium-catalyzed coupling reactions (some below).



Scheme 1.2. Iodination of octaphenylsilsesquioxane.

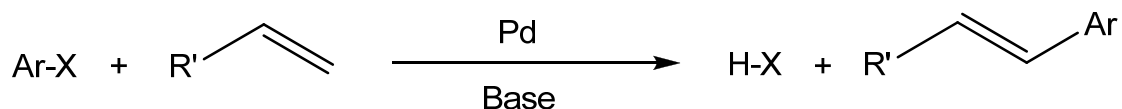
1.4. General Chemical Reactions

Three general chemical reactions were used throughout this work to modify the organic periphery of the T₈, T₁₀, and T₁₂ silsesquioxanes. The Heck and Sonogashira reactions are common organic coupling reactions (reactions that catalytically bring together two neutral organic precursors) and very powerful methods for the formation of carbon-carbon bonds. The third reaction, the olefin cross-metathesis reaction, has recently emerged as a convenient synthetic technique in organic chemistry for reacting two compounds with carbon-carbon double bonds.

1.4.1. The Heck Reaction

The Heck (sometimes referred to as Heck-Mizoroki) reaction (Scheme 1.3) is certainly the most useful and versatile method of C-C formation involving *sp*² carbons. Developed in the late 1970's, the Heck reaction is a palladium-catalyzed cross-coupling reaction of an aryl halide with a vinyl group to afford an aryl alkene. Since its discovery, the general reaction procedure has largely remained unchanged from the original, though

much attention has been devoted to developing new ligands to promote catalytic turnover rates as well as to induce stereoselectivity in appropriate substrates.^{52,53} Reactions are typically carried out in a polar solvent (THF, DMF, DMA, dioxane) at elevated temperatures. Generally the solvents and reaction vessels must be degassed to protect the integrity of the catalyst or the phosphine ligands, as they oxidize in the presence of oxygen.



Scheme 1.3. General Heck reaction.

While the exact mechanism of the Heck reaction is subject to much historical debate,⁵¹⁻⁵⁴ the generally accepted reaction mechanism is shown below in Figure 1.7. It is a variation of the common oxidative-addition/reductive-elimination pathway found in many transition metal-catalyzed reactions.

Historically, a wide variety of conditions and reagents have been used in the Heck reaction, since small changes in the reaction conditions often have mechanistic implications and thus affect the resulting the products. Therefore, no simple procedure works in all cases.⁵⁴⁻⁵⁹ For our T₈, T₁₀, and T₁₂ aryl halide compounds, we have found that we could achieve complete reactions under mild conditions (25 °C, 48 h) using Pd[P(*t*-Bu)₃] and Pd₂(dba)₃ as the catalyst precursor system.⁴³ This system does not require harsh conditions or the use of strong acids or bases, offering the possibility of chemical modification without damaging the silica core.

We have previously shown that a wide variety of compounds can be synthesized by coupling T₈ aryl halides to a variety of olefins.^{42,43,60} This work has been extended to the T₁₀ and T₁₂ analogs and the synthesis and properties of these materials are found in **Chapter 6**.

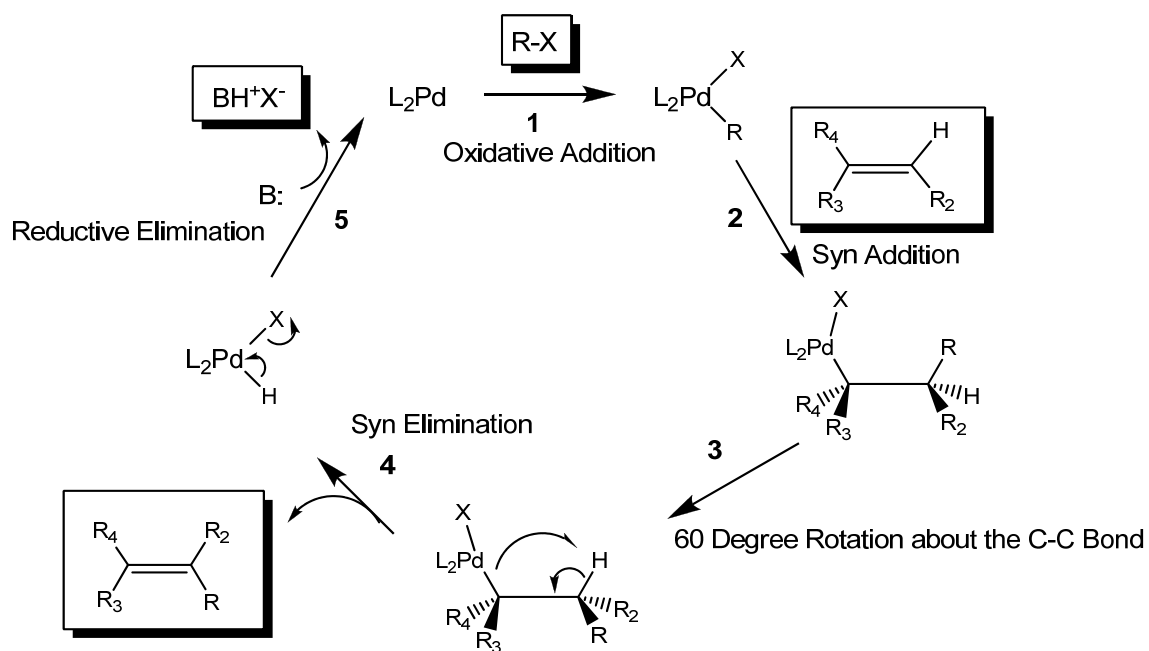
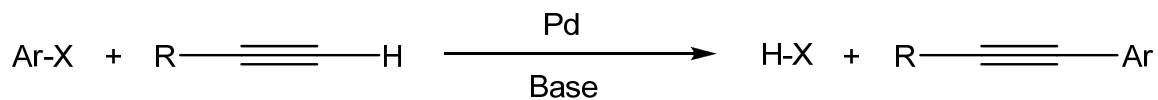


Figure 1.7. Proposed mechanism of the Heck reaction.

1.4.2. The Sonogashira Reaction

The Sonogashira reaction (less commonly known as the Sonogashira-Hagihara or Heck-Cassar-Sonogashira-Hagihara reaction) is similar to the Heck reaction but instead involves the coupling of terminal alkynes with aryl or vinyl halides with catalytic amounts of palladium and Cu (I) halide (Scheme 1.4). The reaction was first reported in 1975 by Kenkichi Sonogashira, Yasuo Toda, and Nobue Hagihara in 1975 as an alternative to the sensitive and sometimes-violent reaction conditions of the Stephens-Castro coupling of copper(I) arylacetylenes with iodoarenes.⁶¹ It is one of the most commonly employed cross-coupling reactions. Reactions with aryl iodides usually occur at room temperature; aryl bromides typically require elevated temperatures under similar reaction conditions.



Scheme 1.4. General Sonogashira reaction.

The proposed reaction mechanism is shown below in Figure 1.8. The Sonogashira reaction was used extensively in the work presented in **Chapter 4**.

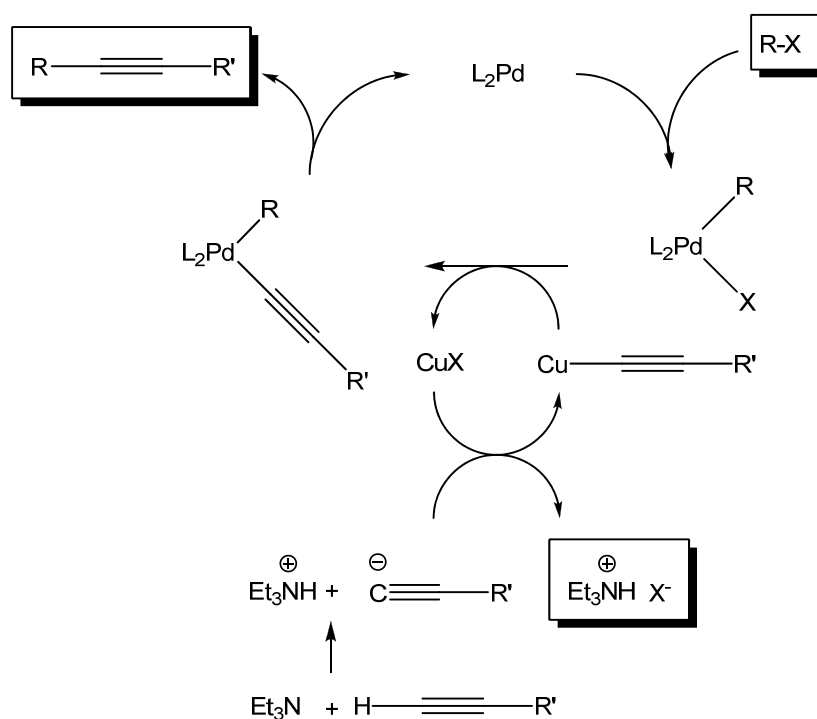


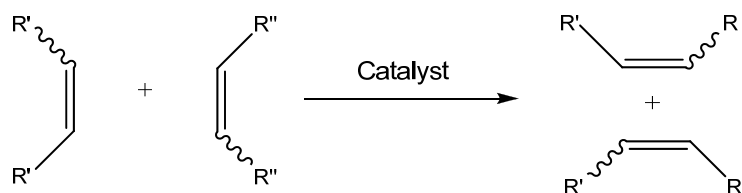
Figure 1.8. Proposed mechanism of the Sonogashira reaction.

1.4.3. Cross Metathesis Reaction

Olefin cross-metathesis is a transalkylidene reaction, which allows for the exchange of substituents between different terminal olefins (Scheme 1.5) in the presence of a catalyst (usually a ruthenium or molybdenum complex). The generally accepted

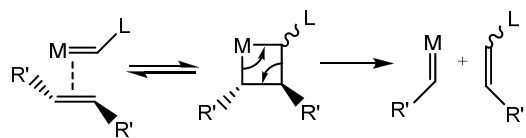
mechanism for metathesis is a chain mechanism, involving the intervention of a metal-carbene complex and a four-membered ring containing a metal (Figure 1.9).⁶²

When the reactants are simple alkenes, the proportions of products are generally statistical, which generally limits the synthetic utility of the reaction since the yield of any one product is low. However, in some cases one alkene may be more or less thermodynamically stable than the rest (due to steric hindrances), so that the proportions are not statistical.⁶³ The olefin cross metathesis reaction is employed to modify compounds in **Chapter 6**.



Scheme 1.5. General olefin cross metathesis.

Initiation:



Catalytic Cycle:

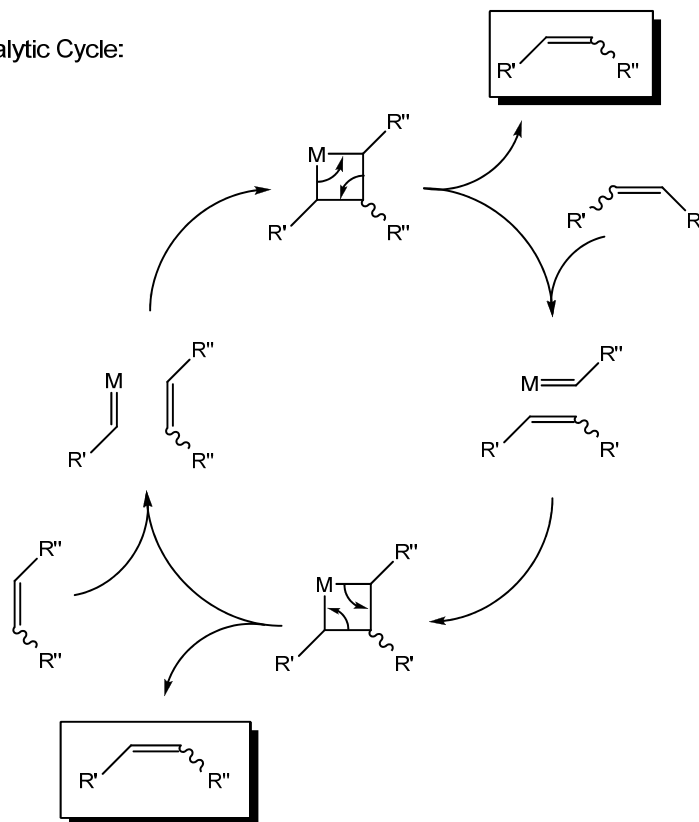


Figure 1.9. Proposed mechanism for olefin cross metathesis reaction.

1.5 References

1. (a) *Organic/Inorganic Hybrid Materials*; Laine, R.M., Sanchez, C., Brinker, C.J., Giannelis, E., Eds.; MRS Symp. Ser. 519; Materials Research Society: Warrendale, PA, 1998. (b) *Organic/Inorganic Hybrid Materials II*; Klein, L. C., Francis, L., DeGuire, M. R., Mark, J. E., Eds.; MRS Symp. Ser. 576; Materials Research Society: Warrendale, PA, 1999. (c) *Organic/Inorganic Hybrid Materials*; Laine, R. M., Sanchez, C., Giannelis, E., Brinker, C. J., Eds.; MRS Symp. Ser. 628; Materials Research Society: Warrendale, PA, 2000. (d) *Organic/Inorganic Hybrid Materials*; Laine, R. M., Sanchez, C., Yang, S., Brinker, C. J., Eds.; MRS Symp. Ser. 726; Materials Research Society: Warrendale, PA, 2002. (e) Sanchez, C.; Soler-Illia, G. J. de A. A.; Ribot, F.; Lalot, T.; Mayer, C. R.; Cabuil, V. *Chem. Mater.* **2001**, *13*, 3061, and references therein.
2. Sellinger, A.; Laine, R. M. *Macromolecules* **1996**, *29*, 2327.
3. Sellinger, A.; Laine, R. M. *Chem. Mater.* **1996**, *8*, 1592.
4. Lichtenhan, J. D.; Otonari, Y. A.; Carr, M. J. *Macromolecules* **1995**, *28*, 8435.
5. Feher, F. J.; Budzichowski, T. A. *J. Organomet. Chem.* **1989**, *379*, 33.
6. Feher, F. J.; Soulivong, D.; Eklud, A. G.; Wyndham, K. D. *Chem. Commun.* **1997**, 1185.
7. Jeon, H. G.; Mather, P. T.; Haddad, T. S. *Polym. Int.* **2000**, *49*, 453.
8. (a) Gilman, J. W.; Schlitzere, D. S.; Lichtenhan, J. D. *J. Appl. Polym. Sci.* **1996**, *60*, 591. (b) Gonzalez, R. I.; Phillips, S. H.; Hoflund, G. B. *J. Spacecr. Rockets* **2000B**, *37*, 463.
9. Sellinger, A.; Laine, R. M.; Chu, V.; Viney, C. *J. Polym. Sci., Part A: Polym. Chem.* **1994**, *2*, 3069.
10. Zhang, C.; Babonneau, F.; Bonhomme, C.; Laine, R. M.; Soles, C. L.; Hristov, H. A.; Yee, A. F. *J. Am. Chem. Soc.* **1998**, *120* (33), 8380.
11. Laine, R. M.; Choi, J.; Lee, I. *Adv. Mater.* **2001**, *13*, 800.
12. Zhang, C.; Laine, R. M. *J. Am. Chem. Soc.* **2000** *122* (29), 6979.
13. (a) Tamaki, R.; Choi, J.; Laine, R.M. *Chem. Mater.* **2003**, *15*, 793. (b) Choi, J.; Tamaki, R.; Kim, S.G.; Laine, R.M. *Chem. Mater.* **2003**, *15*, 3365.

14. Miracle, D.B.; Donaldson, S.L. In *ASM Handbook Composites Vol. 21*, Miracle, D.B. and Donaldson, S.L., Eds. ASM International: Materials Park, OH, **2001**, pp. 3-18.
15. Hull, D.; Clyne, T.W. In *An Introduction to Composite Materials*, 2nd ed., Cambridge University Press, New York, NY **1996**, p. 39.
16. Mathews, F.L.; Rawlings, R.D. In *Composite Materials: Engineering and Science*, CRC Press LLC, Boca Raton, FL **1999**, pp. 13-14.
17. (a) Novak, B. M. *Adv. Mater.* **1993**, *5*, 422. (b) Loy, D. A.; Shea, K. J. *Chem. Rev.* **1995**, *95*, 1431. (c) Ajayan, P. M. *Chem. Rev.* **1999**, *99*, 1787. (d) <http://itri.loyola.edu/nano/final/>.
18. Laine, R. M.; Asuncion, M.Z.; Balia, S.; Dias Filho, N. L.; Harcup, J.; Sutorik, A. C.; Viculis, L.; Yee, A. F.; Zhang, C.; Zhu, Q. In *Organic/Inorganic Hybrid Materials*; Klein, L., De Guire, M., Lorraine, F., Mark, J., Eds.; MRS Symp. Ser. 576; Materials Research Society: Warrendale, PA, 1999; pp 3-14.
19. Laine, R.M. *J. Mater. Chem.* **2005**, *15*, 3725.
20. Sanchez, C.; Ribot, F. *New J. Chem.* **1994**, *18*, 1007.
21. Baney, R.H.; Itoh, M.; Sakakibara, A.; Suzuki, T. *Chem.Rev.* **1995**, *95*, 1409.
22. Pescarmona, P.P.; Maschmeyer, T. *J. Aust. Chem.* **2001**, *54*, 583.
23. Feher, F.J.; Newman, D.A.; Walzer, J.F. *J. Am. Chem. Soc.* **1989**, *111*, 1741.
24. Feher, F.J.; Newman, D.A.; *J. Am.Chem. J. Am. Chem. Soc.* **1990**, *112*, 1931.
25. Feher, F.J.; Budzichowski, T.A.; Rahimian, K.; Ziller, J.W. *J. Am. Chem. Soc.* **1992**, *114*, 2859.
26. Feher, F.J.; Philipps, S.H. *J. Organomet. Chem.* **1996**, *521*, 391.
27. Shchegolikhina, O.I.; Pozdnyakova, Y.A.; Molodtsova, Y.A.; Korin, S.D.; Bukalov, S.S.; Leites, L.A.; Lyssenko, K.A.; Peregodov, A.S.; Auner, N.; Katsoulis, D.E. *Inorg. Chem.* **2002**, *41*, 6892.
28. Gavioli, G.; Battistuzzi, R.; Santi, P.; Zucchi, C.; Palyi, G.; Ugo, R.; Vizi-Orsz, A.; Shchegolikhina, O. I.; Pozdniakova, Yu. A.; Lindeman, S. V.; Zhdanov, A. A. *J. Organomet. Chem.* **1995**, *485*, 257.
29. Zucchi, C.; Mattioli, M.; Cornia, A.; Fabretti, A. C.; Gavioli, G.; Pizzardi, M.; Ugo, R.; Shchegolikhina, O. I.; Zhdanov, A. A.; Palyi, G. *Inorg. Chim. Acta* **1998**, *280*, 282.

30. Cornia, A.; Fabretti, A. C.; Gavioli, G.; Zucchi, C.; Pizzotti, M.; Vizi-Orosz, A.; Shchegolikhina, O. I.; Pozdniakova, Yu. A.; Pa'lyi, G. *J. Cluster Sci.* **1998**, *9*, 295.
31. (a) Feher, F.J.; Budzichowski, T.A.; Blanski, R.L.; Weller, K.J.; Ziller, J.W. *Organometallics* **1991**, *10*, 2526. (b) Feher, F.J.; Soulivong, D.; Eklud, A.G.; Wyndham, K.D. *Chem. Commun.* **1997**, *13*, 1185.
32. (a) Feher, F.J.; Blanski, R.L. *J. Am. Chem. Soc.* **1992**, *114*, 5886. (b) Severn, J.R.; Duchateau, R.; van Santen, R.A.; Ellis, D.D.; Spek, A.L. *Organometallics* **2002**, *1*, 4. (c) Duchateau, R.; Abbenhuis, H.C.L.; van Santen, R.A.; Meetsma, A.; Thiele, S.K.-H.; van Tol, M.F.H. *Organometallics* **1998**, *26*, 5663. (d) Hanssen, R.W.J.M.; van Santen, R.A.; Abbenhuis, H.C.L. *Eur. J. Inorg. Chem.* **2004**, *4*, 675.
33. Maxim, N.; Magusin, P.C.M.M.; Kooyman, P.J.; van Wolput, J.H.M.C.; van Santen, R.A.; Abbenhuis, H.C.L. *Chem. Mater.* **2001**, *13*, 2958.
34. Bonhomme, C.; Toledano, P.; Maquet, J.; Livage, J.; Bohnomme-Coury, L. *J. Chem. Soc., Dalton Trans.* **1997**, *9*, 1617.
35. (a) Bassindale, A.R.; Pourny, M.; Taylor, P.G.; Hursthouse, M.B.; Light, M.E. *Angew. Chem., Int. Ed.* **2003**, *42*, 3488; (b) Bassindale, A.R.; Parker, D.J.; Pourny, M.; Taylor, P.G.; Horton, P.N.; Hursthouse, M.B. *Organometallics* **2004**, *23*, 4400.
36. Tsuchida, A.; Bollin, C.; Sernetz, F.G.; Frey, H.; Mulhaupt, R. *Macromolecules* **1997**, *30*, 2818.
37. (a) Kim, G.-M.; Qin, H.; Fang, X.; Sun, F.C.; Mather, P.T. *J. Polym. Sci. B: Polym. Phys.* **2003**, *41*, 3299. (b) Kim, B.S.; Mather, P.T. *Macromolecules* **2002**, *35*, 8378. (c) Gonzalez, R.I.; Phillips, S.H.; Hoflund, G.B. *J. Spacecraft Rockets* **2000**, *37*, 463.
38. (a) Waddon, A.J.; Coughlin, E.B. *Chem. Mater.* **2003**, *15*, 4555. (b) Cardoen, G.; Coughlin, E.B. *Macromolecules* **2004**, *37*, 5123.
39. (a) Fu, B.X.; Hsiao, B.S.; White, H.; Rafailovich, M.; Mather, P.; Joen, H.G.; Phillips, S.; Lichtenhan, J.; Schwab, J. *Polym. Int.* **2000**, *49*, 437. (b) Fu, B.X.; Zhang, W.; Hsiao, B.S.; Rafailovich, M.; Sokolov, J.; Johansson, G.; Sauer, B.B.; Phillips, S.; Blanski, R. *High Performance Polym.* **2001**, *12*, 565.
40. (a) Baker, E.S.; Gidden, J.; Anderson, S.E.; Haddad, T.S.; Bowers, M.T. *Nano Lett.* **2004**, *4*, 779. (b) Fu, B.X.; Lee, A.; Haddad, T.S. *Macromolecules* **2004**, *37*, 5211. (c) Kopesky, E.T.; Haddad, T.S.; Cohen, R.E.; McKinley, G.H. *Macromolecules* **2004**, *37*, 8992.
41. Tamaki, R.; Tanaka, Y.; Asuncion, M.Z.; Choi, J.; Laine, R.M. *J. Am. Chem. Soc.* **2001**, *123*, 12416.

42. Brick, C.M.; Tamaki, R.; Kim, S.G.; Asuncion, M.Z.; Roll, M.F.; Nemoto, T.; Ouchi, Y.; Chujo, Y.; Laine, R.M. *Macromolecules* **2005**, *38*, 4655.
43. Roll, M.F.; Asuncion, M.Z.; Kampf, J.; Laine, R.M. *ACS Nano* **2008**, *2*, 320.
44. (a) Brown, J.F., Jr. *J. Polym. Sci., Part C* **1963**, *1*, 83. (b) Frye, C.L.; Klosowski, J.M. *J. Am. Chem. Soc.* **1971**, *93*, 4599.
45. (a) Laine, R.M.; Youngdahl, K.A.; Babonneau, F.; Hoppe, M.L.; Zhang, Z.-F.; Harrod, J.F. *Chem. Mater.* **1990**, *2*, 464. (b) Tsumura, M.; Kiyoshi, A.; Kotani, J.; Hiraishi, M.; Iwahara, T. *Macromolecules* **1998**, *31*, 2716. (c) Lee, E.-C.; Kimura, Y. *Polym. J.* **1998**, *30*, 234. (d) Lee, E.-C.; Kimura, Y. *Polym. J.* **1998**, *30*, 730.
46. Wright, J.D.; Sommerdijk, N.A.J.M. *Sol-Gel Materials: Chemicals and Application*, Taylor and Francis, London, **2001**.
47. Sprung, M.M.; Guenther, F.O. *J. Polymer. Sci.* **1959**, *28*, 17.
48. Ollson, K.; Grönwall, C.; *Arkiv. Kemi.* **1961**, *17*, 529.
49. Brown, J.F. Jr.; Vogt, L.H. Jr.; Prescott, O.I. *J. Am. Chem. Soc.* **1964**, *86*, 1120.
50. Kim, S.-G.; Sulaiman, S.; Fargier, D.; Laine, R.M. In *Materials Syntheses: A Practical Guide*, Shubert, U.; Hüsing, N.; Laine, R.M., Eds.; SpringerWien: New York, **2008**, pp. 179-191.
51. Choi, J.; Kim, S.-G.; Laine, R.M. *Macromolecules* **2004**, *37*, 99.
52. Pfaltz, A.; Loiseleur, O.; Hayashi, M.; Keenan, M.; Schemees, N. *J. Organomet.Chem.* **1999**, *576*, 16.
53. (a) Ozawa, F.; Kubo, A.; Hayashi, T. *J. Am. Chem Soc.* **1991**, *113*, 1417. (b) Ozawa, F.; Kobatake, Y.; Hayashi, T. *Tetrahedron Lett.* **1993**, *34*, 2505. (c) Ozawa, F.; Kubo, A.; Hayashi, Nishioka, E.; Yanagi, K.; Moriguchi, K. *Organometallics* **1993**, *12*, 4188. (d) Hayashi, T.; Kubo, A.; Ozawa, F.; *PureAppl. Chem.* **1992**, *64*, 421.
54. (a) Heck, R.F. *Org. React.* N.Y. **1982**, *27*, 345. (b) Plevyak, J.E.; Heck, R.F. *J. Org. Chem.* **1978**, *43*, 2454. (c) Brase, S.; de Meijere, A. In *Metal-catalyzed Cross-coupling Reactions*, Diederich, F., Stang, P.J., Eds.; Wiley-VCH: New York, **1998**, pp. 99-166.
55. Littke, A.; Fu, G. *J. Org. Chem.* **1999**, *64*, 10.
56. Amatore, C.; Jutand A. *J. Organomet. Chem.* **1999**, *576*, 254.

57. Fauvarque, J. F.; Jutand, A. *Bull. Soc. Chim. Fr.* **1976**, 765.
58. Gillie, A.; Stille, J. K. *J. Am. Chem. Soc.* **1980**, *102*, 4933.
59. Fauvarque, J.F.; Jutand, A. *J. Organomet. Chem.* **1977**, *136*, 132.
60. Sulaiman, S.; Bhaskar, A.; Zhang, J.; Guda, R.; Goodson, T. III; Laine, R.M. *Chem. Mater.* **2008**, *20* 5563.
61. Sonogashira, K.; Tohda, Y.; Hagihara, N. *Tetrahedron Lett.* **1975**, *16*, 4467.
62. Grubbs, R.H. *Prog. Inorg. Chem.* **1978**, *24*, 1.
63. Calderon, N.; Ofstead E.A.; Ward, J.P.; Judy, W.A.; Scott K.W. *J. Am. Chem. Soc.* **1968**, *90*, 4133.

Chapter 2

General Experimental Techniques

Dioxane, THF, and toluene were purchased from Fisher and distilled under nitrogen gas from Na/benzophenone prior to use. All other solvents and chemicals were purchased from Fisher or Aldrich and used as received without further purification. All work was performed under nitrogen unless otherwise stated.

2.1 Analytical Procedures

NMR analyses.

All ^1H and ^{13}C -NMR were performed in CDCl_3 or DMSO and recorded on a Varian INOVA 400 spectrometer. ^1H -NMR spectra were collected at 400 MHz using a 6000 Hz spectral width, a relaxation delay of 3.5s, a pulse width of 38° , 30 k data points, and CDCl_3 (7.27 ppm) or DMSO- d_6 (2.50 ppm) as an internal reference. ^{13}C -NMR spectra were collected at 100 MHz using a 25000 Hz spectra width, a relaxation delay of 1.5s, 75k data points, a pulse width of 40° , and CDCl_3 (77.23 ppm) or DMSO- d_6 (39.5 ppm) as the internal reference.

Thermal Gravimetric Analyses (TGA).

Thermal stabilities of materials under N_2 or air were examined using a 2960 simultaneous DTA-TGA Instrument (TA Instruments, Inc., New Castle, DE). Samples (5-10 mg) were

loaded in alumina pans and ramped to 1000 °C while heating at 10 °C/min. The N₂ or air flow rate was 60 mL/min.

Differential Scanning Calorimetry (DSC).

Calorimetry was performed on materials using a DSC 2910 (TA Instruments, Inc., New Castle, DE). The N₂ flow rate was 60 mL/min. Samples (10-15 mg) were placed in a pan and ramped to 400 °C (5 °C/min/N₂) without capping.

Melting Points.

Melting point determinations were performed on samples using a Mel-Temp 3.0 (Laboratory Devices, Inc. Dubuque, IA) with a ramp rate of 5 °C/min.

Fourier-Transform Infrared Spectroscopy (FTIR).

Diffuse reflectance Fourier transform (DRIFT) spectra were recorded on a Nicolet 6700 Series FTIR spectrometer (Thermo Fisher Scientific, Inc., Madison, WI). Optical grade, random cuttings of KBr (International Crystal Laboratories, Garfield, NJ) were ground, with 1.0 wt% of the sample to be analyzed. For DRIFT analysis, samples were packed firmly and leveled off at the upper edge to provide a smooth surface. The FTIR sample chamber was flushed continuously with N₂ prior to data acquisition in the range 4000-400 cm⁻¹.

Gel Permeation Chromatography.

All GPC analyses were done on a Waters 440 system equipped with Waters Styragel columns (7.8 x 300, HT 0.5, 2, 3, 4) with RI detection using Optilab DSP interferometric refractometer and THF as solvent. The system was calibrated using polystyrene standards and toluene as reference. Analyses were performed using PL Caliber 7.04 software (Polymer Labs, Shropshire UK).

Matrix-Assisted Laser-Desorption/Time-of-Flight Spectrometry.

MALDI-TOF was performed on a Micromass TofSpec-2E equipped with a 337 nm nitrogen laser in positive ion reflection mode using poly(ethylene glycol) as the

calibration standard, 1,8,9-anthracenetriol (dithranol) as the matrix, and AgNO₃ as the ion source. Samples were prepared by mixing solutions of five parts dithranol (10 mg/mL in THF), five parts sample (1 mg/mL in THF) and one part AgNO₃ (10 mg/mL in water) and blotting the mixture on the target plate.

X-Ray Diffraction Analysis (XRD).

XRD was performed on a Rigaku Rotating Anode Goniometer (Rigaku Denki., LTD., Tokyo, Japan). The powder sample was packed on a glass specimen holder. XRD scans were made from 10° to 60° 2 θ , using a scan rate of 2° min⁻¹ in 0.05° increments and Cu K α radiation (1.542 Å) operating at 40 kV and 100 mA. The Jade program (Version 3.1 from Materials Data, Inc., Livermore CA) was used to determine the presence of any crystallographic phases.

2.2 General Synthetic Methods

2.2.1 Synthesis of Octaphenylsilsesquioxane (OPS)

OPS was prepared by previously published methods.¹ Phenyltriethoxysilane, PTES, (7 g, 29.1 mmol) was added to a 100 mL round-bottomed flask equipped with a magnetic stir bar and reflux condenser. 50 mL of toluene and potassium hydroxide (0.56 g, 10.0 mmol) was then added under N₂. The solution was heated to reflux at 110 °C, and then water (0.5 mL, 10 wt% water based on PTES) was slowly added in small portions of 0.1-0.2 mL each 3-5 min over 30 min. The reaction was refluxed for 60 h. After about 3 h, a white powder (OPS) begins to precipitate. After 60 h, the precipitated powder is filtered off, washed with methanol (3 x 20 mL), and dried 70 °C/7 h to give 3.41 g (91%) of white powder.

2.2.2 Synthesis of Octa(nitrophenyl)silsesquioxane (ONPS)

ONPS was prepared per Olsson and Grönwall² with several modifications.³ OPS, 50 g (48.4 mmol) was added in small portions to 300 mL of fuming nitric acid with stirring at 0 °C. After addition was complete, the solution was stirred for an additional 30 min and then at room temperature for 20 h. After filtration through glass wool, the solution was poured onto 250 g of ice. A very faintly yellow precipitate was collected, washed with water (~100 mL x 5 until pH ≈ 6.0) and then with ethanol (~100 mL x 2). The obtained powder was dried at ambient to remove residual solvent to yield 60.8 g (43.6 mmol, 90.1%) of material.

2.2.3 Synthesis of Octa(aminophenyl)silsesquioxane (OAPS)

OAPS was prepared³ by introducing ONPS (10.0 g, 7.16 mmol, -NO₂ 57.4 mmol) and 5 wt % Pd/C (1.22 g, 0.574 mmol) into a 250-mL Schlenk flask equipped with a condenser under N₂. Distilled THF (80 mL) and triethylamine (80.0 mL, 0.574 mmol) were then added. The mixture was heated to 60 °C, and 85% formic acid (10.4 mL, 0.230 mol) was added slowly at 60 °C. Carbon dioxide evolved, and the solution separated into two layers. After 5 h, the THF layer was separated, and 50 mL of THF and 50 mL of water were added until the slurry formed a black suspension. The suspension and the THF solution separated previously were mixed and filtered through celite. Another 20 mL of THF and 20 mL of water were added to the flask to dissolve the remaining black slurry, and the suspension was filtered again. All of the filtrates were combined with 50 mL of ethyl acetate and washed 4x with 100 mL H₂O. The organic layer was dried after 5 g of MgSO₄ and precipitated by addition to 2 L of hexane. A white precipitate was collected by filtration, redissolved in 30:50 THF/ethyl acetate and reprecipitated into 1 L hexane. The obtained powder was dried under vacuum. Yield 6.80 g (5.89 mmol, recovery 82%).

2.2.4 Synthesis of Octa(Br_{5,3}phenyl)silsesquioxane (Br_{5,3}OPS)

Br_{5,3}OPS was synthesized according to published methods.⁴ To a 250 mL round-bottom flask equipped with magnetic stirring was added 5.0 g of finely ground OPS (38.7 mmol-phenyl), 570 mg (10.2 mmol) of Fe, and 50 mL of CH₂Cl₂. Then, 1.78 mL (34.8 mmol) of Br₂ was added over the course of 10 min via syringe. The solution was stirred at ambient for 3 h. After this time, 50 mL of 10% NaHSO₃ was added to destroy the remaining Br₂. The organic layer was separated and washed with water three times, and the solvent was removed by rotoevaporation. The resulting white powder was dissolved in 50 mL of ethyl acetate and precipitated into 1000 mL of methanol. The solution was filtered, giving 6.1 g (87%) of a white powder.

2.2.5 Synthesis of Octa(iodophenyl)silsesquioxane (I₈OPS)

I₈OPS was prepared according to the procedures by Roll, et. al.⁵ To an oven-dried, single-neck 1 L flask under flowing N₂ was added 290 mL of 1.0 M ICl/CH₂Cl₂ solution. The solution was cooled to -40 °C using a dry ice/ethanol/ethylene glycol bath, and 26.7 g (25.8 mmol) of powdered OPS was added at an approximate rate of 5 g/min with stirring. HCl evolution began within 1 min of OPS addition. Flowing N₂ flushed the HCl from the reaction system. Residual OPS, sticking to the sides of the flask, was washed into the reaction solution with 40 mL of CH₂Cl₂. The reaction was stirred for 24 h at -40 °C, allowed to warm to room temperature with stirring over another 24 h, and quenched with 300 mL of ~1 M sodium metabisulfite.

When all the ICl was consumed and quenched, the organic layer was extracted, washed three times with water, filtered, and dried over anhydrous sodium sulfate. The volume was subsequently reduced by rotary evaporation to produce a white solid. This solid was further dried under vacuum and then redissolved in 400 mL of THF. This clear solution was then precipitated into 3 L of cold methanol, providing a white powder that was then vacuum-dried to give 47 g (23 mmol, 90% yield). The as-precipitated material could then be recrystallized from hot ethyl acetate to give colorless crystals (~30–40%

yield). Single crystals suitable for X-ray diffraction were grown in using the same recrystallization procedures on a smaller scale.

2.3 References

1. Olsson, K.; Grönwall, C. *Arkiv. Kemi.* **1961**, *17*, 529.
2. Kim, S.-G.; Sulaiman, S.; Fargier, D.; Laine, R.M. In *Materials Syntheses: A Practical Guide*, Shubert, U.; Hüsing, N.; Laine, R.M., Eds.; SpringerWien: New York, **2008**, pp. 179-191.
3. Tamaki, R.; Tanaka, Y.; Asuncion, M.Z.; Choi, J.; Laine, R.M. *J. Am. Chem. Soc.* **2001**, *123*, 12416.
4. Brick, C.M.; Tamaki, R.; Kim, S.G.; Asuncion, M.Z.; Roll, M.F.; Nemoto, T.; Ouchi, Y.; Chujo, Y.; Laine, R.M. *Macromolecules* **2005**, *38*, 4655.
5. Roll, M.F.; Asuncion, M.Z.; Kampf, J.; Laine, R.M. *ACS Nano* **2008**, *2*, 320.

Chapter 3

Silsesquioxane Barrier Materials

Cubic octameric silsesquioxanes, because of their octahedral structures and nanometer size, represent potentially very useful nanoconstruction sites. Here we report the reaction of octaaminophenylsilsesquioxane (OAPS) with a variety of epoxides and dianhydrides and their subsequent heat treatment to form nanocomposite films with exceptional oxygen barrier properties. While solution-cast films give relatively low oxygen transmission rates (OTR), casting followed by warm-pressing lowers the OTR to values competitive with commercially available high-performance barrier films. The lowest OTR measured was obtained with warm-pressed bilayer films consisting of OAPS/tetraglycidyl-*m*-xylenediamine and OAPS/2,4-epoxycyclohexylmethyl-3,4-epoxycyclohexanecarboxylate with OTRs $< 1 \text{ cm}^3 \text{ } 20 \text{ } \mu\text{m}/(\text{m}^2 \cdot \text{day} \cdot \text{atm})$. These silsesquioxane films are thermally very robust, particularly the OAPS/imide films ($>500 \text{ } ^\circ\text{C}$ when fully cured), making them ideal for electronics packaging and encapsulation applications.

3.1 Introduction

One of the oft-repeated objectives of nano-science and nano-technology is to develop methods of constructing materials from the bottom up. However, the potential to realize such approaches is limited by the availability of building blocks that permit the strategic design of materials and thereafter their construction with nanometer by nanometer control. The literature is replete with articles on the design and synthesis of nanosized particles and their assembly to nanostructured materials;¹⁻⁶ however, there are very few building blocks that offer the potential for nanometer by nanometer construction in 1-, 2- or 3-D with control of periodicity over millimeter and even centimeter length scales and therefore global properties.

Octasilsesquioxanes,⁷⁻¹¹ Q_8 $[RMe_2SiOSiO_{1.5}]_8$ and T_8 $[RSiO_{1.5}]_8$ (R = alkyl, alkenyl, alkynyl, aryl, epoxy, methacrylate, aromatic, etc; Figure 3.1) are spherical molecules \approx 1.0 nm in diameter with cubic symmetry that places a functional group in each octant in Cartesian space, thereby, in principle, permitting their assembly one nanometer at a time in 1-, 2- or 3-D with complete control of periodicity. In principle, through control of the architecture of the organic groups connecting the vertices of each silsesquioxane, it is possible to tailor global properties.

We and others have begun to explore their utility for building nanostructured materials, nanocomposites for diverse applications.¹²⁻³⁰ Our initial goal was first to prove that it is possible to both assemble Q_8 and T_8 systems in 3-D covalently linked nanocomposite networks with precise control of the periodicity over extended length scales.^{15,20} A second goal was to demonstrate the potential to tailor global properties through control of the architecture of the organic tethers joining silsesquioxane cage vertices. We focused our efforts on the epoxy and imide chemistries of the Q_8 and T_8 systems, as suggested by Schemes 3.1 and 3.2.^{18,19}

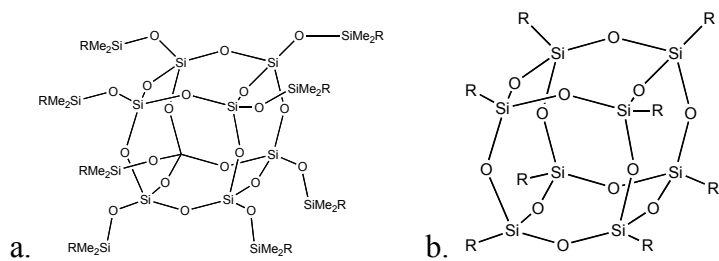
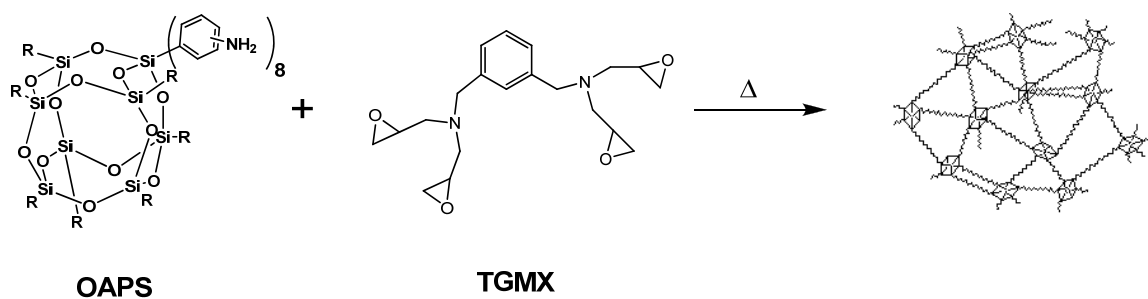
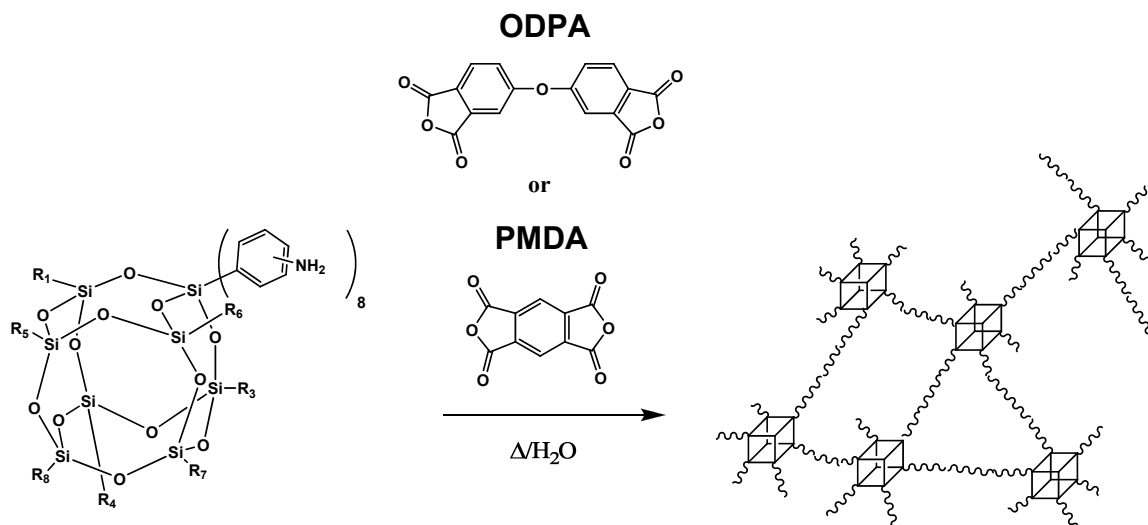


Figure 3.1. Typical (a) Q₈ and (b) T₈ Structures.



Scheme 3.1. Reaction of octaminophenylsilsesquioxane (OAPS) and tetraglycidyl-*m*-xylenediamine (TGMX) to form nanocomposite films.



Scheme 3.2. Reaction of OAPS with oxydiphthalic anhydride (ODPA) or pyromellitic dianhydride (PMDA) to form imide nanocomposite films.

One major finding of this work was that traditional epoxy resin stoichiometries, wherein one -NH_2 group is reacted with two epoxy moieties ($\text{N} = 0.5$), offer poorer mechanical properties than a 1:1 NH_2 :epoxy stoichiometry ($\text{N} = 1$). In this regard, we recently reported the development of simple, low-viscosity epoxy resins with control of coefficients of thermal expansion (CTEs) over an order of magnitude from 25 to 240 $\text{ppm}/^\circ\text{C}$.²² In an extension of these efforts, we report here that it is possible to use nanometer tailoring of the structures of epoxy and imide systems to produce oxygen barrier films that, unoptimized, are equivalent to those produced commercially while offering improved thermal stability.

At the molecular level, transport of gas molecules across membranes is controlled (1) by the solubility of the gas within the membrane materials followed by diffusion through it^{31,32} and (2) the ability to diffuse through the membrane without dissolution via adventitious pores and free volume.³³ Thus, all efforts to make barrier materials must also consider ways of blocking these transport mechanisms.

A review of the literature indicates that superior barrier properties are obtained from polymeric materials modified using an assortment of approaches.³²⁻³⁹ For example, good barrier properties extend from polymers with strong intra-chain forces that induce high packing densities that in turn hinder gas diffusion. Thus strong hydrogen bonding, chain alignment by extrusion, high degrees of crystallinity or liquid crystallinity provide one set of approaches to defeating diffusion of gases. Another approach is to add easily dispersed second phases that can be organic or inorganic inclusions such as exfoliated clay particles or simply silica.³⁹ An extension of this approach is to make bilayer films where transport across the interface is problematic. In the extreme, this can include introduction of an inorganic phase including aluminum (metallized layers). Clearly, the need to disperse or coat a second phase adds to the difficulty and expense of processing as does extrusion or other processing methods that align polymer chains.

If the claim that silsesquioxanes offer tailorability of global properties by assembly at nanometer length scales is to be justified, then it should be possible to develop low-viscosity, single phase silsesquioxane systems that on curing offer good O_2 transport barrier properties. We describe here our efforts to identify useful barrier systems. It is

important to note that the systems developed here also offer considerable potential for modifying CTEs, and abrasion and corrosion resistance.²²

3.2 Experimental

3.2.1 Materials

Tetraglycidyl-*m*-xylenediamine (TGMX, MW 332.4), a gift from Dr. Rafil Basheer of Delphi Corp., and diglycidyl ether of bisphenol A (DGEBA, MW 340.4, Aldrich) were used as received. Standard concentrations (2%, 5%, and 10%) of O₂ in helium were purchased from Cryogenic Gases (Detroit, MI). δ -Alumina nanopowder (Aluminium C, 71 nm APS) was received as a gift from Degussa Inc. and used as received. 4-Vinyl-1-cyclohexene (MW 108.2), pyromellitic dianhydride (PMDA, MW 218.1), 4,4'-oxydianiline (ODA, MW 200.2), 4,4'-oxydiphthalic anhydride (ODPA, MW 310.2), 3,4-epoxy-cyclohexyl-methyl-3,4-epoxy-cyclohexanecarboxylate (ECHX, MW 252.3), resorcinol diglycidyl ether (RDGE, MW 222.2), and N-methylpyrrolidone (NMP) were purchased from Aldrich (Milwaukee, WI) and used without further purification. Octahydridosilsesquioxane (OHS, MW 1018.0) and octaaminophenylsilsesquioxane (OAPS, MW \approx 1153) were synthesized following methods described in the literature.^{16,17} All work was performed under nitrogen.

3.2.2 Curing and Pressing Studies

All samples were cast in round 100 mm diameter Teflon petri dishes. They were heated in a Thelco Laboratory Oven (equipped with temperature controller) according to the conditions described in **Tables 3.1** and **3.2**. Heat-pressed samples were pre-cured and subsequently removed from the molds, sandwiched between aluminum foil sheets, and warm-pressed in air according to the conditions described in **Table 3.2**, from 0.690 – 1.03 MPa (100-150 psi) in a Carver Press Model 3851-0 (equipped with heating platens

and temperature controller) according to the conditions specified in **Table 3.2**. Resulting warm-pressed samples were ~ 200 mm in diameter.

3.2.3 Oxygen Transmission Rate (OTR) Measurements

OTR values were measured using an HP Model 5890 Series 2 GC equipped with permeation cell and calibrated with 2%, 5%, and 10% concentrations of O₂ in helium. A schematic of the components needed to determine OTR by permeation cell and GC is shown in Figure 3.2. Test films were cut and mounted (with typical commercial 2-part epoxy adhesive) on circular aluminum foil holders 100 mm diameter with circle shape openings of 40 mm diameter. Mounted films were then placed in the permeation cell and conditioned under steady flow of test and carrier gas for 2 h. Measurements were taken (at ambient humidity) at room temperature, 18, 50, and 70 °C. The 18 °C measurements were achieved by submerging the permeation cell in an ice bath while measurements at 50 and 70 °C were taken with the permeation cell heated in a temperature controlled oven.

The gas (oxygen) transmission rate **P** (cm³·cm /cm²·s·cm Hg) was obtained by measuring the gas amount **q** (cm³) permeated through membrane in time **t** (sec), as follows:

$$t = \frac{60 \times m}{f} \quad (\text{s})$$

$$P = \frac{q \times l}{a \times t \times 76} \quad (\text{cm}^3 \cdot \text{cm} / \text{cm}^2 \cdot \text{s} \cdot \text{cm Hg})$$

where: **m** = volume of gas sample loop (cm³)
f = gas flow rate (cm³/min)
q = volume of permeated O₂ gas (cm³)
a = area of membrane (cm²)
l = thickness of membrane (cm)

Three separate GC measurements (within $\pm 5\%$) were recorded for each film and averaged. The gas amount q was determined from a calibration curve. The oxygen transmission rate (P) was calculated and standardized to $20\ \mu\text{m}$ thickness. The OTR of the measured films are reported in **Tables 3.1-3.2**.

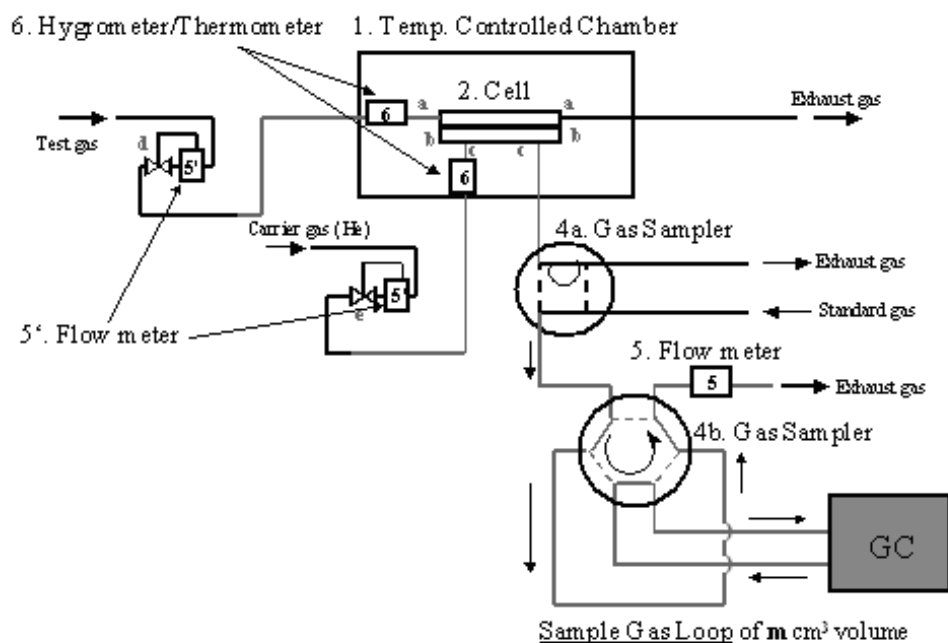


Figure 3.2. Schematic of GC/permeation cell for determination of OTR. (Measurements taken at ambient humidity with HP Model 5890 Series 2 GC.)

3.2.4 Synthetic Methods and Sample Curing Studies

3.2.4.1 Synthesis of Tetrethylcyclohexenyl Silsesquioxane (TCHS) and Curing

OHS, 25.0 g (196.6 mmol Si-H) and 178.6 mg of PtO_2 were placed in a 500 mL Schlenk flask equipped with magnetic stirrer and condenser. The flask was evacuated and flushed three times with N_2 . Toluene (200 mL) and 9.08 mL (122.8 mmol) of 4-vinyl-1-

cyclohexene were added via syringe. The reaction mixture was heated at 85 °C for 24 h. The solid PtO₂ catalyst was separated over celite and residual toluene was removed under vacuum to reveal a white powder (30.9 g, 88%). 2.0 g of TCHS was placed in a round Teflon petri dish and heated at temperatures specified in **Table 2.1** to give a 0.4 mm thick film used in gas transport measurements.

3.2.4.2 Preparation of OAPS/PMDA Imide Films

OAPS, 25.0 g (173.6 mmol NH₂-phenyl) was dissolved in 110 mL (1.13 mol) of NMP. This solution was added to another solution containing 18.9 g (86.8 mmol) of PMDA in 100 mL of NMP. The combined solution was stirred at room temperature for 5 min. An 8.0 g portion of solution was cast into molds and heated at temperatures specified in **Tables 3.1** and **3.2** to give 0.50 mm thick films.

3.2.4.3 Preparation of OAPS/ODA/PMDA Imide Films

OAPS (6.25 g, 43.4 mmol NH₂-Phenyl) and ODA (4.35 g, 43.4 mmol NH₂-Phenyl) were dissolved in 110 mL of NMP. This solution was added to another containing 18.9 g (86.8 mmol anhydride) of PMDA in 100 mL of NMP cooled to 0 °C. The combined solution was stirred at room temperature for 5 min. An 8.0 g portion of solution was cast into molds and heated at temperatures specified in **Tables 3.1** and **3.2** to give 0.50 mm thick films.

3.2.4.4 Preparation of OAPS/ODA/ODPA Imide Films

OAPS (6.25 g, 43.4 mmol NH₂-Phenyl) and ODA (4.35 g, 43.4 mmol NH₂-Phenyl) were dissolved in 110 mL of NMP. This solution was added to another containing 13.5 g (86.8 mmol anhydride) of ODPA in 100 mL of NMP cooled to 0 °C. The combined solution was stirred at 0 °C for 5 min. An 8.0 g portion of this solution was cast into molds and heated at temperatures specified in **Tables 3.1** and **3.2** to give 0.50 mm thick films.

3.2.4.5 Preparation of OAPS/DGEBA Epoxide Films

OAPS (25.0 g, 173.6 mmol NH₂-Phenyl) was dissolved in 110 mL of NMP. This solution was added to another solution containing 32.12 g (173.6 mmol epoxy) of DGEBA in 100 mL of NMP cooled to 0 °C. The combined solution was stirred at for 5 min. 6.0 g of solution cast into molds and heated at temperatures specified in **Tables 3.1** and **3.2** to give 0.45 mm thick films.

3.2.4.6 Preparation of OAPS/ECHX Epoxide Films

OAPS (3.20 g, 22.22 mmol of Ph-NH₂) and ECHX (5.61 g, 44.44 mmol epoxy) were dissolved in 20 mL of DMF and stirred for 5 min. The solution was cast into molds and heated at temperatures specified below in **Tables 3.1** and **3.2** to give 0.50 mm thick films.

3.2.4.7 Preparation of OAPS/TGMX Epoxide Films

OAPS (3.20 g, 22.22 mmol of NH₂) and TGMX (2.29 g, 51.46 mmol of epoxy) were dissolved in 40 mL of THF and stirred for 5 min. The solution was left overnight at room temperature to evaporate THF. The solution was cast into molds and heated at temperatures specified below in **Tables 3.1** and **3.2** to give 0.50 mm thick films.

3.2.4.8 Warm-Pressed OAPS/TGMX-OAPS/ECHX Bilayer Epoxide Films

OAPS/TGMX films were prepared as above. The films were partially cured at 100 °C/1h and 130°C /4h after which it became a flexible solid. OAPS/ECHX films were prepared as above and cast onto the partially cured OAPS/TGMX films. Both layers were again heated at 100 °C/1h and 130 °C/4h, removed from the mold, sandwiched between aluminum foil sheets and heat pressed at 1.03 MPa as specified in **Table 3.2**.

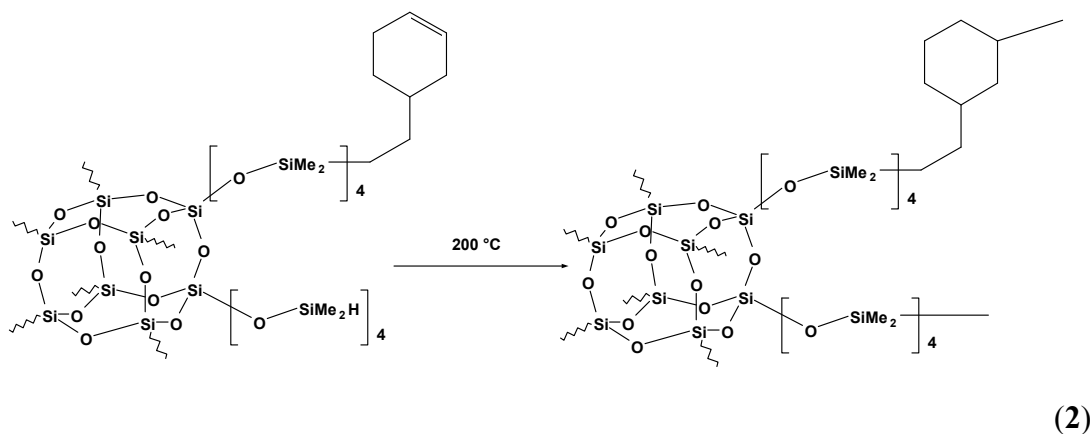
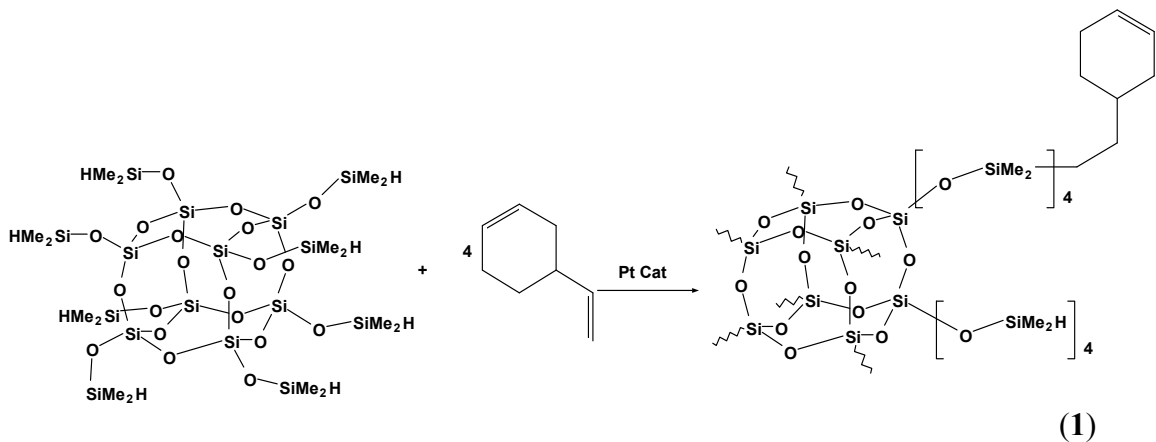
3.2.4.9 Preparation of OAPS/RDGE Films

OAPS (3.20 g, 22.2 mmol of PhNH₂) and RDGE (4.93 g, 44.4 mmol of epoxy) were dissolved in 40 mL of DMF and stirred for 5 min. The solution was cast into molds and heated at temperatures specified in **Tables 3.1** and **3.2** to give 0.50 mm thickness films.

3.3 Results and Discussion

As noted above, traditional barrier materials rely on close packing of polymer molecules coupled with the introduction of both organic and inorganic crystalline second phases as micro and nanocomposite barriers within a standard polymer matrix. Given that octafunctional silsesquioxane cages offer the potential to produce very highly cross-linked materials wherein the silica cage not only acts as the cross-linker but also provides a completely dispersed and highly impermeable inorganic phase,⁴⁰ the initial goal in this work was to form highly cross-linked materials with very short tethers connecting the silsesquioxane cores. Both the epoxy resins of our CTE studies and some of the polyimides studied earlier offer such opportunities.^{18,19,22}

In addition, we were also interested in a novel self-curing oligomer that offers the additional potential of relatively high thermal stability and high hydrophobicity. Thus, we briefly examined the barrier behavior of tetrethylcyclohexenyl silsesquioxanes (TCHS) produced via reaction **1** of Scheme **3.3**. TCHS melts at 120°C and cures at 180°C (reaction **2** of Scheme **3.4**) to give fully dispersed and transparent materials that show no evidence of nanometer-sized pores by BET.



Scheme 3.3. (1) Preparation of TCHS from OHS and 4-vinyl-1-cyclohexene and (2) self-curing of TCHS at 200 °C.

TCHS can be melted, cast as a liquid and subsequently cured to provide high-quality films (see Experimental Section above). Unfortunately, as shown below, it is highly permeable to O₂ but may offer utility for separation of other gases. Thus, the majority of the work reported here maps structure-processing-property relationships of silsesquioxane epoxy and imide nanocomposites as O₂ barrier materials. The types of epoxy compounds studied are shown in Figure 3.3. The oxygen transport values (OTR - measured as a function of film thickness per unit surface area) and curing conditions are shown in **Table 3.1**. We have also characterized these materials via a number of standard techniques; see **Chapter 2**.

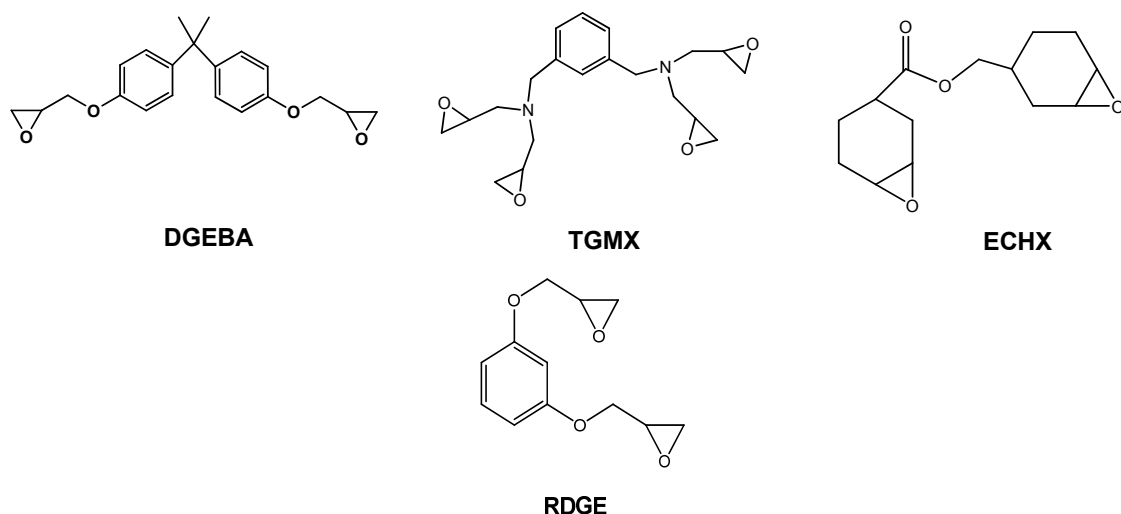


Figure 3.3. Sets of epoxies tested with various amine curing agents.

Table 3.1. Oxygen Transmission Rates (OTR) of cast silsesquioxane films.
 [@ 20 °C and 65% RH; $\text{cm}^3 \cdot 20 \mu\text{m} / \text{m}^2 \cdot \text{day} \cdot \text{atm} \cdot \text{O}_2$, i.e. standardized to 20 μm thickness]

Sample	N NH ₂ groups : Epoxide groups	Curing	OTR (± 0.5) ($\text{cm}^3 \cdot 20 \mu\text{m} / \text{m}^2 \cdot \text{day}$ $\cdot \text{atm}$)
TCHS [Pt(dcp)]	--	170 °C /5 h	24,000
TCHS (PtO ₂)	--	130 °C/6 h, 130 °C/8 h, 150 °C/8 h, 170 °C/8 h	13,000
50% OAPS/PMDA	--	120 °C /4 h, 205 °C /4 h, 215 °C/4 h	31
50% OAPS/PMDA	--	120 °C /4 h, 205 °C /4 h, 215 °C/8 h, 240 °C/8 h	27
50% OAPS/ODPA	--	120 °C /4 h, 205 °C /4 h	35
50% OAPS/ODPA	--	120 °C /4 h, 205 °C /4 h, 215 °C/8 h, 225 °C/8 h	25
50% OAPS/ODPA	--	120 °C /4 h, 205 °C /4 h, 215 °C/8 h, 240 °C/8 h	27
50%OAPS/ODPA /ODA	--	120 °C /4 h, 205 °C /4 h, 215 °C/8 h, 225 °C/8 h	29
OAPS/DGEBA	0.5	130 °C /5 h	110
OAPS/DGEBA	0.5	130 °C /5 h, 150 °C /5 h	21
OAPS/DGEBA	1.0	130 °C /5 h, 150 °C /5 h	24
OAPS/TGMX	0.5	90 °C/2 h	14
OAPS/ECHX	0.5	100 °C/1 h, 130 °C/4 h	8
OAPS/ECHX	1.0	100 °C/1 h, 130 °C/4 h	24
OAPS/ECHX	0.5	100 °C/1 h, 130 °C/4 h, 180 °C/4 h	6
OAPS/RDGE	0.5	95 °C/4 h, 115 °C/4 h	105
OAPS/RDGE	1.0	95 °C/4 h, 115 °C/4 h	115
EVAl F Grade [†]	--	--	< 1.0

[†]Eval F is 32% ethylene-vinyl alcohol copolymer biaxially orientated (3x3) and heat treated to 140 °C.⁴²

In general, the OTR of the films decreases with increasing curing temperatures and times. However, the limiting factor was increased brittleness at higher temperatures, as films cast from solution fractured easily from the stresses of curing in slightly curved molds. In contrast, warm pressing minimized brittle fracture and had a profound effect on barrier properties.

3.3.1 Solution Cast Films

3.3.1.1 TCHS

TCHS films were formed by curing TCHS per conditions described in **Table 3.1**. TCHS is self-curing (Scheme **3.3**); films are completely transparent and have high thermal stability. The 5% mass loss temperature ($T_{d5\%}$) of TCHS is 325 °C, making it ideal for electronics encapsulation. Qualitatively, films have a range of flexibility depending on the temperature and duration of curing. However, no quantitative measurements of flexibility were made. Films cured at 5-h (170 °C) provided the best flexibility and least color while those subjected to step-wise curing (130 °C/6 h, 130 °C/8 h, 150 °C/8 h, 170 °C/8 h) were most rigid and deeply yellow, yet still transparent. The yellow color comes in part from the retained Pt catalyst.

TCHS was initially synthesized using Pt(dcp), a soluble catalyst, which is quenched after the reaction with PPh₃. However, we speculated that the presence of residual PPh₃ inhibited complete curing of TCHS, explaining the unusually high OTR values recorded in **Table 3.1**. According to solid state NMR studies, 130 °C/5 h and 170 °C/5 h TCHS films are 69% and 79% cured.⁴¹ In response to this, we examined PtO₂ catalyzed hydrosilylation, and filtered off the solid catalyst while eliminating the need for PPh₃. While the OTR values using PtO were lower by approximately half [13,000 vs. 24,000 cm³·20 μm/(m²·day·atm)], they were not as low as expected or desired. Thus, we focused on the polyimide and epoxy systems.

3.3.1.2 Polyimide Films

We previously described the synthesis, processing, and mechanical properties of two polyimide nanocomposite systems, OAPS/PMDA and OAPS/ODPA.^{18,19} Although the OAPS/PMDA materials are very brittle, we were able to successfully process a number of films suitable for OTR measurements. Note that in our earlier studies, these materials cured most effectively on heating to ≥ 300 °C.

As expected, the barrier performance of these films improved with higher temperature (more complete) curing, but cast OAPS/PMDA films could not be heated above 240 °C without fracturing into unusable fragments. Even so, films heated step-wise (to minimize cracking) 120 °C /4 h, 205 °C /4 h, 215 °C/8 h, 225 °C/8 h exhibited promising barrier properties [**Table 3.1**; $27 \pm 0.5 \text{ cm}^3 \cdot 20 \mu\text{m}/(\text{m}^2 \cdot \text{day} \cdot \text{atm})$] where commercial, biaxially stretched hot and oriented EVAL offer transport values of $1 \pm 0.005 \text{ cm}^3 \cdot 20 \mu\text{m}/(\text{m}^2 \cdot \text{day} \cdot \text{atm})$. Note that these values are far superior to those obtained for TCHS and reflect the length (~1.8 nm) and rigidity of the tethers that join the vertices of two cubes.^{18,19}

We also measured the barrier properties of analogous OAPS/ODPA films, which also exhibited barrier properties directly related to the degree of curing. Again, while cast OAPS/ODPA samples could not be heated directly to ≥ 225 °C without cracking, samples cured step-wise to that temperature showed barrier properties [$25 \text{ cm}^3 \cdot 20 \mu\text{m}/(\text{m}^2 \cdot \text{day} \cdot \text{atm})$] competitive with commercial PVA films [$20 \text{ cm}^3 \cdot 20 \mu\text{m}/(\text{m}^2 \cdot \text{day} \cdot \text{atm})$]⁴² but offering air stability to 550 °C when fully cured. In contrast, the decomposition temperatures of PVA films are very close to their melting temperatures (between 150 °C and 250 °C), which in turn are dependent on the degree of hydrolysis.⁴³

In order to make the films more flexible with the goal of curing to higher temperatures, we introduced ODA (Figure 3.4) as a diluent in the OAPS/ODPA systems. Reactions of equal stoichiometric amounts of OAPS and ODPA with ODA gave films that were much less brittle than undiluted films, with comparable oxygen permeabilities [$29 \text{ cm}^3 \cdot 20 \mu\text{m}/(\text{m}^2 \cdot \text{day} \cdot \text{atm})$ for OAPS/ODPA/ODA and $25 \text{ cm}^3 \cdot 20 \mu\text{m}/(\text{m}^2 \cdot \text{day} \cdot \text{atm})$ for OAPS/ODPA] under identical curing conditions (120 °C /4 h, 205 °C /4 h, 225 °C/8 h, 225 °C/8 h).

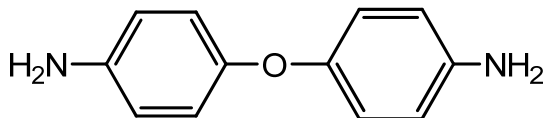


Figure 3.4. Chemical structure of oxydianiline (ODA).

As **Table 3.1** shows, the use of ODA gives essentially the same barrier performance. However, the resulting films are qualitatively more flexible and also could be cured to somewhat higher temperatures (240 °C) before fracturing.

3.3.1.3 Epoxy Resin Films

The bulk of our study focused on OAPS/epoxy resin systems, since they offer access to films with very high cross-link densities in addition to strong hydrogen bonding, as well as the incorporation of an inorganic silica core. Figure 3.3 provides a complete list of epoxy compounds studied and their structures.

The flexibility of OAPS/epoxy films also depended on cure times and temperatures. In general, OAPS/TGMX films were more flexible compared to other epoxide films cured under similar conditions. All of the transparent films were colored from light yellow to dark orange. OTR values for OAPS/epoxy films exhibited the best properties of all the cast films studied, with OAPS/ECHX (100°C/1 h, 130°C/4 h, 180 °C/4 h) exhibiting the lowest OTR [$6 \text{ cm}^3 \cdot 20 \mu\text{m}/(\text{m}^2 \cdot \text{day} \cdot \text{atm})$] observed.

Again, barrier properties generally improved at higher temperatures and longer cure times. For example, O_2 permeability for OAPS/DGEBA (130 °C/5h) falls from 110 to $21 \text{ cm}^3 \cdot 20 \mu\text{m}/(\text{m}^2 \cdot \text{day} \cdot \text{atm})$ when heated for 5 h more at 150 °C. In addition, these films also benefit from the heat capacity of the silica framework and the ability of the cube to control polymer (tether) chain motion at elevated temperatures. For example, the $T_{d5\%}$ of OAPS/DGEBA is 180 °C, compared to 165 °C for DGEBA alone. However, RDGE films did not offer the same barrier performance as ECHX, DGEBA, or TGMX. While it can be predicted that higher temperature curing may be necessary to reduce the O_2 permeability of OAPS/RDGE films, these films could not be heat treated higher than 115

°C without cracking. Since the epoxide functionalities of RDGE are *meta* to each other across the aromatic ring and because the separation (by measuring number of bonds) between them is relatively short compared to DGEBA and TGMX, there might not be enough flexibility in the tethers to limit cracking as the films cure. However, the ability of the ECHX cyclohexyl epoxides to adopt flexible chair conformations could explain why OAPS/ECHX films do not crack under similar curing conditions to those used for OAPS/RDGE.

We also manipulated the ratio “N” (NH₂ groups : epoxide groups) in OAPS/epoxide films to measure the effects on OTR values. In general, a lower N value led to improved OTR performance, which corresponds to an increase in cross-link density. The materials with N = 1.0 and N = 0.5 stoichiometries are most important here because these are the ratios that can give perfectly matched curing to form one or two cross-links per each vertex, respectively. For example, OAPS/ECHX impermeability improves from 24 to 8 cm³·20 μm/(m²·day·atm) under the same conditions (100 °C/1 h, 130 °C/4 h) when the N ratio is changed from 1.0 to 0.5, respectively.

3.3.2 Warm-Pressed Films

While ‘cube’ films exhibit excellent barrier properties when cast from solution, warm pressing dramatically lowers the OTR of the OAPS/imide and epoxide films, see **Table 3.2**. Initially the films are pre-cured (**Table 3.2**) to remove solvent and then cured under pressure between heated platens (see experimental details). Note that the **Table 3.2** conditions represent maximum temperatures and loads during curing; higher temperatures and pressures cause films to crack.

There is significant improvement in the barrier properties of both OAPS/imide and epoxide systems when cured under pressure. It is reasonable to assume that heating under pressure eliminates voids and pores resulting from residual solvent eliminated in the pre-curing step.

Table 3.2. Oxygen Transmission Rates (OTR) of heat-pressed silsesquioxane films. [$@ 20\text{ }^{\circ}\text{C}$ and 65% RH; $\text{cm}^3 \cdot 20\text{ }\mu\text{m} / (\text{m}^2 \cdot \text{day} \cdot \text{atm}) - \text{O}_2$, i.e. standardized to $20\text{ }\mu\text{m}$ thickness]

Sample	N NH ₂ groups : Epoxide groups	Initial Curing	Curing w/Pressure	OTR (± 0.5) ($\text{cm}^3 \cdot 20$ $\mu\text{m}/\text{m}^2 \cdot \text{day} \cdot \text{atm}$)
50% OAPS/PMDA	--	120 °C /4 h	240 °C/8 h @ 1.03 MPa	17
50% OAPS/ODPA	--	120 °C /4 h	240 °C/8 h @ 1.03 MPa	12
50% OAPS/ODPA/ODA	--	120 °C /4 h	240 °C/8 h @ 1.03 MPa	13
OAPS/DGEBA	0.5	120 °C /4 h	200 °C /10 h @ 0.690 MPa	7
OAPS/DGEBA	0.5	120 °C /4 h	200 °C /10 h @ 0.862 MPa	5
OAPS/DGEBA	0.5	120 °C /4 h	200 °C /10 h @ 1.03 MPa	3.9
OAPS/TGMX	0.5	100 °C/1 h, 130 °C/4 h	200 °C/4 h @ 1.03 MPa	3.2
OAPS/ECHX	0.5	100 °C/1 h, 130 °C/4 h	200 °C/4 h @ 1.03 MPa	5.2
OAPS/TGMX	0.5	100 °C/1 h, 130 °C/4 h	200 °C/4 h @ 1.03 MPa	1.2
OAPS/ECHX (i) & OAPS/TGMX (ii) Bilayer	0.5 0.5	i. 100 °C/1 h, 130 °C/4h ii. 100 °C/1 h, 130 °C/4h	iii. 200 °C/4 h @ 1.03 MPa	0.8

This is not unexpected given that it is known that a combination of heat treatment and orientation will improve gas barrier properties in ordinary polymer films, but improvement by orientation alone without heat treatment is usually marginal.⁴³ This suggests that thermal treatment of film systems has a direct influence on chain-chain ordering (crystallinity), which determines the performance of barrier films. Heat treatment under pressure may allow the cubes and tethers to order under conditions where they usually do not crystallize. Future powder XRD studies could elucidate whether or not this is the case.

The improvement in the polyimide films was significant, but not as dramatic as for the epoxide systems. The OTR of OAPS/TGMX films, for example, drops from 14 (as cast) to 3.2 when cured at 1.03 MPa. Warm pressing reduces the propensity of films to crack permitting higher cure temperatures. In addition, the curing times for all systems are shortened without sacrifice to barrier performance.

A bilayer of OAPS/TGMX and OAPS/ECHX film cured under pressure exhibits the best OTR of the cube films, $1.2\text{ cm}^3 \cdot 20\text{ }\mu\text{m}/(\text{m}^2 \cdot \text{day} \cdot \text{atm})$. We have obtained values as low as $\approx 0.8\text{ cm}^3 \cdot 20\text{ }\mu\text{m}/(\text{m}^2 \cdot \text{day} \cdot \text{atm})$ for this same system, but are hindered by the

detection limits of our instrumentation and thus these systems may actually be better than we are currently able to report. The transparent dark purple bilayer film offers excellent adhesion between the layers. Unfortunately efforts to form OAPS/DGEBA bilayers with OAPS/TGMX or OAPS/ECHX were not possible due to delamination after curing. More work and the possibility of making tri and tetra-layer films offers further potential to improve barrier properties. In addition, it may be possible to spray coat the individual layers since these materials will cure near room temperature.⁴⁴

3.3.3 Temperature Dependence

The dependence of OTR on temperature was investigated for OAPS/TGMX and OAPS/ODPA (Figure 3.5), as they represent the most flexible epoxy and imide films that still maintain excellent barrier properties.

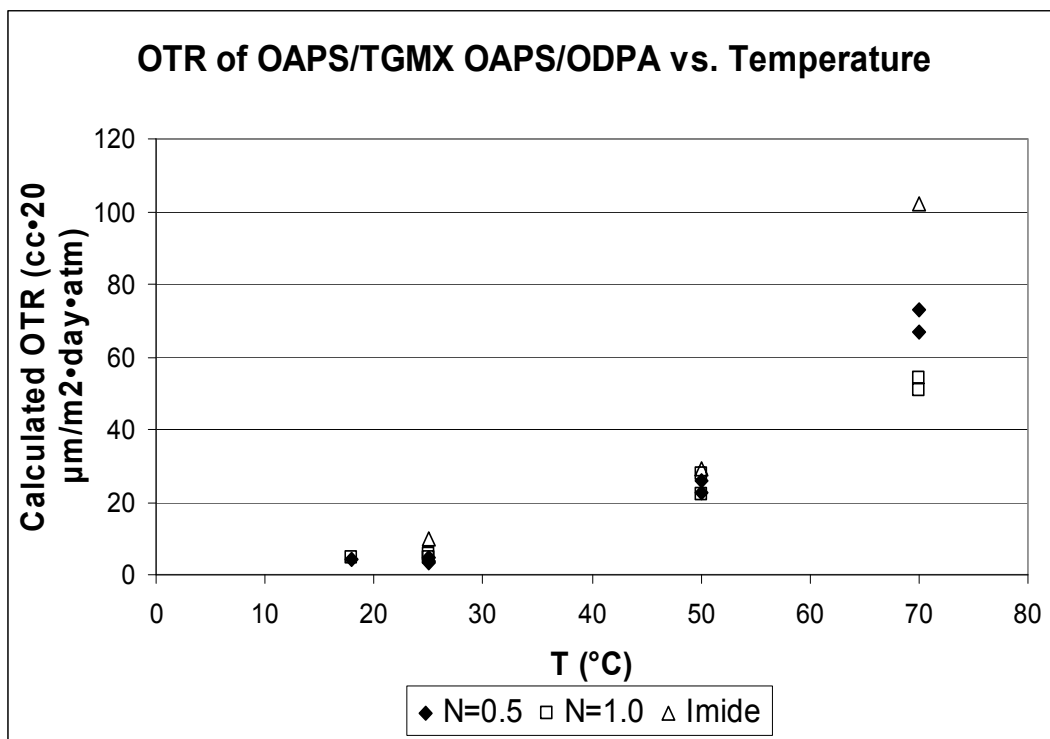


Figure 3.5. OTR vs. Temperature. OAPS/TGMX (100 °C/1 h, 200 °C/4 h @ 1.03MPa) and OAPS /ODPA (120 °C /4 h, 275 °C/8 h @ 1.03MPa). $E_a \approx 10 \pm 2$ kcal.

As expected, the permeability of each film increases at temperatures above room temperature due to increased molecular motion of polymer segments in these films even though they rarely exhibit significant T_g s. Conversely, at lower temperatures the decreased motion of these segments improves OTR. In addition, the temperature-dependent asymptotic decrease in permeability is also attributed to the corresponding decrease in kinetic energy of the permeating O_2 molecules at lower temperatures.⁴⁵

At room temperature, the majority of epoxide films with $N = 0.5$ exhibit better barrier performance while films with $N = 1.0$ perform better at higher temperatures. This suggests that the increased cross-link density for OAPS/TGMX films improves OTR but only at low temperatures. The decrease in barrier performance at elevated temperatures, however, may be attributed to both a significant increase in motion of the permeant gas and the organic tethers, which leads to increased O_2 transport. This suggests that a high degree of cross-linking is unfavorable since any significant increase in tether motion could lead to nano-sized cracks in the films.

At $N = 1.0$, the degree of cross-linking is essentially halved, and the film may be able to relieve any strain caused by motion via flexing at the molecular level. This strain relief may explain why polyimide films behave relatively poorly at elevated temperatures, due to the short length and rigidity of cross-linking units. At lower temperatures, however, increased cross-link density is not a problem due to both the decreased motion of the tethers and lower gas mobility.

Since increased cross-link density improves OTR performance at temperatures < 50 °C yet presents a liability at higher temperatures, it may be possible to tailor these films across a broad temperature range by maintaining maximum cross-link density with longer and somewhat more flexible epoxy tethers. Theoretically these systems should present the same barriers to oxygen permeation at lower temperatures while decreasing OTR at increased temperatures by flexing to avoid strain that leads to cracking. It could also lead to easier processing and perhaps the opportunity to align tethers through uniaxial or biaxial stretching.

3.4 Conclusions

We have found that OAPS/imide and OAPS/epoxide films exhibit excellent barrier properties, competitive with current commercial grade barrier films.⁴² While cast OAPS/ODPA and OAPS/ECHX epoxide films have promising OTRs of 25 and 6 $\text{cm}^3 \cdot 20 \mu\text{m}/(\text{m}^2 \cdot \text{day} \cdot \text{atm})$ (at optimum curing conditions), a significant improvement is achieved with warm pressing. A combination warm-pressed, bilayer film system consisting of OAPS/ECHX and OAPS/TGMX was found to have OTR of $< 1 \text{ cm}^3 \cdot 20 \mu\text{m}/(\text{m}^2 \cdot \text{day} \cdot \text{atm})$. It should be noted that commercial barrier films with similar performance are usually achieved with 3- or 4 different film layers and may utilize adhesives to keep the films together.⁴⁶

The structure of the organic tethers, as well as cross-link densities, determine O_2 permeability. Long and flexible organic tethers improve the film's overall flexibility, an important factor during warm pressing. While increasing cross-link density traditionally improves OTR, high cross-link density of short and stiff tethers leads either to cracking during curing or nano-sized cracks or more free volume at elevated temperatures for reasons stated above. At low temperatures, however, the movement of short and stiff tethers is minimized and high cross-link density improves OTR. We have determined that the ideal silsesquioxanes film would have a high cross-link density of long, flexible tethers, to achieve maximum performance at a wide range of temperatures.

Silsesquioxane films, particularly OAPS/imide and OAPS/epoxide films, provide excellent O_2 barrier properties potentially of use for a wide variety of packaging applications. The silsesquioxanes films can in principle be further functionalized to tailor barrier properties or for selected transport of specific gases for separation applications. It was recently demonstrated both theoretically and experimentally that silsesquioxanes offer higher barriers to N_2 diffusion than O_2 .⁴⁰ They also offer high thermal stability of potential use in high temperature applications such as electronics packaging.

Note that our results contrast considerably with polysiloxane films, which are well known to have high oxygen permeabilities [$>19,000 \text{ cm}^3 \cdot 20 \mu\text{m}/(\text{m}^2 \cdot \text{day} \cdot \text{atm})$] due to the high degree of chain flexibilities.⁴⁴ Consequently, our results again support the utility of

using nanoscale tailoring with nanoscopic silsesquioxane units to closely control global properties.

3.5 References

1. Kamat, P.V. *J. Phys. Chem. B.* **2002**, *106*, 7729.
2. Champion Y.; H.-J. Fecht Eds. *Nano-Architected and Nanostructured Materials: Fabrication, Control and Properties*; Wiley-VCH: Weinheim, 2005.
3. Wang, Z.L.; Liu, Y.; Zhang, Z. Eds. *Handbook of Nanophase and Nanostructured Materials, Vol 3. Materials Systems and Applications*; Kluwer Academic/Plenum Publ: New York, 2002.
4. Shen, Y.; Friend, C.S.; Jiang, Y.; Jakubczyk, D.; Swiatkiewicz, J.; Prasad, P.N. *J. Phys. Chem. B.* **2000**, *104*, 7577.
5. Davis, M.E.; Katz, A.; Ahmad, W.R. *Chem. Mater.* **1996**, *8*, 1820.
6. Moriarty, P. *Rep. Prog. Phys.* **2001**, *64*, 297.
7. Voronkov, M.G.; Lavrent'yev, V.I. *Top. Curr. Chem.* **1982**, *102*, 199.
8. Baney, R.H.; Itoh, M.; Sakakibara, A.; Suzuki, T. *Chem. Rev.* **1995**, *95*, 1409.
9. Lichtenhan, J. In *Polymeric Materials Encyc.*; Salmone, J.C. Ed.; Vol. 10; CRC Press: New York, NY, 1996; pp 7768-7777.
10. Provatas, A.; Matisons, J.G. *Trends Polym. Sci.* **1997**, *5*, 327.
11. Laine, R.M. *J. Mater. Chem.* **2005**, *15*, 3725.
12. Sellinger, A.; Laine, R.M. *Macromolecules* **1996**, *29*, 2327.
13. Sellinger, A.; Laine, R.M. *Chem. Mater.* **1996**, *8*, 1592.
14. Zhang, C.; Laine, R.M. *J. Organomet. Chem.* **1996**, *521*, 199.
15. Zhang, C.; Babonneau, F.; Bonhomme, C.; Laine, R.M.; Soles, C.L.; Hristov, H.A.; Yee, A.F. *J. Am. Chem. Soc.* **1998**, *120*, 8380.
16. Zhang, C.; Laine R.M. *J. Am. Chem. Soc.* **2000**, *122*, 6979.
17. Tamaki, R.; Tanaka, Y.; Asuncion, M.Z.; Choi, J.; Laine, R.M. *J. Am. Chem. Soc.* **2001**, *123*, 12416.
18. Tamaki, R.; Choi, J.; Laine, R.M. *Chem. Mater.* **2003**, *15*, 793.

19. Choi, J.; Tamaki, R.; Kim, S.G.; Laine, R.M. *Chem. Mater.* **2003**, *15*, 3365.
20. Laine, R.M.; Choi, J.; Lee, I. *Adv. Mater.* **2001**, *13*, 800.
21. Choi, J.; Yee, A.F.; Laine, R.M. *Macromolecules* **2003**, *15*, 5666.
22. Sulaiman, S.; Brick, C.M.; De Sana, C.M.; Katzenstein, J.M.; Laine, R.M.; Basheer, R.A. *Macromolecules* **2006**, *39*, 5167.
23. Kim, G.M.; Qin, H.; Fang, X.; Sun, F.C.; Mather, P.T. *J. Polym. Science: Part B: Polym. Phys.*, **2003**, *41*, 3299.
24. Ramirez, C.; Abad, M.J.; Barral, L.; Cano, J.; Diez F.J.; Lopez, F.J.; Montes, R.; Polo, J. *J. Therm. Analysis and Calorimetry* **2003**, *72*, 421.
25. Leu, C-M.; Chang, Y-T.; Wei, K-H. *Chem. Mater.* **2003**, *15*, 3721.
26. Seino, M.; Kawakami, Y. *Poly. J.* **2004**, *36*, 422.
27. Huang, J.C.; Xiao, Y.; Mya, K.Y.; Liu, X.M.; He, C.B.; Dai, J.; Siow, Y.P. *J. Mater. Chem.* **2004**, *14*, 2858.
28. Zheng, L.; Farris, R.J.; Coughlin, E.B. *Macromolecules* **2001**, *34*, 8034.
29. Neumann, D.; Fisher, M.; Tran, L.; Matison, J.G. *J. Am. Chem. Soc.* **2002**, *124*, 13998.
30. Pittman, C.U.; Li, G.Z.; Ni, H. *Macromolecules Symp.* **2003**, *196*, 301.
31. Camper, D.; Bara, J.; Koval, C.; Noble, R. *Ind. Eng. Chem. Res.* **2006**, *45*, 6279 and references therein.
32. Van der Bruggen, B.; Jansen, J.C.; Figoli, A.; Geens, J.; Van Baelen, D.; Drioli, E.; Vandecasteele, C. *J. Phys. Chem. B* **2004**, *108* 13273 and references therein.
33. Ha, S.Y.; Park, H.B.; Lee, Y.M. *Macromolecules* **1999**, *32*, 2394 and references therein.
34. Okahata, Y.; Shimizu, A. *Langmuir* **1989**, *5*, 954.
35. Nishide, H.; Tsukahara, Y.; Tsuchida, E. *J. Phys. Chem. B.* **1998**, *102*, 8766.
36. Wilson, M.A.; Pohorille, A. *J. Am. Chem. Soc.* **1996**, *118*, 6580.
37. Solovyov, S.E. *J. Phys. Chem. B.* **2006**, *110*, 17977.

38. Sweeny, R.F.; Rose, A. *I & EC Product Res. and Development* **1965**, 4, 248.
39. Abe, A.; Albertsson, A.-C.; Duncan, R.; Dusek, K.; Jeu, W.H.d.; Joanny, J.F.; Kausch, H.-H.; Kobayashi, S.; Lee, K.-S.; Leibler, L.; Long, T.E.; Manners, I.; Möller, M.; Nuyken, O.; Terentjev, E.M.; Voit, B.; Wegner, G.; Wiesner, U. *Inorganic Polymeric Nanocomposites and Membranes. Advances in Polymer Science*, 179; Springer: Berlin, Heidelberg, New York, 2005.
40. Tejerina, B.; Gordon, M.S. *J. Phys. Chem. A* **2002**, 106, 11764.
41. Takamura, N.; Viculis, L.; Zhang, C; Laine, R.M submitted to *Macromolecules*.
42. Eval Americas Technical Bulletin No. 110 *Barrier Properties of EvalTM Resins* (2000).
43. Mark, J.E. Ed. *Physical Properties of Polymers Handbook 2nd Ed. AIP Series in Polymers and Complex Materials*; AIP Press: Woodbury, NY, 1996.
44. Laine, R.M.; Roll, M.; Asuncion, M.Z.; Sulaiman, S.; Popova, V.; Bartz, D.; Krug, D.J.; Mutin, P.H. *J. Sol-Gel Sci. Tech.* **2008**, 46, 335.
45. Hong, S.-I.; Krochta, J.M. *Journal of Food Engineering* **2006**, 77, 739.
46. Massey, L.K. *Permeability Properties of Plastics and Elastomers - A Guide to Packaging and Barrier Materials (2nd Edition)*; William Andrew Publishing/Plastics Design Library: Norwich, NY, 2003.

Chapter 4

Octalkynylsilsesquioxanes, Nano Sea Urchin Molecular Building Blocks for 3-D-Nanostructures

The design and construction of 3-D molecular scaffolds is currently an area of extreme interest for a variety of reasons including hydrogen storage, gas separation and molecular sieving. Octahedral silsesquioxanes, $[\text{RSiO}_{1.5}]_8$, represent a class of unusually robust, nanometer size molecules with cubic symmetry that places each functional group in a different octant in Cartesian space. This 3-D array of functional groups offers the potential to design nanobuilding blocks to construct multifunctional, nanocomposite materials including molecular scaffolds. We describe here detailed studies on the synthesis of octaalkyne silsesquioxanes using Sonogashira coupling of octaiodophenyl-silsesquioxane, $[p\text{-IC}_6\text{H}_4\text{SiO}_{1.5}]_8$ (I_8OPS) and a related bromine derivative with terminal alkynes. We describe versatile and reliable methods for synthesizing octaalkyne silsesquioxanes in moderate to high yields with 100% conversion of the I_8OPS to the octaalkynes. The inorganic core provides 3-D rigidity and the heat capacity of crystalline SiO_2 making them quite robust in many environments. The alkyne “spines” provide excellent solubility in organic solvents and the ability to polymerize on heating, to form robust 3-D polyalkyne networks with air stabilities to $>500\text{ }^\circ\text{C}$ suggesting potential utility as matrix materials for high temperature composites. With appropriate functionality on the external point of the spine, all of these molecules should also serve as 3-D connection points for the construction of molecular scaffolds.

4.1 Introduction

The design and construction of 3-D molecular scaffolds is currently an area of extreme interest for a variety of reasons including hydrogen storage, gas separation and molecular sieving, for molecular recognition, non-linear optical properties, synthesis of hyperbranched and dendrimeric species, protection and stabilization of catalytic sites, the creation of well-defined arrays of addressable functional groups for computational purposes, and for micromechanical devices, etc.¹⁻¹⁴ Extensive work has been devoted to developing rigid rod components for molecular scaffolds,^{1,2} and through the use of transition metal centers there are now extensive sets of work on developing connection points for these rigid rods.³⁻⁸ To date, however, very little work has been directed towards developing connection points with symmetry higher than tetrahedral.^{1,2,4} To our knowledge there are no components that provide connection points with cubic symmetry although the potential utility of cubane materials as difunctional connection points has been described.¹

Part of the problem lies in the fact that aside from cubane, only one other easily accessible class of materials offers perfect cubic symmetry, the cubic silsesquioxanes.⁹⁻¹⁵ We have recently developed a synthetic route to $[p\text{-I-C}_6\text{H}_4\text{SiO}_{1.5}]_8$,¹⁶ with the pure octasubstituted isomer isolated in $\geq 40\%$ yields (at scales of 100 g of starting material) following recrystallization and where iodide substitution is reproducibly $\geq 93\%$ para offering the potential to create cubic connection points for 3-D molecular scaffolds. Given the considerable interest in using alkyne and oligoalkyne rods as the bridging components in such scaffolds, we have undertaken to develop synthetic routes to a number of alkynes some of which offer potential as octafunctional, cubic connection points. These same systems polymerize on heating to generate materials that exhibit very high temperature oxidative stability offering the potential to serve as composite matrix materials.

4.2 Experimental

4.2.1 Materials

Dioxane was purchased from Fisher and distilled under N₂ prior to use. Octa(iodophenyl)silsesquioxane was synthesized according to recently published methods.¹⁶ All other chemicals were purchased from Fisher or Aldrich and used as received. All work was performed under nitrogen unless otherwise stated.

4.2.2 Synthetic Methods

4.2.2.1 Sonogashira Coupling of Br_{5,3}OPS and Phenylacetylene

To a dry 50 mL Schlenk flask under N₂ and equipped with a magnetic stir bar was added 0.500 g of Br_{5,3}OPS (1.83 mmol Br), CuI (18.2 mg, 0.096 mmol, 5%), Pd₂(dba)₃ (22.08 mg, 0.048 mmol), bis(tri-*tert*-butylphosphine)-palladium(0) (24.5 mg, 0.096 mmol), 5.0 mL 1,4 dioxane (previously distilled under N₂), 0.36 mL (2.6 mmol) of triethylamine, and phenylacetylene (0.21 mL, 1.8 mmol). The solution was stirred at 25 °C for 48 h, during which time it turned dark gray-brown. The mixture was poured into excess methanol to deactivate the catalyst. Volatiles were removed by rotary evaporation. The residue was dissolved in 5.0 mL of ethyl acetate, filtered through celite, and precipitated into 100 mL of methanol. The light orange powder was collected by filtration and dried in vacuo for 5 h, giving 0.418 g (90%). Characterization data: TGA (air, 1000 °C): Found 25.4%; Calculated 27.0%; T_{d5%} 518 °C. GPC: M_n 1349; M_w 1538; PDI 1.14.

4.2.2.2 Sonogashira Coupling of Br_{5,3}OPS and 4-Ethynyltoluene

To a dry 50 mL Schlenk flask under N₂ and equipped with a magnetic stir bar was added 0.500 g of Br_{5,3}OPS (1.83 mmol Br), CuI (18.2 mg, 0.096 mmol, 5%), Pd₂(dba)₃

(22.08 mg, 0.048 mmol), bis(tri-*tert*-butylphosphine)-palladium(0) (24.5 mg, 0.096 mmol), 5.0 mL 1,4 dioxane (previously distilled under N₂), 0.36 mL (2.6 mmol) of triethylamine, and 4-Ethynyltoluene (0.23 mL, 1.8 mmol). The solution was stirred at 25 °C for 48 h, during which time it turned dark gray-brown. The mixture was poured into excess methanol to deactivate the catalyst. Volatiles were removed by rotary evaporation. The residue was dissolved in 5.0 mL of ethyl acetate, filtered through celite, and precipitated into 100 mL of methanol. The light orange powder was collected by filtration and dried in vacuo for 5 h, giving 0.421 g (86%). Characterization data: TGA (air, 1000 °C): Found 22.5%; Calculated 25.4%; T_{d5%} 482 °C. GPC: M_n 1575; M_w 1654; PDI 1.09.

4.2.2.3 Sonogashira Coupling of Br_{5,3}OPS and 4-Ethynylanisole

To a dry 50 mL Schlenk flask under N₂ and equipped with a magnetic stir bar was added 0.500 g of Br_{5,3}OPS (1.83 mmol Br), CuI (18.2 mg, 0.096 mmol, 5%), Pd₂(dba)₃ (22.08 mg, 0.048 mmol), bis(tri-*tert*-butylphosphine)-palladium(0) (24.5 mg, 0.096 mmol), 5.0 mL 1,4 dioxane (previously distilled under N₂), 0.36 mL (2.6 mmol) of triethylamine, and 4-Ethynylanisole (0.24 mL, 1.8 mmol). The solution was stirred at 25 °C for 48 h, during which time it turned dark gray-brown. The mixture was poured into excess methanol to deactivate the catalyst. Volatiles were removed by rotary evaporation. The residue was dissolved in 5.0 mL of ethyl acetate, filtered through celite, and precipitated into 100 mL of methanol. The light orange powder was collected by filtration and dried in vacuo for 5 h, giving 0.451 g (87%). Characterization data: TGA (air, 1000 °C): Found 21.2%; Calculated 23.8%; T_{d5%} 502 °C. GPC: M_n 1643; M_w 1791; PDI 1.15.

4.2.2.4 Sonogashira Coupling of Br_{5,3}OPS and 4-Ethynyl- α - α -trifluorotoluene

To a dry 50 mL Schlenk flask under N₂ and equipped with a magnetic stir bar was added 0.500 g of Br_{5,3}OPS (1.83 mmol Br), CuI (18.2 mg, 0.096 mmol, 5%), Pd₂(dba)₃ (22.08 mg, 0.048 mmol), bis(tri-*tert*-butylphosphine)-palladium(0) (24.5 mg, 0.096

mmol), 5.0 mL 1,4 dioxane (previously distilled under N₂), 0.36 mL (2.6 mmol) of triethylamine, and 4-Ethynyl- α - α -trifluorotoluene (0.25 mL, 1.8 mmol). The solution was stirred at 25 °C for 48 h, during which time it turned dark gray-brown. The mixture was poured into excess methanol to deactivate the catalyst. Volatiles were removed by rotary evaporation. The residue was dissolved in 5.0 mL of ethyl acetate, filtered through celite, and precipitated into 100 mL of methanol. The light orange powder was collected by filtration and dried in vacuo for 5 h, giving 0.376 g (64%). Characterization data: TGA (air, 1000 °C): Found 22.5%; Calculated 20.7%; T_{d5%} 417 °C. GPC: M_n 1761; M_w 2132; PDI 1.21.

4.2.2.5 Sonogashira Coupling of Br_{5,3}OPS and Trimethylsilylacetylene

To a dry 50 mL Schlenk flask under N₂ and equipped with a magnetic stir bar was added 0.500 g of Br_{5,3}OPS (1.83 mmol Br), CuI (18.2 mg, 0.096 mmol, 5%), Pd₂(dba)₃ (22.08 mg, 0.048 mmol), bis(tri-*tert*-butylphosphine)-palladium(0) (24.5 mg, 0.096 mmol), 5.0 mL 1,4 dioxane (previously distilled under N₂), 0.36 mL (2.6 mmol) of triethylamine, and Trimethylsilylacetylene (0.13 mL, 1.8 mmol). The solution was stirred at 25 °C for 48 h, during which time it turned dark gray-brown. The mixture was poured into excess methanol to deactivate the catalyst. Volatiles were removed by rotary evaporation. The residue was dissolved in 5.0 mL of ethyl acetate, filtered through celite, and precipitated into 100 mL of methanol. The light orange powder was collected by filtration and dried in vacuo for 5 h, giving 0.471 g (80%). Characterization data: TGA (air, 1000 °C): Found 17.8%; Calculated 27.5%; T_{d5%} 423°C. GPC: M_n 1045; M_w 1275; PDI 1.22.

4.2.2.6 Sonogashira Coupling of Br_{5,3}OPS and Methyl Propiolate

To a dry 50 mL Schlenk flask under N₂ and equipped with a magnetic stir bar was added 0.500 g of Br_{5,3}OPS (1.83 mmol Br), CuI (18.2 mg, 0.096 mmol, 5%), Pd₂(dba)₃ (22.08 mg, 0.048 mmol), bis(tri-*tert*-butylphosphine)-palladium(0) (24.5 mg, 0.096 mmol), 5.0 mL 1,4 dioxane (previously distilled under N₂), 0.36 mL (2.6 mmol) of

triethylamine, and Methyl Propriolate (0.15 mL, 1.8 mmol). The solution was stirred at 25 °C for 48 h, during which time it turned dark gray-brown. The mixture was poured into excess methanol to deactivate the catalyst. Volatiles were removed by rotary evaporation. The residue was dissolved in 5.0 mL of ethyl acetate, filtered through celite, and precipitated into 100 mL of methanol. The light orange powder was collected by filtration and dried *in vacuo* for 5 h, giving 0.242 g (56%). Characterization data: TGA (air, 1000 °C): Found 31.8%; Calculated 29.3%; $T_{d5\%}$ 398 °C. GPC: M_n 1110; M_w 1410; PDI 1.27.

4.2.2.7 Sonogashira Coupling of I₈OPS and Phenylacetylene

To a dry 50 mL Schlenk flask under N₂ and equipped with a magnetic stir bar under was added 0.5g I₈OPS (2.4 mmol I-Phenyl), 0.29 mL (2.6 mmol) phenylacetylene, 18.2 mg (0.096 mmol, 4%) CuI, 194 mg (0.168 mmol, 7%) tetrakis(triphenylphosphine)palladium(0), 5.0 mL 1,4 dioxane (previously distilled and degassed), and 0.808 mL (4.9 mmol) triethylamine. The solution was stirred at 60 °C for 24 hours. The solution turned dark gray-brown. The mixture was passed through a short celite column and poured into an excess of methanol to deactivate the catalyst. The resulting precipitate was collected by filtration. The residue was redissolved in 5.0 mL ethyl acetate and precipitated into 100 mL methanol. The light brown-orange powder was collected by filtration and dried *in vacuo* for 5 h, giving 0.403 g (90%). Characterization data: TGA (air, 1000 °C): Found 26.4%; Calculated 27.0%; $T_{d5\%}$ 526 °C. GPC: M_n 1112; M_w 1128; PDI 1.02.

4.2.2.8 Sonogashira Coupling of I₈OPS and 4-Ethynyltoluene

To a dry 50 mL Schlenk flask under N₂ and equipped with a magnetic stir bar under was added 0.5g I₈OPS (2.4 mmol I-Phenyl), 0.33 mL (2.6 mmol) 4-Ethynyltoluene, 18.2 mg (0.096 mmol, 4%) CuI, 194 mg (0.168 mmol, 7%) tetrakis(triphenylphosphine)palladium(0), 5.0 mL 1,4 dioxane (previously distilled and degassed), and 0.808 mL (4.9 mmol) triethylamine. The solution was stirred at 60 °C for

24 hours. The solution turned dark gray-brown. The mixture was passed through a short celite column and poured into an excess of methanol to deactivate the catalyst. The resulting precipitate was collected by filtration. The residue was redissolved in 5.0 mL ethyl acetate and precipitated into 100 mL methanol. The light brown-orange powder was collected by filtration and dried *in vacuo* for 5 h, giving 0.423 g (89%). Characterization data: TGA (air, 1000 °C): Found 24.5%; Calculated 24.7%; $T_{d5\%}$ 475 °C. GPC: M_n 1150; M_w 1165; PDI 1.01.

4.2.2.9 Sonogashira Coupling of I₈OPS and 4-Ethynylanisole

To a dry 50 mL Schlenk flask under N₂ and equipped with a magnetic stir bar under was added 0.5g I₈OPS (2.4 mmol I-Phenyl), 0.34 mL (2.6 mmol) 4-Ethynylanisole, 18.2 mg (0.096 mmol, 4%) CuI, 194 mg (0.168 mmol, 7%) tetrakis(triphenylphosphine)palladium(0), 5.0 mL 1,4 dioxane (previously distilled and degassed), and 0.808 mL (4.9 mmol) triethylamine. The solution was stirred at 60 °C for 24 hours. The solution turned dark gray-brown. The mixture was passed through a short celite column and poured into an excess of methanol to deactivate the catalyst. The resulting precipitate was collected by filtration. The residue was redissolved in 5.0 mL ethyl acetate and precipitated into 100 mL methanol. The light brown-orange powder was collected by filtration and dried *in vacuo* for 5 h, giving 0.456 g (90%). Characterization data: TGA (air, 1000 °C): Found 22.6%; Calculated 23.8%; $T_{d5\%}$ 508 °C. GPC: M_n 1327; M_w 1346; PDI 1.01.

4.2.2.10 Sonogashira Coupling of I₈OPS and 4-Ethynyl- α - α - α -trifluorotoluene

To a dry 50 mL Schlenk flask under N₂ and equipped with a magnetic stir bar under was added 0.5g I₈OPS (2.4 mmol I-Phenyl), 0.36 mL (2.6 mmol) 4-Ethynyl- α - α - α -trifluorotoluene, 18.2 mg (0.096 mmol, 4%) CuI, 194 mg (0.168 mmol, 7%) tetrakis(triphenylphosphine)palladium(0), 5.0 mL 1,4 dioxane (previously distilled and degassed), and 0.808 mL (4.9 mmol) triethylamine. The solution was stirred at 60 °C for 24 hours. The solution turned dark gray-brown. The mixture was passed through a short

celite column and poured into an excess of methanol to deactivate the catalyst. The resulting precipitate was collected by filtration. The residue was redissolved in 5.0 mL ethyl acetate and precipitated into 100 mL methanol. The light brown-orange powder was collected by filtration and dried *in vacuo* for 5 h, giving 0.406 g (70%). Characterization data: TGA (air, 1000 °C): Found 21.7%; Calculated 20.7%; $T_{d5\%}$ 423 °C. GPC: M_n 2017; M_w 2144; PDI 1.15.

4.2.2.11 Sonogashira Coupling of I₈OPS and Trimethylsilylacetylene

To a dry 50 mL Schlenk flask under N₂ and equipped with a magnetic stir bar under was added 0.5g I₈OPS (2.4 mmol I-Phenyl), 0.184 mL (2.6 mmol) Trimethylsilylacetylene, 18.2 mg (0.096 mmol, 4%) CuI, 194 mg (0.168 mmol, 7%) tetrakis(triphenylphosphine)palladium(0), 5.0 mL 1,4 dioxane (previously distilled and degassed), and 0.808 mL (4.9 mmol) triethylamine. The solution was stirred at 60 °C for 24 hours. The solution turned dark gray-brown. The mixture was passed through a short celite column and poured into an excess of methanol to deactivate the catalyst. The resulting precipitate was collected by filtration. The residue was redissolved in 5.0 mL ethyl acetate and precipitated into 100 mL methanol. The light brown-orange powder was collected by filtration and dried *in vacuo* for 5 h, giving 0.406 g (81%). Characterization data: TGA (air, 1000 °C): Found 27.6%; Calculated 27.5%; $T_{d5\%}$ 418 °C. GPC: M_n 1050; M_w 1098; PDI 1.02.

4.2.2.12 Sonogashira Coupling of I₈OPS and Methyl Propriolate

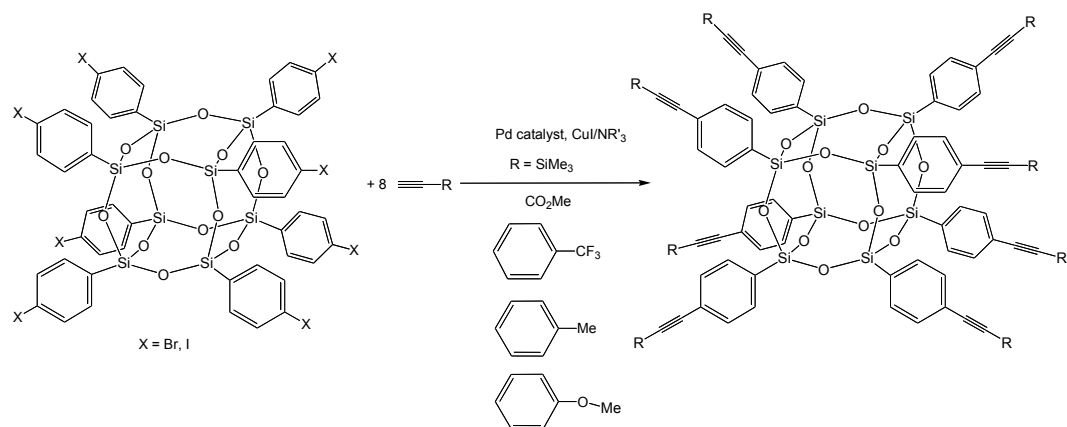
To a dry 50 mL Schlenk flask under N₂ and equipped with a magnetic stir bar under was added 0.5g I₈OPS (2.4 mmol I-Phenyl), 0.215 mL (2.6 mmol) Methyl Propriolate, 18.2 mg (0.096 mmol, 4%) CuI, 194 mg (0.168 mmol, 7%) tetrakis(triphenylphosphine)palladium(0), 5.0 mL 1,4 dioxane (previously distilled and degassed), and 0.808 mL (4.9 mmol) triethylamine. The solution was stirred at 60 °C for 24 hours. The solution turned dark gray-brown. The mixture was passed through a short celite column and poured into an excess of methanol to deactivate the catalyst. The

resulting precipitate was collected by filtration. The residue was redissolved in 5.0 mL ethyl acetate and precipitated into 100 mL methanol. The light brown-orange powder was collected by filtration and dried *in vacuo* for 5 h, giving 0.276 g (67%). Characterization data: TGA (air, 1000 °C): Found 29.3%; Calculated 29.3%; T_{d5%} 403 °C. GPC: M_n 1101; M_w 1123; PDI 1.02.

4.3 Results and Discussion

The objectives of the current study are to develop molecular “sea urchins,” molecules that have alkyne groups pointing to each octant in Cartesian space (cubic symmetry). Such structures offer the opportunity to build 3-D molecular scaffolds by serving as connection points, especially for example the trimethylsilyl compound which can be expected to be susceptible to facile proto-desilylation providing a point for further elaboration.¹⁷ In addition, reaction of the alkyne groups with perphenylcyclopentadienones can be expected to provide access to 3-D graphene like structures akin to the novel 2-D structures developed by the Mullen group over the last decade.¹⁸ Finally, alkyne monomers are known to undergo polymerization to provide novel, high temperature matrix materials for high strength, carbon fiber-reinforced composite materials for aerospace applications.¹⁹ A further possible application of these materials is as starting points for the synthesis of robust 3-D star networks of polyacetylenes.²⁰

Our initial approach focused on using Br_{5,3}OPS as the substrate for alkylation via Pd catalyzed Sonogashira reactions.²¹ Unfortunately the complex substitution patterns found for Br_{5,3}OPS were not conducive to producing highly symmetrical products. In addition, this approach suffered other problems as noted below. Thus with the successful synthesis of very pure *p*-I₈OPS, we switched to this substrate for more extensive efforts (Scheme 4.1).



Scheme 4.1. Synthesis of octaalkyne silsesquioxane via Br_{5,3}OPS and I₈OPS.

4.3.1 Sonogashira Reactions from Br_{5,3}OPS

Both I₈OPS and the previously reported²⁰ Br_{5,3}OPS were reacted with various terminal acetylenes (**Table 4.1**) under slightly different conditions with different Pd catalysts (see Experimental Section). A catalyst system containing bis(*tri-tert*-butylphosphine)-palladium(0) and Pd₂(dba)₃ was employed for Br_{5,3}OPS because previous work showed that this system catalyzed both Heck and Sonogashira reactions from aryl bromides at ambient temperature, exclusive of unwanted side polymerizations associated with higher temperature reaction conditions.²¹

Table 4.1. Alkyne product yields, conversions, and GPC data from Br_{5,3}OPS²¹ and I₈OPS.¹⁶

Acetylene	Br _{5,3} OPS				I ₈ OPS				Ceramic Yield (Theory)
	Yield (%) [†]	%Conv. [*] (NMR)	GPC PDI	Ceramic Yield	Yield (%) [†]	%Conv. [*] (NMR)	GPC PDI	Ceramic Yield	
Phenylacetylene	90	n/a	1.14	25.4%	90	n/a	1.02	26.4%	27.0%
4-Ethynyltoluene	86	130	1.09	22.5%	89	>99	1.01	24.5%	25.4%
4-Ethynylanisole	87	130	1.15	21.2%	90	>99	1.01	22.6%	23.8%
4-Ethynyl- α,α,α -trifluorotoluene	64	120	1.21	22.5%	70	>99	1.15	21.1%	20.7%
Trimethylsilyl-acetylene	80	110	1.23	17.8%	81	>99	1.02	27.6%	27.5%
Methylpropiolate	56	110	1.23	17.8%	67	>99	1.02	29.3%	29.3%

[†] Isolated yield calculated relative to complete conversion of aryl halide. ^{*} Conversion calculated as ratio of aromatic to non-aromatic protons in ¹H NMR compared to the theoretical ratio.

Br_{5.3}OPS was used as the starting aryl halide since “octa-functional” Br₈OPS is actually a mixture of mono- and di-substituted isomers.²¹ The use of Br_{5.3}OPS ensures that the majority (>97%) of the resulting products are mono-substituted and predominantly (40%) *p*-isomers.

Early attempts to synthesize *p*-alkynes from Br_{5.3}OPS resulted in the coincident formation of alkenyl bromides, as evidenced by characteristic alkenyl C-H peaks (\approx 6.5 ppm) present in the ¹H NMR of each sample. These peaks suggest that HBr byproduct adds across the alkyne triple bond, resulting in a C=C bond and a vinyl bromide that offers another site for further reaction. Multiple substitution products are reflected in greater-than-unity % conversions (determined by ¹H NMR as the ratio of aromatic to non-aromatic protons compared to the theoretical ratio) for alkyne products from Br_{5.3}OPS. Consequently, MALDI-TOF data collected for the reaction of Br_{5.3}OPS with 4-ethynyltoluene indicates an average degree of substitution of 7.5 whereas the starting material was only 5.3. Residues at 1000 °C in air, which indicate the SiO₂ content (ceramic yields) of the materials, are all lower than theory, indicating higher-than-expected substitution. Furthermore, the PDIs determined by GPC are somewhat broader than expected for typical octa-substituted cubic silsesquioxanes (which usually have very narrow polydispersities), and may signify the presence of asymmetrical, multiply-substituted products. Even when a deficiency of acetylene is used compared to the aryl-bromide (4 eq. acetylene: 5.3 eq. Ph-Br), the presence of multi-substituted products is detected by ¹H NMR and TGA.

In an effort to capitalize on such uncontrolled substitution, we attempted to create exhaustively substituted “hyperbranched” oligoalkynes. Thus, Br_{5.3}OPS was reacted with a 2:1 excess of phenylethyne under Sonogashira conditions. Unfortunately, attempts to obtain effective alkyne hyper-branching were unsuccessful, as determined by the TGA, the maximum degree of substitution was \approx 9 for Br_{5.3}OPS, regardless of additional addition of catalyst or alkyne.

Since Br_{5.3}OPS is a mixture of isomers with only 40% *p*-isomer and the remaining 61% a mixture of unsubstituted phenyl and *m*- and *o*-isomers, the resulting Sonogashira products are expected to be a mixture of isomers as well. This fact is reflected in the rather broad ¹H NMR signals for phenyl-CH₃ and phenyl-OCH₃ substituted alkynes.

Since highly symmetric octa-alkynes offer considerable potential for the reasons discussed above, the low symmetry of alkynes from Br_{5,3}OPS increases the probability of defects in higher ordered structures derived from them.

4.3.2 Sonogashira Reactions from I₈OPS

The problem of multiple substitution products and isomer mixtures was remedied by using I₈OPS as the starting aryl halide. Apart from the aryl-iodide being more reactive¹⁶ in Sonogashira and similar coupling reactions, I₈OPS is $\geq 93\%$ *p*-substituted and 99% octa-substituted after recrystallization, highly soluble in organic solvents and preparable in 100 g quantities.¹⁶ In theory, the use of highly symmetrical I₈OPS should lead selectively to symmetrical *p*-octa-alkynes, “sea urchin”-like molecules.

The catalyst system for alkynylation from I₈OPS was changed from (tri-*tert*-butylphosphine)-palladium(0)/Pd₂(dba)₃ to the less expensive (Ph₃P)₄Pd, due to the increased reactivity of the aryl iodide towards substitution. We found that heating the reaction mixture at 60 °C for 24 h drove the reactions to completion in the shortest possible time. As expected from aryl iodides, I₈OPS is so reactive towards substitution that $\approx 70\%$ conversion can be achieved even at ambient temperature if stirred for 2.5 d. However, we found that mild heating could achieve higher conversion in less time. There was no evidence of unwanted double addition of the starting alkyne on heating.

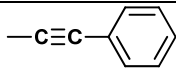
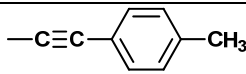
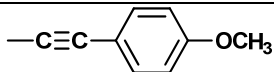
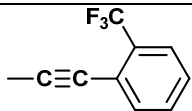
Compared to alkyne products from Br_{5,3}OPS, I₈OPS products by GPC are very monodisperse, representative of typical octa-functionalized cubic silsesquioxanes (see **Table 4.1**). Moreover, ¹H NMR does not reveal the presence of any alkenyl H's from addition side reactions as for Br_{5,3}OPS. Note that we were unable to obtain MALDI-TOF data for this set of materials although we tried multiple times using several procedures, e.g. with and without Ag⁺.

4.3.3 Thermal Studies

The octaalkynes from I₈OPS exhibit exceptional thermal robustness in air (**Table 4.2**). The 5% mass loss temperatures (T_{d5%}) determined by TGA predictably are the

highest for the phenylethyne derivatives (475 - 526 °C) and the lowest for the non-aromatic propiolate and trimethylsilyl derivatives (ca. 400 and 420 °C, respectively). Residues at 1000 °C (ceramic yields, **Table 4.1**) in air for all derivatives are very close to theory (± 1 weight %).

Table 4.2. $T_{d5\%}$ for octa-alkynes from I₈OPS (in air).

R	$T_{d5\%}$ (°C)
	526
	475
	508
	423
$-\text{C}\equiv\text{C}-\text{Si}(\text{CH}_3)_3$	418
$-\text{C}\equiv\text{C}-\text{COOCH}_3$	403

When heated treated to 400 °C/4 h, the materials thermally cross-link. Following polymerization, the cross-linked materials exhibit even greater stability. The $T_{d5\%}$ for Ph-OCH₃ increases from ≈ 510 °C to 560 °C as shown in Figure 4.1, which is typical behavior for these materials.^{19,22} These properties make octa-alkynes ideal cross-linking agents for high performance resins.²²

Evidence for self-polymerization is seen in the DRIFTS spectra of the diphenylethyne derivative before and after heat treatment. Before heating, we see typical $\nu\text{C}\equiv\text{C}$ at ≈ 2217 cm^{-1} , as well as $\nu\text{C-H}$ aromatic ring and $\nu\text{Si-O}$ stretches at ≈ 3050 and 1120 cm^{-1} , respectively, which are consistent with the proposed structure of the material. After heating at 400 °C/4h, however, there is a notable absence of $\nu\text{C}\equiv\text{C}$ peaks in the spectrum (Figure 4.2b). This seems to indicate exhaustive polymerization of the alkyne groups.

ν C-H aromatic ring and ν Si-O stretching peaks are still found in the DRIFTS spectrum after heat treatment, indicating retention of the tether aromatic rings as well as the silica cage. Thus the material is still polymeric (and not charred) after heating.

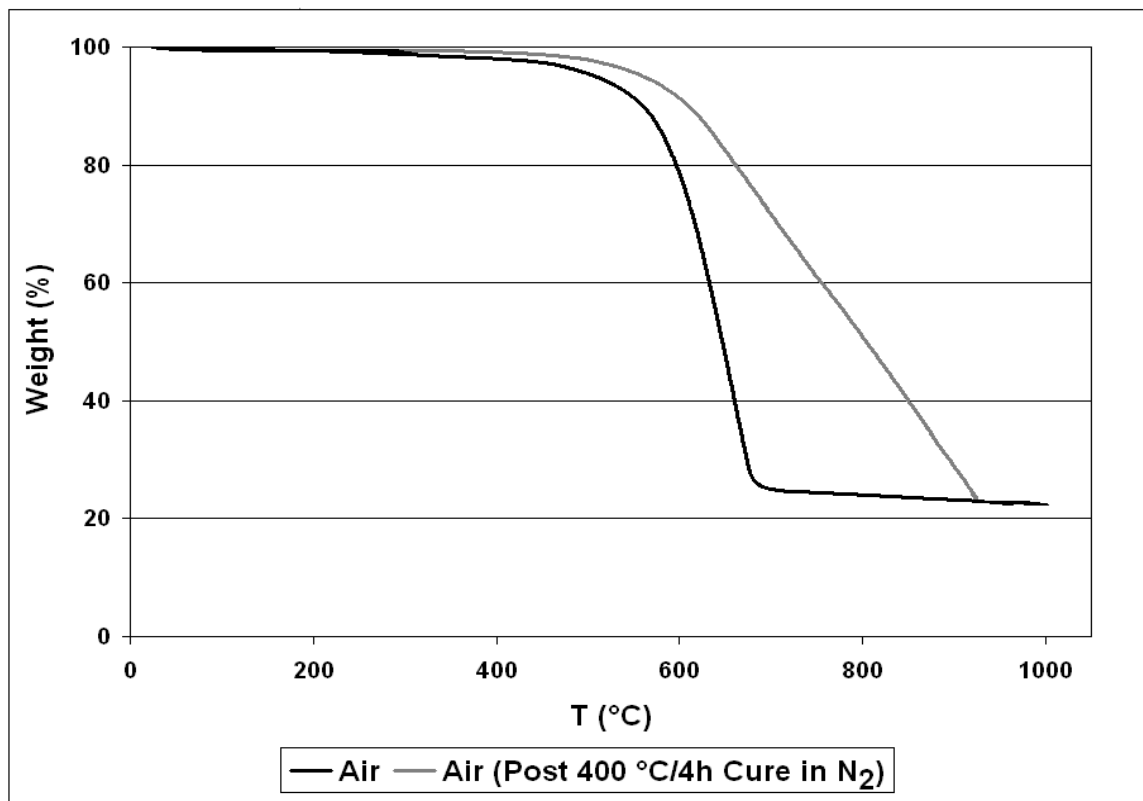


Figure 4.1. TGA of *p*-methoxydiphenylethyne derivative before/after 400 °C/4 h heat treatment.

The DSC of [diphenylethyneSiO_{1.5}]₈ is shown in Figure 4.3. Most notable are two exotherms with maxima at 190 ° and 285 °C, and an exotherm onset at \approx 325 °C. We believe that the first exotherm corresponds some form of ordering, e.g. T_c , since materials heated to this temperature and subsequently cooled remain soluble. However, heating to temperatures \geq 285 °C, results in much reduced solubility, suggesting some form of polymerization occurs during the second exotherm. Materials heated past this temperature are brittle and completely insoluble in any organic solvents suggesting that the 325 °C exotherm onset corresponds to bulk polymerization. While we do not observe the appearance of an endotherm corresponding to T_m , it is possible that the endotherm is

masked by the other two exotherms (simultaneous melting and polymerization). The other octa-alkyne derivatives exhibit similar DSC plots. In no instance are we able to observe melting via DSC or using standard melting point studies.

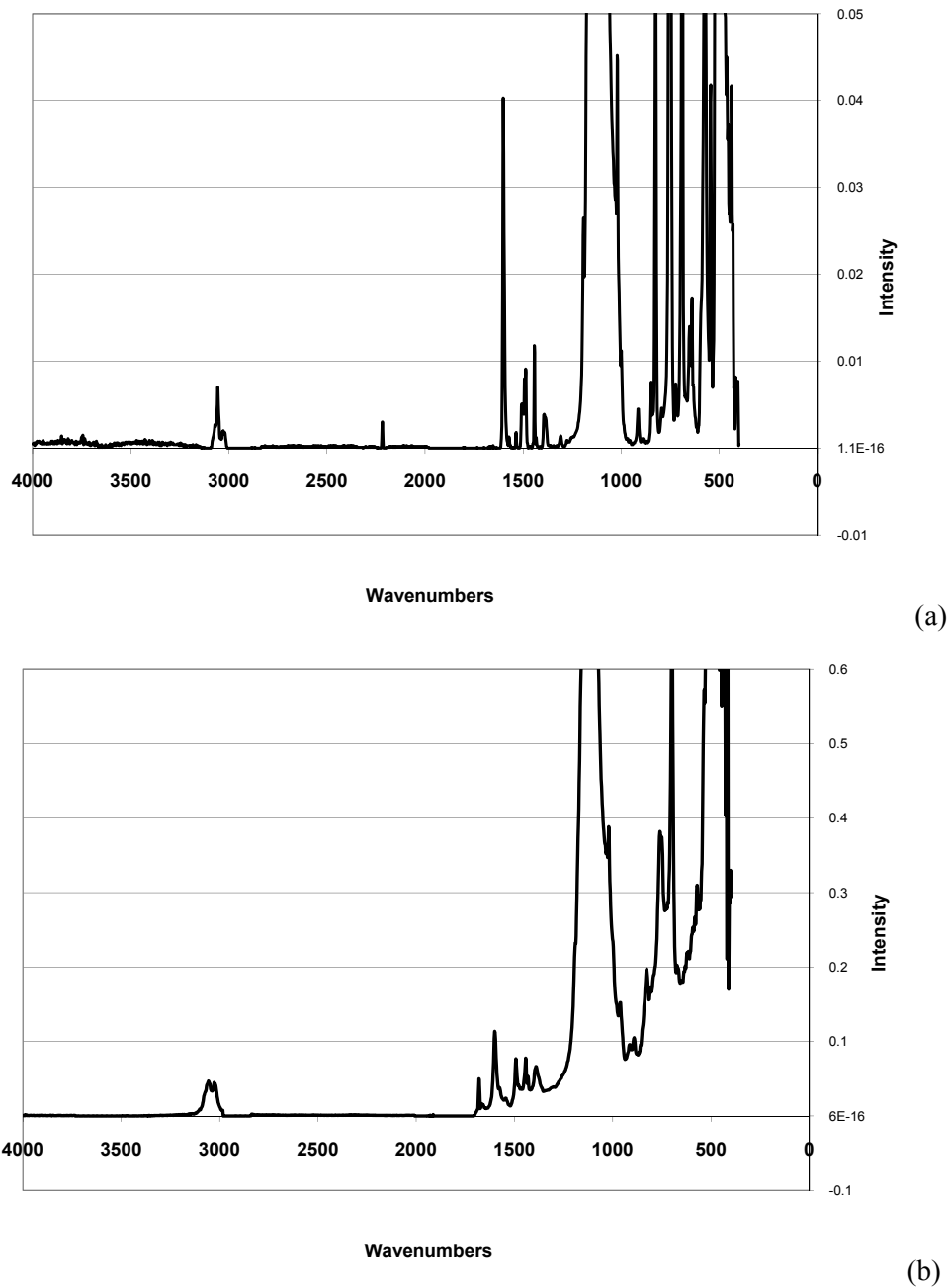


Figure 4.2. DRIFT spectra of [diphenylethyneSiO_{1.5}]₈ (a) before, (b) after heating to 400 °C/4h.

While the precise mode of cross-linking is unclear, the presence of IR peaks ≈ 1680 cm^{-1} in the heat treated material (Figure 4.2b) could be attributed to C=C bond peaks resulting from polymerization. If this is indeed the case, the resulting thermoset could have a structure such as shown in Figure 4.4. The weakness of this reasoning is that there does not seem to be a reasonable source of protons during thermal self-polymerization to support this mechanism. However, thermolysis of aromatic acetylenes has been reported to give various π -conjugated products, such as fused rings, by means of intra and inter-molecular cyclization.²²⁻²⁶

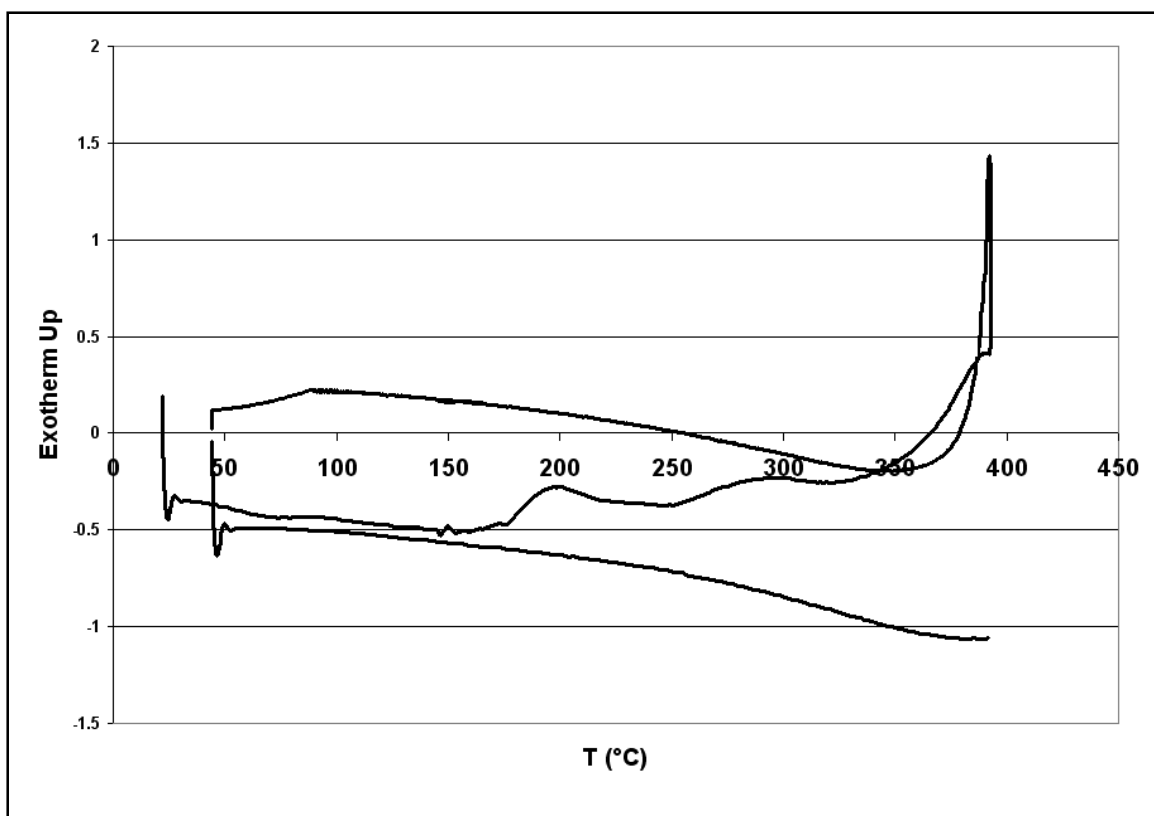


Figure 4.3. DSC thermogram of diphenylethyne derivative (N_2).

While further analysis is needed to identify the exact cross-linking mechanism whereby these materials polymerize, we find that they readily self-polymerize at temperatures ≈ 400 $^\circ\text{C}$ to produce cross-linked materials with thermal stabilities in air

above 500°C. This level of thermal stability is among the best for alkyne derived polymers currently known.²²⁻²⁶ In part these stabilities must result as a consequence of generating full dispersed nanosilica particles within the polymer matrix that provide extra heat capacity not found in simple cross-linked polyalkynes.

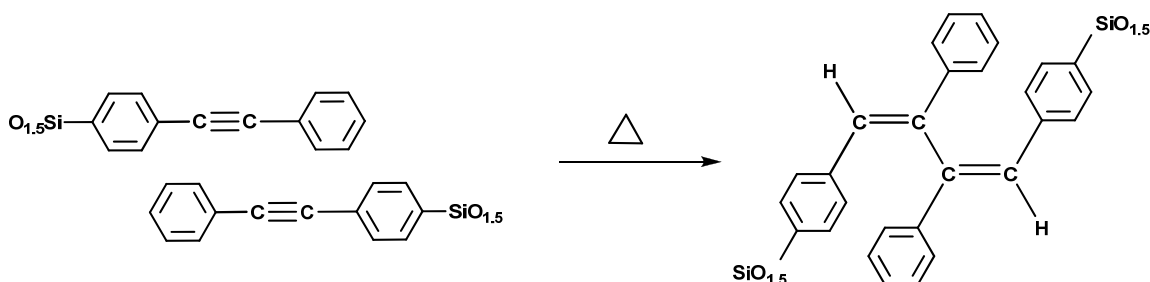


Figure 4.4. Possible structure of octa-acetylenes after thermal polymerization.

In a future paper we will explore the reaction of selected octaalkynes with tetraphenylcyclopentadienone to first produce, for example, an octahexaphenylbenzene silsesquioxane, a soluble, robust molecule with 56 phenyl rings that offers potential access to an octagraphene silsesquioxane.

4.4 Conclusions

Octa-alkynes are readily synthesized in >70% yields with 100% conversions from I₈OPS via Sonogashira reactions under mild conditions. While the formation of octa-alkynes from Br_{5,3}OPS resulted in unwanted addition reactions, the reactivity of the aryl iodide and near-perfect symmetry makes I₈OPS a suitable platform for the construction of octa-alkynes with corresponding geometry. The resulting alkyne compounds are thermally robust, yet highly soluble and have been shown to self-polymerize at temperatures \approx 400 °C to form highly cross-linked star polyalkynes with exceptional high temperature oxidative stability in air.

Finally, given that we now have developed a simple, high yield route to 3-D “Nano-Sea Urchin” molecules, it appears reasonable to suggest that the introduction of appropriate functionality at the external alkyne position will offer the potential to use these compounds as 3-D connectors for the construction of nanostructured materials. It also appears that these compounds, made in two steps from OPS could be used as new matrix materials for structural composites.

4.5 References

1. Schwab, P. F. H.; Levin, M. D.; Michl, J. *Chem. Rev.* **1999**, *99*, 1863-1934.
2. Levins, C.G.; Schafmeister, C.F. *J. Am. Chem. Soc.* **2003**, *125*, 4702-4703.
3. Yaghi, O.M.; Li, H.; Davis, C.; Richardson, D.; Groy, T.L. *Acc. Chem. Res.* **1998**, *31*, 474-484.
4. Eddaoudi, M.; Moler, D.B.; Li, H.; Chen, B.; Reineke, T.M.; O'Keeffe, M.; Yaghi, O.M. *Acc. Chem. Res.* **2001**, *34*, 319-330.
5. Wong-Foy, A. G.; Matzger, A. J.; Yaghi, O. M. *J. Am. Chem. Soc.* **2006**, *128*, 3494-3495.
6. Yang, H.-B.; Ghosh, K.; Arif, A. M.; Stang, P. J. *J. Org. Chem.* **2006**, *71*, 9464-9469.
7. Olenyuk, B.; Levin, M.D., Whiteford, J. A.; Shield, J.E., Stang, P.J. *J. Am. Chem. Soc.* **1999**, *121*, 10434-10435.
8. Addicott, C.; Das, N.; Stang, P.J. *Inorg. Chem.* **2004**, *43*, 5335-5338.
9. Lanznaster, M.; Heeg, M.J.; Yee, G.T.; McGarvey, B.R., Verani, C.N. *Inorg. Chem.* **2007**, *46*, 72-78.
10. Shin, J-S.; Pierce, N.A. *Nano Lett.* **2004**, *4*, 905-909.
11. Sasaki, T.; Osgood, A. J.; Alemany, L.B.; Kelly, K.F.; Tour, J.M. *Organic Lett.* **2008**, *10*, 229-232.
12. Mitkin, O.D.; Kurchan, A.N.; Wan, Y.; Schiwal, B.F.; Kutateladze, A.G. *Organic Lett.* **2001**, *3*, 1841-1844.
13. Menzel, H.; Mowery, M.D.; Cai, M.; Evans, C.E. *Macromolecules* **1999**, *32*, 4343-4350.
14. Majoros, I.J.; Keszler, B.; Woehler, S.; Bull, T.; Baker, J.R. Jr. *Macromolecules* **2003**, *36*, 5526-5529.
15. Silsesquioxane reviews: (a) Voronkov M.G., Lavrent'yev, V. I. *Top. Curr. Chem.* **1982**, *102*, 199-236. (b) R.H. Baney, M. Itoh, A. Sakakibara, T. Suzuki *Chem. Rev.* **1995**, *95*, 1409-1430. (c) Provatas, A.; Matisons, J.G. *Trends Polym. Sci.* **1997**, *5*, 327-333. (d) Lichtenhan, J. in Polymeric Materials Encyc., Salmone, J.C. Ed. Vol.

- 10, CRC Press, N.Y., **1996**, 7768-7777. (e) Laine, R.M. *J. Mater. Chem.* **2005**, *15*, 3725-3744.
16. Roll, M.F.; Asuncion, M.Z.; Kampf, J.; Laine, R.M. *ACS Nano* **2008**, *2*, 320-326.
17. (a) Horita, A.; Tsurugi, H.; Satoh, S.; Maiura, M. *Organic Lett.* **2008**, *10*, 1751-1754.
(b) Rahm, A.; Wulff, W.D. *Organometallics* **1993**, *12*, 597-599.
18. See for example: (a) Wiesler, U.-M.; Berresheim, A.J.; Morgenroth, F.; Lieser, G.; Müllen, K. *Macromolecules* **2001**, *34*, 187-199. (b) Tracz, A.; Jeszka, J.K.; Watson, M.D.; Pisula, W.; Mullen, K.; Pakula, T. *J. Am. Chem. Soc.* **2003**, *125*, 1682-1683.
(c) Zhi, L.; Wu, J., Mullen, K. *Org. Lett.* **2005**, *7*, 5761-5764.
19. See for example: (a) Melissaris, A.P.; Sutter, J.K.; Litt, M.H.; Scheiman, D.P.; Schuerman, M.A. *Macromolecules* **1995**, *28*, 860-865. (b) Melissaris, A.P.; Litt, M.H.; *Macromolecules* **1994**, *27*, 2675-2684. (c) Archibald, T.G.; Malik, A.A.; Baum, K.; Unroe, M.R. *Macromolecules* **1991**, *24*, 5261-5265.
20. Kaneko, T.; Horie, T.; Asano, M.; Aoki, T.; Oikawa, E. *Macromolecules*, **1997**, *30*, 3118-3121.
21. Brick, C. M.; Tamaki, R.; Kim, S-G.; Asuncion, M.; Roll, M. F.; Nemoto, T.; Laine, R.M. *Macromolecules*, **2005**, *38*, 4655-4660.
22. (a) Hergenrother, P.M.; Encyclopedia of Polymer Science and Engineering, J. Wiley, Chichester, **1985**, *1*, 61-86. (b) Meador, M.A. *Ann. Rev. Mater. Sci.* **1998**, *28*: 599-630.
23. Gandon, S.; Mison, P.; Bartholin, M.; Mercier, R.; Sillion, B.; Geneve, E.; Grenier, P.; Grenier-Loustalot, M.-F. *Polymer*, **1997**, *38*, 1439-1447.
24. Gandon, S.; Mison, P.; Bartholin, M.; Mercier, R.; Sillion B. *Polymer* **1997**, *38*, 1449-1459.
25. Nakamura, K.; Ando, S.; Takeichi, T. *Polymer* **2001**, *42*, 4045-4054.
26. Ochiai, B.; Tomita, I.; Endo, T. *Polymer* **2001**, *42*, 8581-8586.

Chapter 5

Synthesis, Characterization and Functionalization of Incompletely Condensed “Half Cube” $[\text{RSi}(\text{OH})\text{O}]_4$ or $[\text{RSi}(\text{ONa})\text{O}]_4$ Silsesquioxanes as a Potential Route to Nanoscale Janus Particles

Multiple literature reports describe the synthesis of $[\text{RSiO}(\text{OH})]_4$ or $[\text{RSiO}(\text{ONa})]_4$ compounds. Surprisingly, in the majority of cases the OH or ONa groups all lie on the same face of the cyclomers or half cubes. Consequently, it appears possible to couple R containing half cubes with R' containing half cubes to form bi-functional (Janus) silsesquioxane cages or cubes. We report here synthesis of $[\text{PhSiO}(\text{ONa})]_4$ and $[p\text{-IPhSiO}(\text{ONa})]_4$ half cubes. We thereafter discuss efforts to react the $[\text{PhSiO}(\text{ONa})]_4$ salt with RSiCl_3 (R = Me, vinyl, and cyclohexyl) in MeOH to produce the compounds $\{\text{PhSiO}[\text{OSi}(\text{OMe})_2\text{R}]\}_4$ species which were characterized using traditional spectroscopic procedures. These compounds were then subjected to acid catalyzed hydrolysis to hydrolytically remove the OMe groups to generate Janus cubes. While it is possible to isolate the target compounds, which were also characterized in detail, the yields were lower than expected perhaps because of competitive hydrolytic cleavage of the Si-O-SiR(OMe)₂ linkage.

5.1 Introduction

The synthesis and perfect assembly of 2- and 3-D structures from molecular components (nanobuilding blocks) is of immense current interest due to the potential to realize novel properties in nanosized and nanostructured materials, since materials reduced to the nanoscale often exhibit very different properties or phenomena compared to the macroscale. In fact, *the* essential challenge is to control materials' structures at these dimensions because the ability to tailor global properties precisely is dependent on manipulating component organization at the finest length scales. Indeed the construction of materials nanometer-by-nanometer should lead to the design of a variety of materials with well-defined nanoarchitectures and predictable behaviors.

Consequently highly symmetrical nanobuilding blocks are required, particularly those that offer both diverse functionality coupled with ease of synthesis, because it follows that breaks in periodicity (defects) in assembled 2- and 3-D structures should be minimized with higher component symmetry. The energy required to create a defect is offset by a gain in entropy; in theory, defects can be minimized by using highly symmetrical and well-ordered components that minimize the entropy of a given system. It can be expected then that misaligned but highly symmetrical components would require the least energy (associated with the least movement) to reorient and align with other assembled components. Accordingly, cubic structures (offering the highest symmetry) would also require the least energy to assemble.¹ Note that defects will still occur due to temperature-dependent entropic effects (TAS).

Cubic silsesquioxanes are one of the few groups of 3-D molecules with structures that offer high symmetry, ease of synthesis and/or modification, and octafunctionality such that each octant in Cartesian space contains one functional group. It is the positioning of functional groups, the variety possible, and their nm size that provide unique opportunities to build nanocomposites in 1-, 2- or 3-D, one nm at a time.²⁻³³ In addition, the core adds the rigidity and heat capacity of silica (in essence “the smallest single crystal sand particle”) making these compounds thermally robust at elevated temperatures.

As nanoconstruction sites, completely condensed silsesquioxanes can be further functionalized by direct chemical modification of the organic moieties to form larger, well-defined structures. However, similar “bottom-up” construction possibilities may also exist by employing *incompletely* condensed silsesquioxanes as nanobuilding blocks. Recently, incompletely condensed silsesquioxanes $[(\text{RSiO}_{1.5})_a(\text{H}_2\text{O})_{0.5b}]_n$, where a , b , n are integers: $a + b = 2n$, $b \leq a + 2$ have attracted attention as models for silica-supported systems, ligands for homogeneous catalysts, and comonomers in silsesquioxane-siloxane polymers.³⁴ Of particular interest to us is the all *cis*- $(\text{RSiO}_{1.5})_4(\text{H}_2\text{O})_2$ “half cube” (Figure 5.1a), since it represents a proposed intermediate in the formation of completely condensed cubic silsesquioxanes^{34,35}.

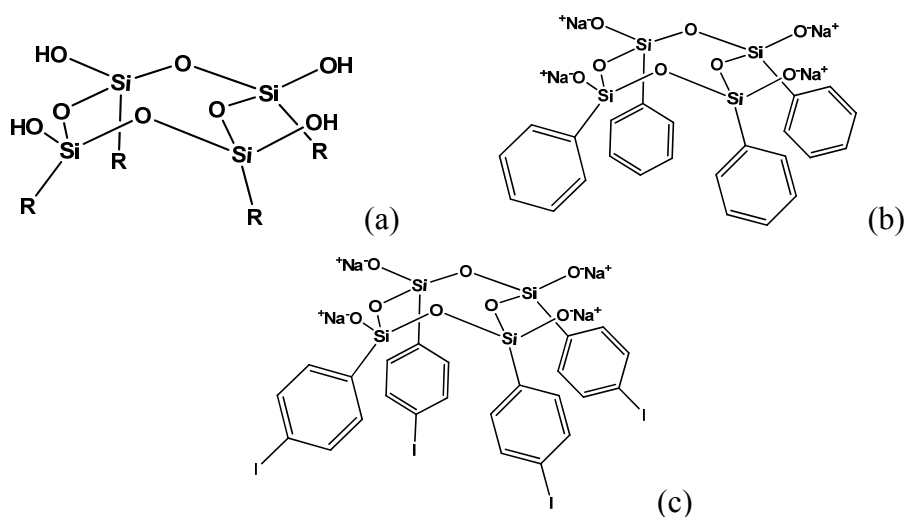


Figure 5.1. Structure of a. $(\text{RSiO}_{1.5})_4(\text{H}_2\text{O})_2$ “half cube” b. $[\text{Ph}_4\text{SiO}(\text{ONa})]_4$ half cube salt c. $[p\text{-IPhSiO}(\text{ONa})]_4$ half cube salt.

In principle such incompletely condensed half cube silsesquioxanes may provide potential access to “perfectly” defined surfaces via “Janus” (two-faced) cubes and may also help explain the unique emission characteristics of stilbene silsesquioxane derivatives, which are red-shifted up to 80 nm (0.75 eV).³⁶ The synthesis of a Janus cube such as suggested by Figure 5.2 could help support (or refute) the existence of 3-D

excited state conjugation through the center of the silsesquioxane cage, which density functional theory (DFT) HOMO-LUMO calculations have deemed quite possible.³⁷

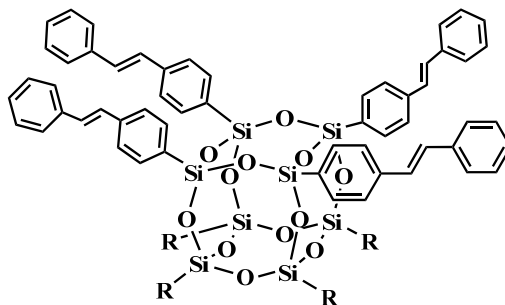


Figure 5.2. Target structure of a tetrastilbene Janus cube.

In addition, bi-functional or Janus cubes in principle can be tailored to modify surfaces and/or thin films with nanometer-scale control of the compositions and properties of individual layers. Moreover, one could also introduce bifunctionality allowing layer-by-layer coatings of hydrophobic/hydrophilic or hard/flexible layers with defined length scales. Janus cubes can also serve as interfaces between different domains or to guide self-assembly wherever complementary or dissimilar chemical functionalities are used. Here we describe efforts to develop routes to Janus cubes through studies on the functionalization of compounds like that shown in Figure 5.1b.

5.2 Experimental

5.2.1 Materials

All trichlorosilanes were purchased from Gelest, Inc. and used without further purification. All other chemicals were purchased from Fisher or Aldrich and used as received. Octaphenylsilsesquioxane (OPS) and octaiodophenylsilsesquioxane (I₈OPS)

were synthesized following methods described in the literature.^{38,39} All work was performed under nitrogen unless otherwise stated.

5.2.2 Synthetic Methods

5.2.2.1 Synthesis of Tetraphenyl Sodium Salt from OPS

To a dry 250 mL round bottom flask under N₂ and equipped with a magnetic stir bar and reflux condenser was added 5.00 g OPS (4.84 mmol, 38.8 mmol Si), 1.71 g NaOH (42.6 mmol), and 150 mL n-BuOH. The solution was stirred at 110 °C for 24-48 h, during which time it turns yellowish green. The hot solution was gravity filtered to remove the insolubles and allowed to cool to room temperature. The solution was then placed in a freezer and after 24 h white needle-like crystals form. The solid was filtered and dried *in vacuo* at 50 °C for 6 h, giving 4.97 g [(80%) - Figure 5.1b]. Characterization data: ¹H NMR (400 MHz, DMSO): 7.1 (1 H, m, *para* Ar-H), 7.2 (2 H, m, *meta* Ar-H), 7.7 (2 H, m, *ortho* Ar-H).

5.2.2.2 Reaction of Tetraphenyl Sodium Salt and Me₃SiCl₃

To a 250 mL round bottom flask under N₂ and equipped with magnetic stir bar was added 8.23 mL Me₃SiCl (65.0 mmol) and 2.83 mL pyridine (35.0 mmol) in 50 mL of toluene. 5.00 g of tetraphenyl sodium salt (8.22 mol) was added in one portion and the resulting mixture was refluxed for 1.5 h. The mixture was allowed to cool to room temperature and the insolubles were gravity filtered. The toluene filtrate was washed with water and dried over sodium sulfate. Benzene was removed *in vacuo* at 50 °C for 12 h to give 6.23 g (90.0 %) of white crystalline solid. Characterization data: ¹H NMR (400 MHz, CDCl₃): 0.2 (36 H, s, CH₃), 7.1 (4 H, m, Ar-H), 7.3 (4 H, m, Ar-H), 7.4 (8 H, m, Ar-H) ppm.

5.2.2.3 Synthesis of Tetra(*p*-iodophenyl) Sodium Salt from I₈OPS

To a dry 250 mL round bottom flask under N₂ and equipped with a magnetic stir bar and reflux condenser was added 3.40 g I₈OPS (1.66 mmol, 13.28 mmol Si), 0.53 g NaOH (13.25 mmol), and 100 mL n-BuOH. The solution was stirred at 110 °C for 12 h, during which time it turns colorless after 40 mins. The hot solution was gravity filtered to remove the insolubles and allowed to cool to room temperature. The solvent was removed slowly under reduced pressure at 35 °C for ~5 h at which point white needle-like crystals form. The solid was filtered and dried *in vacuo* at 50 °C for 6 h, giving 2.82 g [(74%) – Figure 5.1c]. Characterization data: ¹H NMR (400 MHz, CD₃OD): 7.3 (2 H, m, *meta* Ar-*H*), 7.6 (2 H, m, *ortho* Ar-*H*).

5.2.2.4 Synthesis of Tetramethyltetraphenyl Dimethoxy Derivative

To a 500 mL round bottom flask under N₂ and equipped with magnetic stir bar was added a suspension of 5.00 g of tetraphenyl sodium salt (8.22 mmol) in 100 mL MeOH. 4.25 mL of CH₃SiCl₃ (36.2 mmol) was dissolved in 100 mL of hexane and added to the MeOH suspension via addition funnel over 30 minutes. The heterogeneous reaction mixture was allowed to stir for 24 h at room temperature at which point insoluble NaCl formed. The salt was filtered from the reaction mixture and the hexane layer was separated, dried over Na₂SO₄, and rotary evaporated to give a viscous light-yellow oil. The oil was dried *in vacuo* at 80 °C for 6 h to give 6.20 g (82%). Characterization data: ¹H NMR (400 MHz, CDCl₃): 0.4 (3 H, s, CH₃), 3.2 (6 H, s, OCH₃), 7.2 (3 H, m, Ar-*H*); 7.6 (2 H, m, Ar-*H*) ppm. GPC: M_n 658; M_w 684; PDI 1.09.

5.2.2.5 Hydrolysis of Tetramethyltetraphenyl Dimethoxy Derivative

To a 25 mL round bottom flask under N₂ and equipped with magnetic stir bar was added 0.500 g (0.516 mmol) of tetramethyltetraphenyl dimethoxy derivative dissolved in 10 mL of hexane. 5 mL of H₂O and 1 mL of concentrated HCl were added dropwise to the solution and allowed to react 24 h at room temperature. The white insoluble

precipitate (0.344 g, 85%) was filtered and dried *in vacuo* at 80 °C for 12 h. Characterization data: TGA (air, 1000 °C): Found 61.2%; Calculated 61.2%; T_{d5%} 450 °C. IR: $\nu_{\text{C}=\text{H}}$ (3048-2939), ν_{CH_3} (2838), $\nu_{\text{C}=\text{C}}$ (Ar ring, 1591), $\nu_{\text{Si}-\text{CH}_3}$ (1269), $\nu_{\text{Si}-\text{O}}$ (1132) cm^{-1} .

5.2.2.6 Bromination of Tetramethyltetraphenyl Janus Cube

To a 50 ml Schlenk flask under N₂ and equipped with a magnetic stir bar was added granular iron (0.060 g, 1.00 mmol), tetramethyltetraphenylsilsesquioxane (2.00 g, 2.56 mmol), and CH₂Cl₂ (15 mL). The suspension was cooled to 0°C and bromine (3.30 g, 21.0 mmol) was slowly added. The suspension was stirred for 2 days and then more bromine (0.1 mL) and iron (0.02 g) were added and stirred for an additional 2 days. The suspension was filtered and the organic layer was washed with a sodium bicarbonate solution and then dried over Na₂SO₄. The solvent was removed under reduced pressure and the solid was collected and washed with water (3 x 10 mL), acetone (3 x 10 mL) and diethylether (3 x 10 mL) and dried *in vacuo* to give 1.2 g as white solid (64%). Characterization data: IR: $\nu_{\text{C}=\text{H}}$ (2870), $\nu_{\text{Si}-\text{C}}$ (1274), $\nu_{\text{Si}-\text{O}}$ (1142, 1041) cm^{-1} . MALDI-TOF: m/z (Ag⁺ adduct) = 897 [AgSi₈O₁₂(C₆H₅)₃(CH₃)₄], 970 [AgSi₈O₁₂(C₆H₄Br)(C₆H₅)₃(CH₃)₄], 1205 [AgSi₈O₁₂(C₆H₄Br)₄(CH₃)₄] amu.

5.2.2.7 Synthesis of Tetraphenyltetra vinyl Dimethoxy Derivative

To a 500 mL round bottom flask under N₂ and equipped with magnetic stir bar was added a suspension of 5.00 g of tetraphenyl sodium salt (8.22 mmol) in 100 mL MeOH. 4.60 mL of C₂H₃SiCl₃ (36.2 mmol) was dissolved in 100 mL of hexane and added to the MeOH suspension via addition funnel over 30 minutes. The heterogeneous reaction mixture was allowed to stir for 24 h at room temperature at which point insoluble NaCl formed. The salt was filtered from the reaction mixture and the MeOH layer was separated, dried over Na₂SO₄, and rotary evaporated to give a viscous colorless oil. The oil was dried *in vacuo* at 80 °C for 6 h to give a white crystalline solid 6.91 g (87%). Characterization data: ¹H NMR (400 MHz, CD₃OD): 3.2 (6 H, s, OCH₃), 5.9 (3 H, m, -

$CH=CH_2$), 7.2 (3 H, m, Ar-*H*), 7.6 (2 H, m, Ar-*H*) ppm. GPC: M_n 705; M_w 741; PDI 1.05.

5.2.2.8 Hydrolysis of Tetraphenyltetravinyl Dimethoxy Derivative

To a 25 mL round bottom flask under N_2 and equipped with magnetic stir bar was added 0.500 g (0.492 mmol) of tetraphenyltetravinyl dimethoxy derivative dissolved in 10 mL of MeOH. 5 mL of H_2O and 1 mL of concentrated HCl were added dropwise to the solution and allowed to react 24 h at room temperature. The white insoluble precipitate (0.377 g, 92%) was filtered and dried *in vacuo* at 80 °C for 12 h. Characterization data: TGA (air, 1000 °C): Found 51.5%; Calculated 57.7%; $T_{d5\%}$ 424 °C. IR: $\nu_{C=H}$ (3048-2950), $\nu_{C=C}$ (1630), $\nu_{C=C}$ (Ar ring, 1593), ν_{Si-O} (1134) cm^{-1} . MALDI-TOF: m/z (Ag^+ adduct) = 755, 900, 941 [$AgSi_8O_{12}(C_6H_5)_4(C_2H_3)_4$], 1060, 1080, 1130, 1180, 1230 amu.

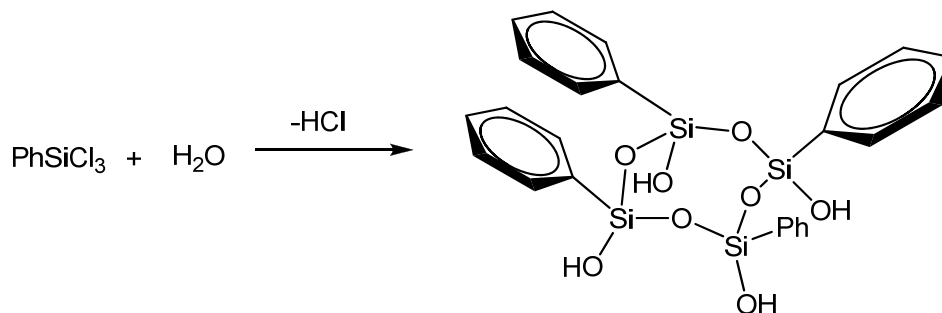
5.2.2.9 Synthesis of Tetracyclohexyltetraphenyl Dimethoxy Derivative

To a 500 mL round bottom flask under N_2 and equipped with magnetic stir bar was added a suspension of 5.00 g of tetraphenyl sodium salt (8.22 mmol) in 100 mL MeOH. 6.45 mL of $C_6H_9SiCl_3$ (36.2 mmol) was dissolved in 100 mL of hexane and added to the MeOH suspension via addition funnel over 30 minutes. The heterogeneous reaction mixture was allowed to stir for 24 h at room temperature at which point insoluble NaCl formed. The salt was filtered from the reaction mixture and the hexane layer was separated, dried over Na_2SO_4 , and rotary evaporated to give a viscous light-yellow oil. The oil was dried *in vacuo* at 80 °C for 6 h to give 7.76 g (76%). Characterization data: 1H NMR (400 MHz, $CDCl_3$): 0.8 (3 H, m, aliphatic-*H*), 1.2 (4 H, m, aliphatic-*H*), 1.7 (4 H, m, aliphatic-*H*), 3.5 (7 H, m, OCH_3), 7.4 (2 H, m, Ar-*H*), 7.7 (3 H, m, Ar-*H*) ppm. GPC: M_n 934; M_w 1037; PDI 1.18.

5.3 Results and Discussion

The objectives of the current study are to develop straightforward routes to half cube silsesquioxanes that in turn may be tailored by simple silanization. The resulting modified half cubes could then be hydrolyzed to form fully condensed Janus cubes with different moieties on each defined “face” of the cube. For example, any effort to functionalize just four of the eight p-iodo groups in I₈OPS,³⁹ see Scheme 5.3 below, would lead to a statistical distribution of functional groups at all corners rather than just *cis*-functionalization. It would also lead to sets of products where the average degree of substitution would be four rather than only four functional groups.

Thus, one can only expect to form a true Janus cube (where each face has one specific functionality) exclusively via a half cube intermediate. Previous work³⁵ by others and members of our team⁴⁰ focused on using acid-catalyzed hydrolysis of aromatic trichloro- or triethoxysilanes to form half cubes as suggested in Scheme 5.1.



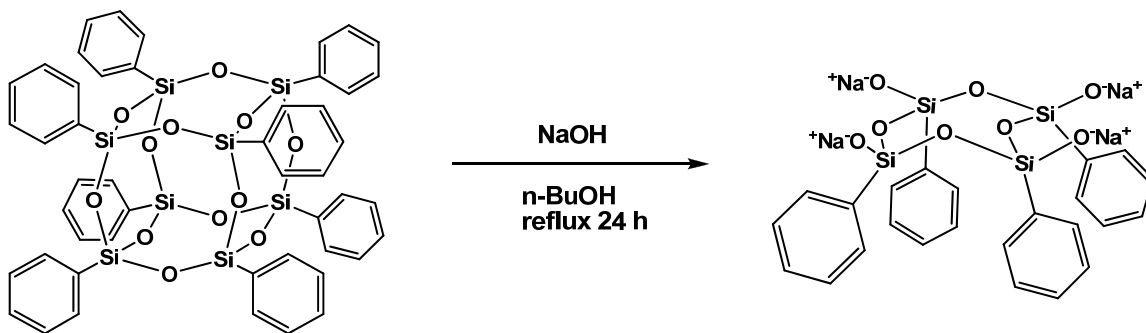
Scheme 5.1. Hydrolysis of PhSiCl₃ to form [PhSiO(OH)]₄.

However, the tendency of incompletely condensed half cubes (Figure 5.1a or the product of Scheme 5.1) to further condense even at room temperature in the solid state severely limits their utility and makes subsequent modification of the phenyl groups (i.e. by electrophilic aromatic substitution) essentially impossible without encountering extensive amounts of undesirable side products. In the past, the incorporation of tailorable moieties on the half cube required prior functionalization of the starting

monosilane via multiple step reactions involving both air and moisture sensitive intermediates followed by careful purification.⁴⁰ We report here an alternate route that permits access to perfectly functionalized half cube intermediates and also, initial efforts to produce Janus cages.

5.3.1 Synthesis of Tetra(*p*-iodo)phenyl Tetrasilesquioxane (I₄Ph₄) Sodium Salt

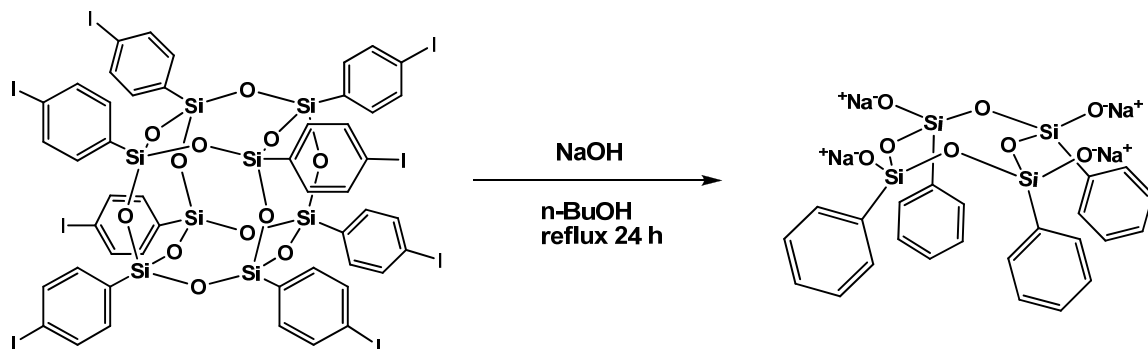
Shchegolikhina et al⁴¹ reported the high yield synthesis of the sodium salt of tetraphenyl tetrasilesquioxane [(Ph₄ half cube) - Figure 5.1b] from OPS, Scheme 5.2. The structure of the Ph₄ half cube salt was corroborated by ¹H NMR, and physical properties identical to those as described previously in the literature.⁴¹



Scheme 5.2. Reaction of OPS with NaOH to form Ph₄ sodium salt.

A similar approach was extended to NaOH cleavage of I₈OPS to produce tetra(*p*-iodo)phenyltetrasilesquioxane (I₄Ph₄) sodium salt, Figure 5.1c and Scheme 5.3, which incorporates a modifiable *para* iodo on the aromatic ring. This compound is readily synthesized in *one step* in high yield (see experimental section) and eliminates the need for Grignard modification of a triethoxysilane.⁴⁰ The structure of the I₄Ph₄ sodium salt was confirmed by ¹H NMR and the absence of a *para* aromatic proton (due to *p*-iodo substitution) is observed in the spectrum. A single crystal XRD data set was collected⁴² and while the data are not suitable for publication at this time, the structure clearly shows

the I-Ph- groups entirely *cis* with the half cube assuming a distorted boat conformation.^{40,41}

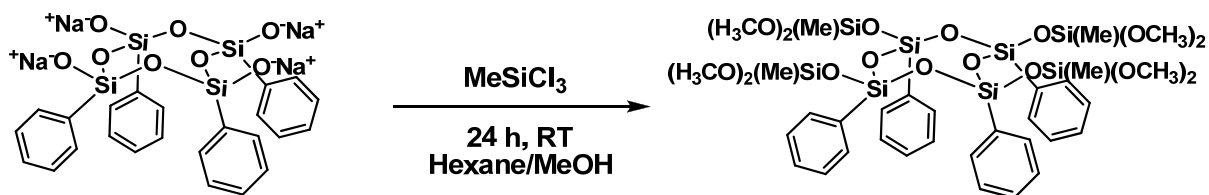


Scheme 5.3. Reaction of I₈OPS with NaOH to form I₄Ph₄ sodium salt.

5.3.2 Synthesis of Tetramethyltetraphenyl (Me₄Ph₄) silsesquioxane

In an effort to make fully condensed Janus cubes, the Ph₄ half cube sodium salt was reacted with MeSiCl₃ in the presence of methanol at room temperature to form the tetramethyltetraphenyl (Me₄Ph₄) dimethoxy half cube derivative {PhSiO[OSi(OCH₃)₂Me]}₄, (Scheme 5.4) in 85% yield. ¹H NMR (see experimental) confirmed the product structure and demonstrated facile methanolysis of the {PhSiO[OSiCl₂Me]}₄ intermediate's chloro groups by reaction with methanol solvent. GPC analysis reveals a single peak with M_n = 658 and M_w = 684 (vs. 969 amu theory) as has been seen previously because the GPC is calibrated using polystyrene standards that do not take into account silsesquioxane compounds' 3-D structures.³⁰ Mass spectroscopy using MALDI-ToF was unsuccessful as such compounds appear to not be readily ionizable.

Hydrolysis of Me₄Ph₄ dimethoxy derivative and subsequent cage closure were achieved by reaction with dilute HCl to form the Me₄Ph₄ Janus cube (Figure 5.3). Figure 5.4 provides TGA data indicating a ceramic yield (61.23%) essentially identical to theory (61.21%), supporting the formation of Me₄Ph₄ silsesquioxane. Unfortunately, the yields of this material are rather low, 10 %.



Scheme 5.4. Reaction of Ph_4 half cube sodium salt with MeSiCl_3 .

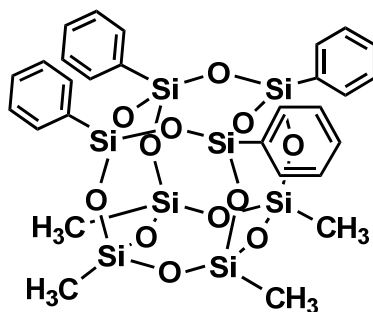


Figure 5.3. Tetramethyltetraphenyl (Me_4Ph_4) silsesquioxane cube.

While the TGA data indicate that the hydrolysis process likely works and that at least some of the $-\text{O}(\text{Me})\text{Si}(\text{OCH}_3)_2$ groups of the starting material are *cis* on the same face of the half cube. The low yields might suggest that only some of the intermediate compound has the dimethoxy groups all *cis*. Alternately, subsequent reaction with aqueous acid could lead to formation of high MW oligomeric condensation products and or oligomers that are not seen by GPC for any number of reasons. One they could be so crosslinked as to be insoluble or just insoluble because the parent cage compounds $[\text{MeSiO}1.5]_8$ and $[\text{PhSiO}1.5]_8$ are not particularly soluble. Indeed, the isolated Me_4Ph_4 cube is not very soluble. However in addition to the excellent correlation between the found and calculated TGA data, we also find that the melting point of the Me_4Ph_4 cube (112-114 °C) is essentially the same (116-118 °C) as reported by Andrianov et al.⁴³ Andrianov et al successfully synthesized the Me_4Ph_4 cube by the reaction of *cis*-1,3,5,7-tetrahydroxy-1,3,5,7-tetraphenylcyclotetrasiloxane with tetra-methylcyclotetrasiloxane in low concentrations. Their yields were only 1-2 %.

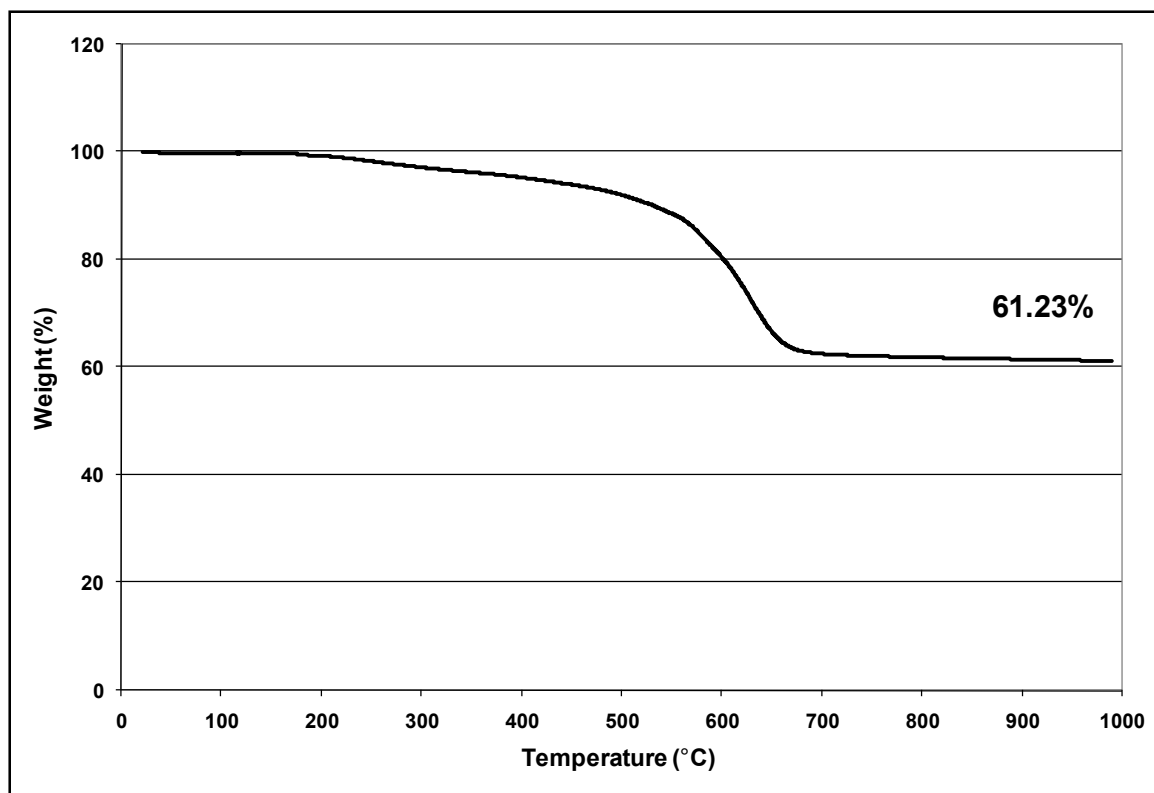


Figure 5.4. TGA (air) of tetramethyltetraphenyl (Me_4Ph_4) cubic silsesquioxane.

The FTIR of the Me_4Ph_4 cube, Figure 5.5, exhibits characteristic aromatic $\nu\text{C-H}$ vibrations ($3070\text{-}2970\text{ cm}^{-1}$), aliphatic $\nu\text{C-H}$ bands (2490 cm^{-1}), a $\nu\text{Si-C}$ band (1270 cm^{-1}), and $\nu\text{Si-O}$ attributed to the silsesquioxane cage (1130 cm^{-1}). Perhaps most important, no $\nu\text{O-H}$ bands ($3200\text{-}3400\text{ cm}^{-1}$) are seen, thus no unreacted -OH groups remain. Because it is insoluble in both nonpolar and polar solvents (CHCl_3 , DMSO, THF, MeOH, etc.) we were unable to further characterize it by NMR or MALDI-TOF. MALDI characterization requires THF solubility to allow intimate mixing with aqueous AgNO_3 , for sample preparation.

The low yields of this product mean that efforts to reproduce this synthesis often fail. The inconsistency in forming the intended product signifies a more complicated hydrolysis mechanism than originally predicted. We tried a variety of hydrolysis conditions and varied solvents, concentrations of reactants, reaction time, temperature, etc. with no clear insight into hydrolysis optimization. A more precise and rigorous study into the optimization of the hydrolysis conditions to form the Me_4Ph_4 Janus cube exclusively via a unimolecular pathway is necessary.

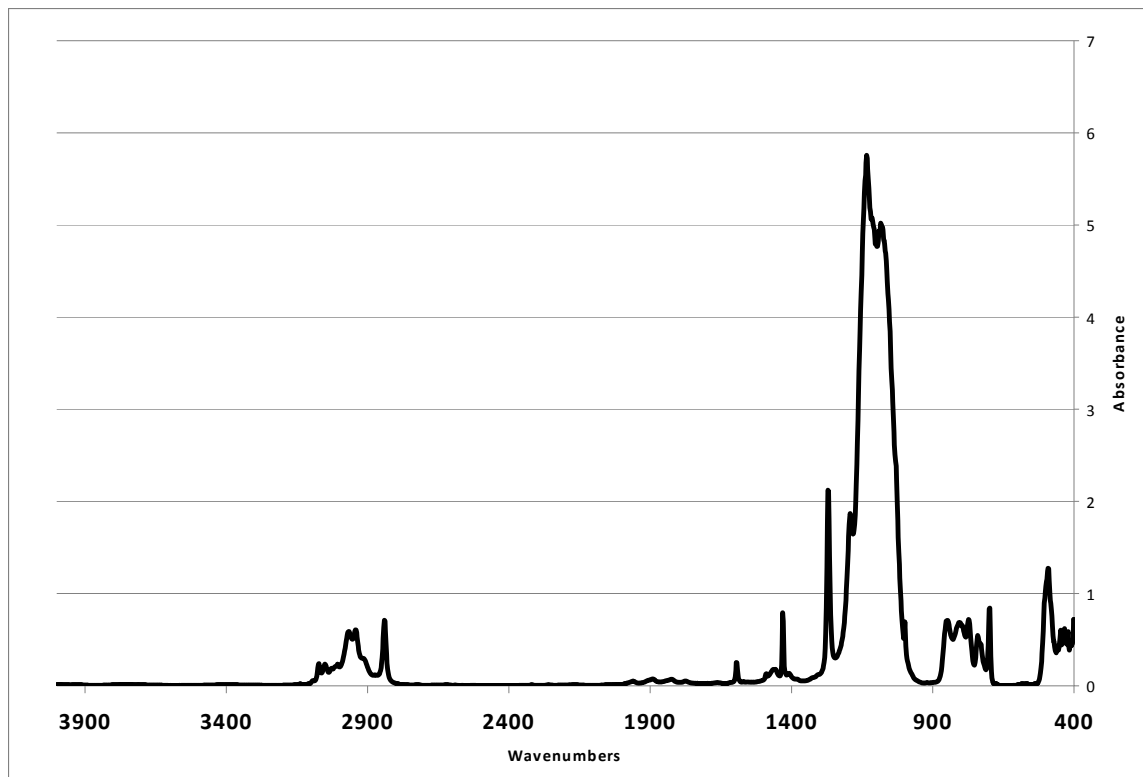
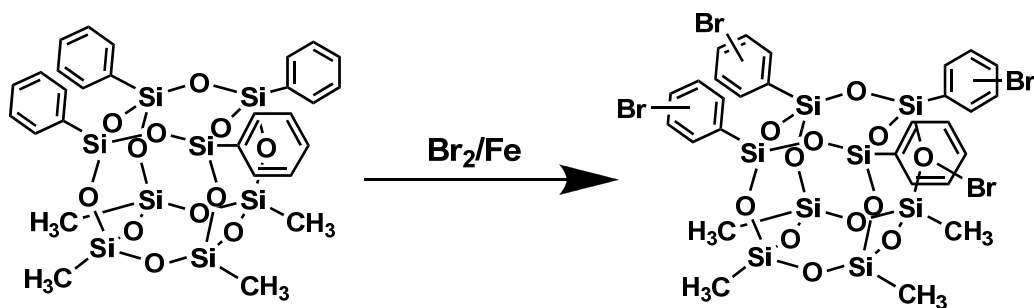


Figure 5.5. FTIR of tetramethyltetraphenyl (Me_4Ph_4) cubic silsesquioxane.



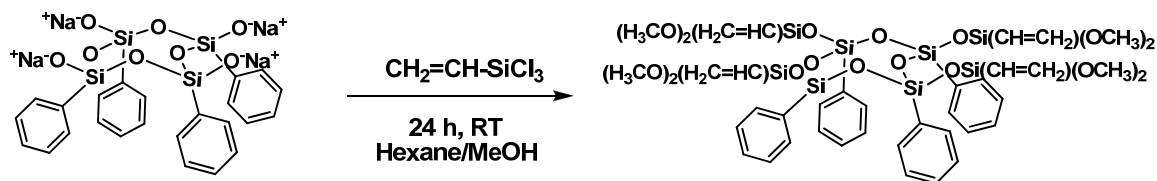
Scheme 5.5. Bromination of Me_4Ph_4 Janus cube.

As a result of these shortcomings, we sought to improve solubility by attempting bromination (Scheme 5.5) without purification. We found evidence for the Ag^+ adduct of both *mono*- [$\text{Me}_4(\text{Br-Ph})_1\text{Ph}_3$] and *tetra*-brominated [$\text{Me}_4(\text{Br-Ph})_4$] Janus cubes. However,

we were unable to develop a well defined route to any one easily isolated product and further efforts ceased.

5.3.3 Synthesis of Tetravinyltetraphenyl (vinyl₄Ph₄) silsesquioxane

Similarly the tetraphenyltetravinyl dimethoxy derivative $\{\text{PhSiO}[\text{OSi}(\text{OCH}_3)_2\text{vinyl}]\}_4$, was also easily prepared by reaction of the Ph₄ half cube sodium salt with vinyltrichlorosilane at room temperature in the presence of methanol, reaction (6). Unlike the Me₄Ph₄ dimethoxy derivative (a viscous oil), the vinyl₄Ph₄ derivative is a white crystalline solid. The structure of the vinyl₄Ph₄ dimethoxy derivative was confirmed by ¹H NMR, Figure 5.6 showing characteristic aromatic (7.0-8.0 ppm), vinyl (~5.9 ppm), and methoxy (~3.2 ppm) peaks with the correct integration (1.9:1.0:2.2 actual vs. 1.7:1.0:2.0 theory, respectively). GPC analysis showed a single peak consistent with the proposed molecular weight.



Scheme 5.6. Reaction of Ph₄ half cube sodium salt with VinylSiCl₃.

Again we attempted to hydrolyze the vinyl₄Ph₄ dimethoxy derivative using dilute HCl to form the vinyl₄Ph₄Janus cube (Figure 5.7). The MALDI spectrum of the hydrolysis product is shown in Figure 5.8. While the spectrum indicates the presence of the MW (Ag⁺ adduct) of the proposed structure, higher MW peaks in the MALDI also suggests the existence of oligomeric or polymeric condensation products in addition to the desired compound. Moreover, since the resulting product is insoluble in both aqueous and organic solvents, GPC and ¹H NMR analyses of the hydrolyzed product are impractical in this case.

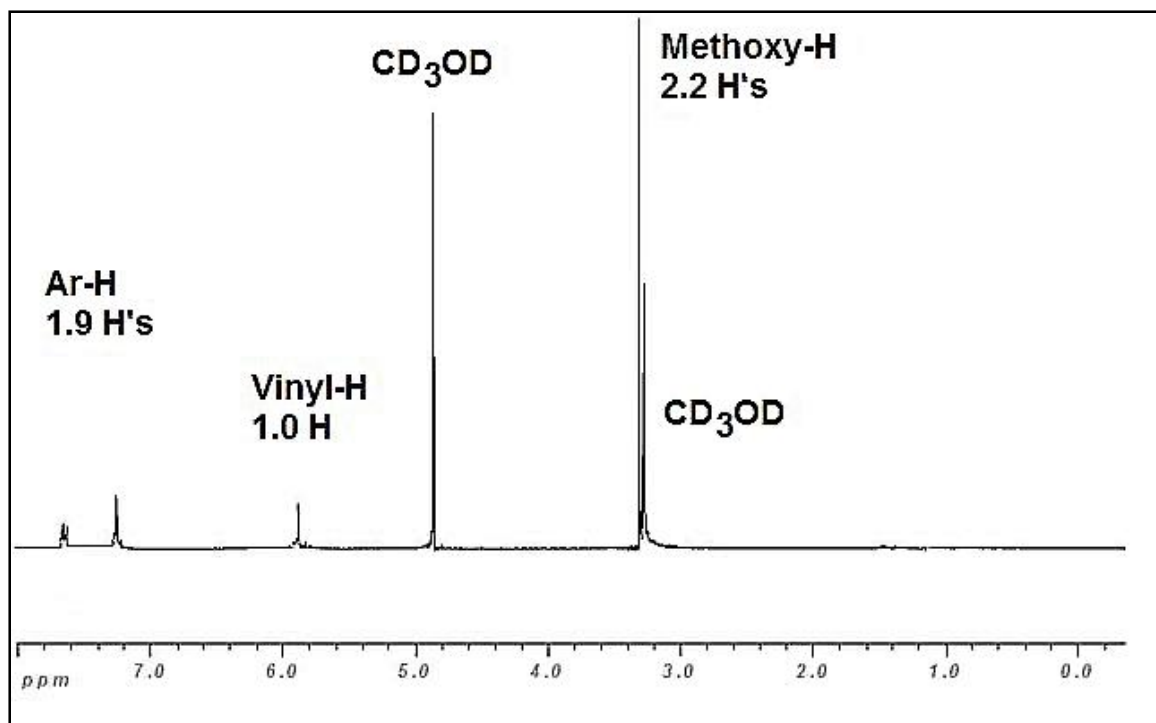


Figure 5.6. ^1H NMR of tetravinyltetraphenyl ($\text{vinyl}_4\text{Ph}_4$) dimethoxy derivative (CD_3OD).

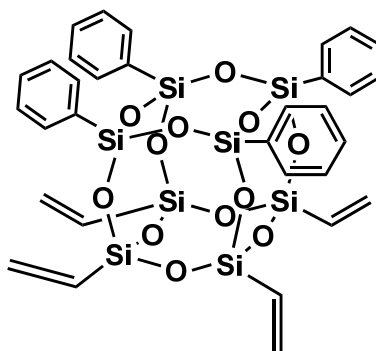


Figure 5.7. Tetravinyltetraphenyl ($\text{vinyl}_4\text{Ph}_4$) silsesquioxane.

As in the case of Me_4Ph_4 derivative, the hydrolysis of the $\text{vinyl}_4\text{Ph}_4$ dimethoxy derivative may proceed via bimolecular pathways because of the competing reactivity of the $\text{Si}(\text{OMe})_2\text{vinyl-O-Si}$ linkages. Again, further optimization of hydrolysis conditions is

needed. However, the vinyl₄Ph₄ Janus cube is definitely a product that forms during hydrolysis, albeit one of many products that are not easily isolated.

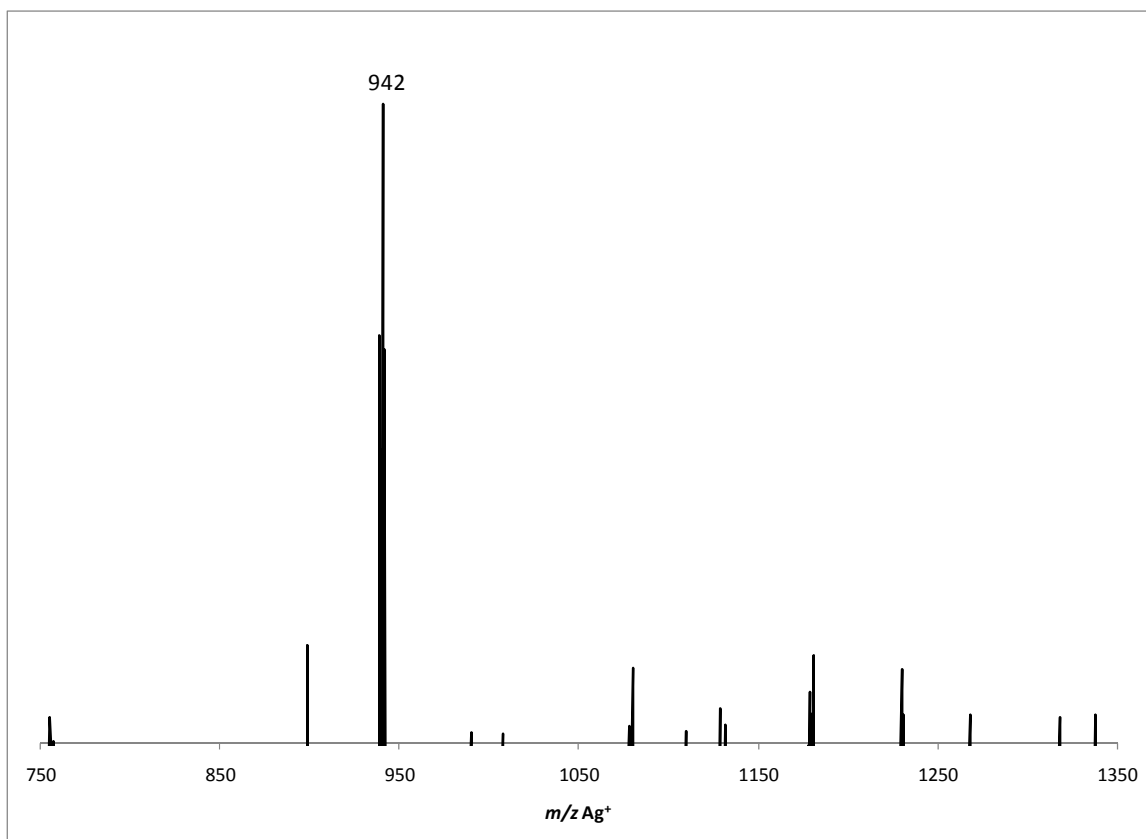
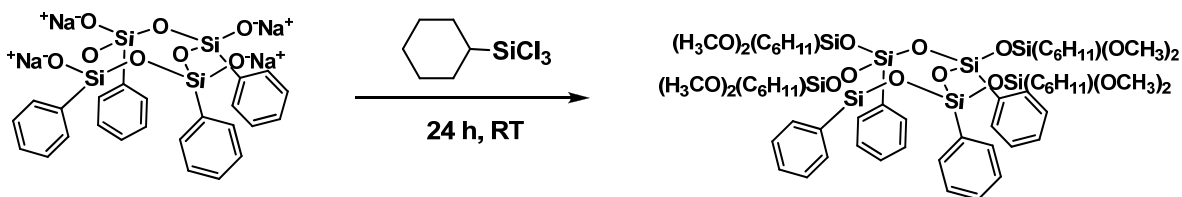


Figure 5.8. MALDI of tetravinyltetraphenyl (vinyl₄Ph₄) Janus cube (m/z Ag⁺). 942 Da is the expected MW of the proposed product.

5.3.4 Tetracyclohexyltetraphenyl (Cyclohexyl₄Ph₄) Dimethoxy Derivative

The Ph₄ half cube sodium salt was reacted with cyclohexyltrichlorosilane in MeOH in order to make {PhSiO[OSi(OCH₃)₂cyclohexyl]}₄, Scheme 5.7. Again, the anticipated structure is supported by ¹H NMR and GPC analyses. Unfortunately, we were unsuccessful in hydrolyzing this derivative to form the intended, fully-condensed cube. As above, we examined a wide variety of hydrolysis conditions and were only able to isolate high MW liquid product(s). We surmise that the mechanism of hydrolysis with

aqueous HCl is particularly inefficient in this case because of the bulky alkyl groups, which when hydrolyzed most likely form oligomeric products because of the tendency of $\{\text{PhSiO}[\text{OSi}(\text{OCH}_3)_2\text{cyclohexyl}]\}_4$ to phase separate from the acid phase rather than mix intimately as required for uniform and rapid hydrolysis of the methoxy groups. Perhaps this problem could be overcome using a miscible organic acid (e.g. glacial acetic acid).



Scheme 5.7. Reaction of Ph_4 half cube sodium salt with CyclohexylSiCl_3 .

5.4 Conclusions

Half cube sodium salts are readily synthesized in one step and $>70\%$ yields from OPS and I_8OPS . In particular, the I_4 half cube sodium salt shows potential for further modification at the iodo moiety by a host of Pd-catalyzed substitution reactions (after protection of the hydroxyl group with Me_3SiCl). We have also shown evidence for the syntheses of the $\{\text{PhSiO}[\text{OSi}(\text{OCH}_3)_2\text{R}]\}_4$ where $\text{R} = \text{Me}$, vinyl and cyclohexyl as well as their hydrolysis products Me_4Ph_4 and $\text{vinyl}_4\text{Ph}_4$. However, extensive efforts to optimize their hydrolysis to form Janus cubes in high yields suggests that further studies are needed to avoid formation of unwanted higher MW products. Base-catalyzed hydrolysis may also be considered as an alternative to acid-catalyzed conditions. The purity of the dimethoxy derivatives as assessed by ^1H NMR and GPC suggest that the critical stage of Janus cube formation occurs during hydrolysis. Regardless, while such optimization may not be trivial, the dimethoxy derivatives still remain a potential route to nanoscale Janus cubes.

5.5 References

1. Eaton, P.E. *Angew.Chem. Int. Ed. Engl.* **1992**, *31*, 1421.
2. (a) Feher, F.J.; Blanski, R.L. *J. Am. Chem. Soc.* **1992**, *114*, 5886. (b) Feher, F.J.; Soulivong, D.; Eklud, A.G.; Wyndham, K.D. *Chem. Comm.* **1997**, 1185. (c) Severn, J.R.; Duchateau, R.; van Santen, R.A.; Ellis, D.D.; Spek, A.L. *Organomet.* **2002**, *21*, 4. (d) Duchateau, R.; Abbenhuis, H.C.L.; van Santen, R.A.; Meetsma, A.; Thiele, S.K.-H.; van Tol, M.F.H. *Organomet.* **1998**, *17*, 5222.
3. Maxim, N.; Magusin, P.C.M.M.; Kooyman, P.J.; van Wolput, J.H.M.C.; van Santen, R.A.; Abbenhuis, H.C.L. *J. Phys. Chem. B.* **2002**, *106*, 2203.
4. Bonhomme, C.; Toledano, P.; Maquet, J.; Livage, J.; Bonhomme-Coury, L. *J. Chem. Soc. Dalton Trans.*, **1997**, 1617.
5. (a) Bassindale, A.R.; Pourny, M.; Taylor, P.G.; Hursthouse, M.B.; Light, M.E. *Angew. Chem. Inter. Ed.* **2003**, *42*, 3488. (b) Bassindale, A.R.; Parker, D.J.; Pourny, M.; Taylor, P.G.; Horton, P.N.; Hursthouse, M.B. *Organomet.* **2004**, *23*, 4400.
6. Tsuchida, A.; Bolln, C.; Sernetz, F.G.; Frey, H.; Mülhaupt, R. *Macromolecules* **1997**, *30*, 2818.
7. Reviews: (a) Voronkov, M. G.; Lavrent'yev, V. I. *Top. Curr. Chem.* **1982**, *102*, 199. (b) Baney, R.H.; Itoh, M.; Sakakibara, A.; Suzuki, T. *Chem. Rev.* **1995**, *95*, 1409. (c) Provatas, A.; Matison, J.G. *Trends Polym. Sci.* **1997**, *5*, 327. (d) Loy, D.A.; Shea, K.J. *Chem. Rev.* **1995**, *95*, 1431. (e) Lichtenhan, J. "Silsequioxane-based Polymers," in *Polymeric Materials Encyc.*, J.C. Salamone Ed. Vol. 10, CRC Press, N.Y., **1996**, 7768-77. (e) Laine, R.M. *J. Mater. Chem.* **2005**, *15*, 3725. (f) Calzaferri, G. "Silsequioxanes," in *Tailor-made Silicon-Oxygen Compounds, from molecules to materials*, R. Corriu and P. Jutzi eds. Publ. Friedr. Vieweg & Sohn mbH, Braunschweig/Weisbaden, Germany 1996. pp. 149-169.
8. (a) Lichtenhan, J.D.; Vu, H.Q.; Carter, J.A.; Gilman, J.W.; Feher, F.J. *Macromolecules* **1993**, *26*, 2141. (b) Gilman, J.W.; Schlitzer, D.S.; Lichtenhan, J.D. *J. Appl. Poly. Sci.* **1996**, *60*, 591. (c) Gonzalez, R.I.; Phillips, S.H.; Hoflund, G.B. *J. Spacecraft and Rockets* **2000**, *37*, 463.
9. (a) Weidner, R.; Zeller, N.; Deubzer, B.; Frey, V. U.S. Patent 5,047,492, Sept., **1991**. (b) S. Dathe, E. Popowski, G. Sonnek, T. Feiher, H. Jancke, U. Schelm, Euro. Patent 0,348,705 A1 **1989**. (c) C. Freyer, J. Wolferseder, U. Peetz, Euro. Patent 0,624, 691 A1 **1993**.
10. (a) Stewart, M.D., Willson, C.G. *MRS Bulletin* **2005**, *30*, 947. (b) Stewart, M.D.; Wetzel, J.T.; Schmid, G.M.; Palmieri, F.; Thompson, E.; Kim, E.K.; Wang, D.;

- Sotodoeh, K.; Jen, K.; Johnson, S.C.; Hao, J.; Dickey, M.D.; Nishimura, Y.; Laine, R.M.; Resnick, D.J.; Willson, C.G.; *Proc. SPIE-Int. Soc. Opt. Eng.* **2005**, 5751, 219.
11. (a) Hasegawa, I.; Sakka, S.; Sugahara, Y.; Kuroda, K.; Kato, C. *J. Chem. Soc., Chem. Commun.* **1989**, 4, 208. (b) Hasegawa, I.; Moto-jima, S. *J. Organomet. Chem.* **1992**, 441, 373. (c) Hasegawa, I.; Sakka, S.; *Chem. Lett.* **1988**, 8, 1319.
12. Agaskar, A. *Inorg. Chem.* **1991**, 30, 2707.
13. (a) Hoebbel, D.; Endres, K.; Reinert, T.; Pitsch, I. *J. Noncryst. Sol.* **1994**, 176, 179. (b) Hoebbel, D.; Pitsch, I.; Heidmann, D. "Inorganic organic polymers with defined silicic acid units," *Eurogel '91*, Elsevier Sci. Publ. **1992**, pp 467-73.
14. Pach, M.; Stösser, R. *J. Phys. Chem. A.* **1997**, 101, 8360.
15. (a) Hong, B.; Thoms, T.P.S.; Murfee, H.J.; Lebrun, H.J. *Inorg. Chem.* **1997**, 36, 6146. (b) Feher, F.J.; Wyndham, K.D. *Chem. Comm.* **1998**, 323. (c) Dvornic, P.R.; Hartmann-Thompson, C.; Keinath, S.E.; Hill, E.J. *Macromolecules* **2004**, 37, 7818.
16. (a) Kim, G.-M.; Qin, H.; Fang, X.; Sun, F.C.; Mather, P.T. *J. Poly. Sci. B-Polymer Physics*, **2003**, 41, 3299. (b) Kim, B.S.; Mather, P.T. *Macromolecules* **2002**, 35, 8378.
17. (a) Waddon A.J.; Coughlin, E.B. *Chem. Mater.* **2003**, 15, 4555. (b) Cardoen, G.; Coughlin, E.B. *Macromolecules* **2004**, 37, 5123-6.
18. (a) Fu, B.X.; Hsiao, B.S.; White, H.; Rafailovich, M.; Mather, P.; Joen, H.G.; Phillips, S.; Lichtenhan, J. and Schwab, J. *Poly. Inter.*, **2000**, 49, 437. (b) Fu, B.X.; Zhang, W.; Hsiao, B.S.; Rafailovich, M.; Sokolov, J.; Johansson, G.; Sauer, B.B.; Phillips, S. and Blanski, R. *High Performance Poly.*, **2001**, 12, 565.
19. Lin, H-C.; Kuo, S-W; Huang, C-F; Chang, F-C. *Macromol. Rapid Comm.* **2006**, 27, 537.
20. (a) Baker, E.S.; Gidden, J.; Anderson, S.E.; Haddad, T.S.; Bowers, M.T. *Nano Lett.*, **2004**, 4, 779. (b) Fu, B.X.; Lee, A.; Haddad, T.S. *Macromolecules* **2004**, 37, 5211. (c) Kopesky, E.T.; Haddad, T.S.; Cohen, R.E.; McKinley, G.H. *Macromolecules* **2004**, 37, 8992.
21. Brown, J.F.; Vogt, L.H.; Perescott, P.I. *J. Am. Chem. Soc.* **1964**, 86, 1120.
22. Zhang, C.; Babonneau, F.; Bonhomme, C.; Laine, R.M.; Soles, C.L.; Hristov, H.A.; Yee, A.F. *J. Am. Chem. Soc.* **1998**, 120, 8380.
23. Sellinger, A.; Laine, R.M. *Macromolecules* **1996**, 29, 2327.

24. Choi, J.; Harcup, J.; Yee, A.F.; Zhu, Q.; Laine, R.M. *J. Am. Chem. Soc.* **2001**, *123*, 11420.
25. Sellinger, A.; Laine, R.M. *Chem. Mater.* **1996**, *8*, 1592.
26. Zhang, C.; Laine, R.M. *J. Am. Chem. Soc.* **2000**, *122*, 6979.
27. Laine, R.M.; Choi, J.; Lee, I. *Adv. Mater.* **2001**, *13*, 800.
28. Zhang, C.; Laine, R.M. *J. Organomet. Chem.* **1996**, *521*, 199.
29. Tamaki, R.; Tanaka, Y.; Asuncion, M. Z.; Choi, J.; Laine, R.M. *J. Am. Chem. Soc.* **2001**, *123*, 12416.
30. Costa, R.O.R.; Vasconcelos, W.L.; Tamaki, R. and Laine, R.M. *Macromolecules* **2001**, *34*, 5398.
31. Laine, R.M.; Zhang, C.; Sellinger, A.; Viculis, L.; *J. Appl. Organometallic Chem.* **1998**, *12*, 715.
32. (a) Tamaki, R.; Choi, J.; Laine, R.M. *Chem. Mater.* **2003**, *15*, 793. (b) Choi, J.; Tamaki, R.; Kim, S.G.; Laine, R.M. *Chem. Mater.* **2003**, *15*, 3365.
33. Choi, J.; Yee, A.F.; Laine, R.M. *Macromolecules* **2003**, *15*, 5666.
34. Pescarmona, P.P.; Maschmeyer, T. *J. Aust. Chem.*, **2001**, *54*, 583.
35. Feher, F.; Schwab, J.J.; Soulivong, D.; Ziller, J.W. *Main Group Chem.* **1997**, *2*, 123.
36. Neurock, M.; Filhol, J.-S.; Lee, C.-Y.; Laine, R.M.; Brick, C.M.; Roll, M.F. unpublished work.
37. Sulaiman, S.; Bhaskar, A.; Zhang, J.; Guda, R.; Goodson, T. III; Laine, R.M. *Chem. Mater.* **2008**, *20*, 5563.
38. Brown, J. F., Jr.; Vogt, L. H., Jr.; Prescott, P. I. *J. Am. Chem. Soc.* **1964**, *86*, 1120.
39. Roll, M.F.; Asuncion, M.Z.; Kampf, J.; Laine, R.M. *ACS Nano* **2008**, *2*, 320.
40. Ronchi, M.; Pizzotti, M.; Orbelli Biroli, A.; Macchi, P.; Lucenti, E.; Zucchi, C. *J. Organometallic Chem.* **2007**, *692*, 1788.
41. Shchegolikhina, O.; Pozdniakova, Y.; Antipin, M. *Organomet.* **2000**, *19*, 1077.
42. Asuncion, M.Z.; Kampf, J.; Laine, R.M. unpublished results.

43. K.A. Andrianov, K.A.; V.S. Tikhonov, V.S.; G.P. Makhneva, G.P.; G.S. Chernov, G.S. *Izvestiya Akademii Nauk SSSR, Seriya Khimicheskaya*, **1973**, 4, 956.

Chapter 6

Fluoride Rearrangement Reactions of Polyphenyl- and Polyvinylsilsesquioxanes as a Facile Route to Fluorescent Oligomers

The objectives of the work described in this chapter are to demonstrate novel, facile routes to fluorescent oligomers via fluoride-mediated rearrangement of polyphenylsilsesquioxane (PPS) and polyvinylsilsesquioxane (PVS). PPS and PVS are polymeric by-products of the syntheses of the related T_8 octamers and as such lack the perfect 3-D symmetry of their polyhedral counterparts. Here we demonstrate that random-structured PPS and PVS rearrange in the presence of catalytic amounts of $Bu_4N^+F^-$ in THF to form mixed polyhedral T_{10} and T_{12} cages in high yield. Furthermore, through control of the ratio of starting materials, we can statistically tailor the numbers and types of moieties on these cages, $vinyl_xPh_{10-x} T_{10}$ and $vinyl_xPh_{12-x} T_{12}$.

Simple metathesis chemistry on cages with $x \sim 2$ vinyl groups and 4-bromostyrene followed by Heck coupling with other vinyl cages leads to “string of beads” silsesquioxane oligomers joined by conjugated organic tethers. The functionalized T_{10} and T_{12} cages, metathesis compounds, and Heck compounds were characterized by standard analytical methods (MALDI-TOF MS, 1H and ^{13}C NMR spectroscopy, TGA, and GPC). MALDI confirms the elaboration of the cages after each synthetic step and GPC verifies the presence of higher MW silsesquioxane oligomer. TGA shows that all of these compounds are thermally stable in air (>300 °C). Investigation of the UV-Vis absorption and photoluminescence behavior of the Heck oligomers reveals exceptional red shifts (≈ 120 nm) that suggest electronic interaction with the silica cores. Such phenomena may imply 3-D conjugation through the cores themselves.

6.1 Introduction

Polyhedral silsesquioxanes, in particular the T_8 octasilsesquioxane “cubes” $[(RSiO_{1.5})_8]$ Figure **6.1a**], represent a versatile class of highly symmetrical three-dimensional organosilicon compounds with well-defined nanometer structures. The combination of a rigid silica core and a more flexible, modifiable organic shell make these compounds extremely useful as platforms for hybrid nanocomposite materials with properties intermediate between the properties of ceramics and organics.¹⁻¹²

Silsesquioxanes have been used in recent years to (1) model catalytic surfaces,^{13,14} (2) generate new catalysts¹⁵ and (3) novel porous media,¹⁶ serve as (4) NMR standards,¹⁷ and (5) encapsulants.¹⁸ The T_{10} decameric and T_{12} dodecameric cages (Figure **6.1b** and **6.1c**, respectively) are frequently formed alongside the T_8 cube^{19,20} and their derivatives often exhibit similar chemical, thermal, and mechanical properties parallel to those of T_8 derivatives.^{19b}

Cubic silsesquioxanes are typically prepared via acid or base-catalyzed hydrolytic condensation of trifunctional organosilanes or by chemical transformation of the pendant groups on pre-existing cages. Since their initial discovery in 1946,²¹ there have been numerous studies on the synthesis of polyhedral silsesquioxanes. However, no universal preparative procedures have been established for reasons mentioned below.¹⁹

Many factors are known to influence the formation (and hence structure) of silsesquioxanes from the hydrolytic condensation of $RSiX_3$ (where X is typically a halogen or alkoxy group); they are: the nature of the R group, nature of X group, solvent, concentration of starting materials, reaction time, rate of addition and quantity of H_2O , pH, solubility of product, etc.²⁰ It has proven difficult to quantify the effects of these factors, either individually or collectively, because each reaction appears to be uniquely sensitive to a combination of many (if not all) of the above variables.

Researchers have shown that acid-catalyzed hydrolysis of trialkoxysilanes often forms the corresponding cubic silsesquioxane very slowly and with poor yields (~5-30%) depending on the nature of the starting silane.²²⁻²⁴ In contrast, base-catalyzed conditions generally improve reaction times and yields,²⁵ but the use of excessively strong base usually leads to undesired cage scission. Among the base promoted syntheses recently,

work by others^{25,26} used F^- as a base to synthesize T_8 silsesquioxanes, because it is also a strong nucleophile and forms kinetically reactive Si-F bonds.²⁷ For example, F^- is effective in rapidly catalyzing gel formation of tetraethylorthosilicate in sol-gel processes at 25 °C.²⁸ Tetrabutylammonium fluoride²⁵ and KF ²⁶ were used because solutions of these compounds are only slightly basic ($pK_a \sim 3.20$ in H_2O).

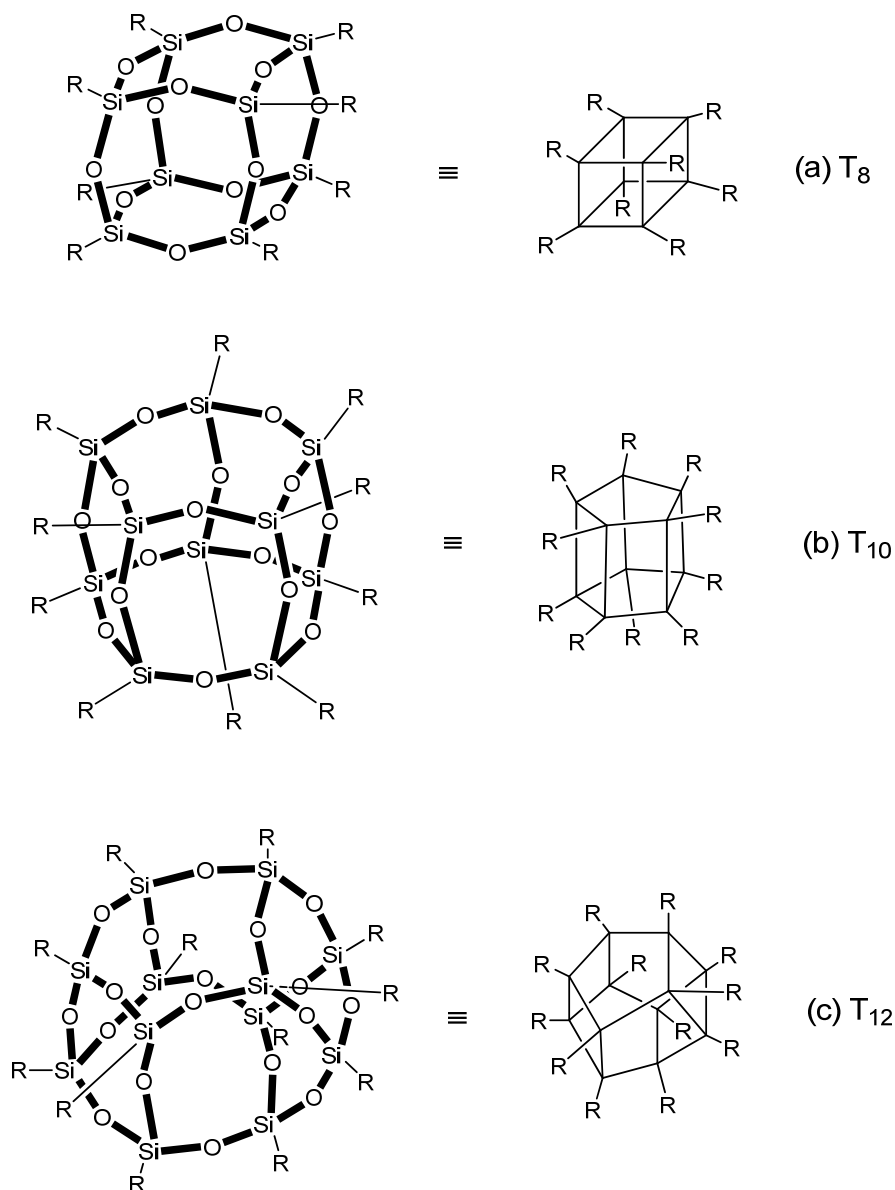
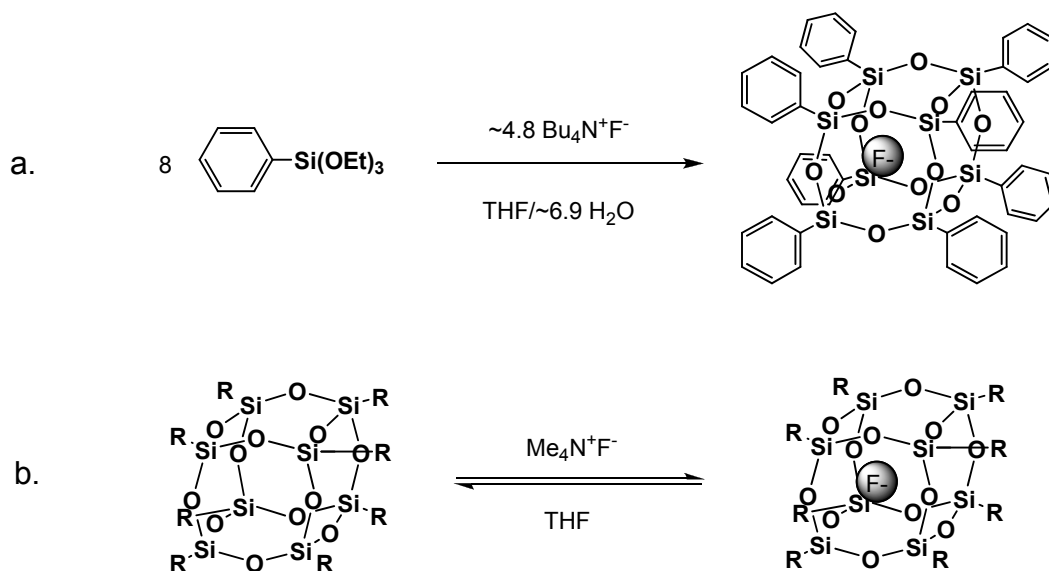


Figure 6.1. Idealized structures of (a) T_8 octasilsesquioxane “cube”, (b) T_{10} decasilsesquioxane, and (c) T_{12} dodecasilsesquioxane.



Scheme 6.1. Synthesis and structure of $\text{F}^-@(\text{PhSiO}_{1.5})_8$ from (a) reaction of phenyltriethoxysilane and TBAF^{29a} and by (b) reaction of OPS and TMAF.^{30a}

Recently Bassindale^{29a} reported the encapsulation of F^- in the center of a phenyl T_8 cage (octaphenylsilsesquioxane, OPS; Scheme 6.1a) by removal of solvent after the hydrolysis of phenyltriethoxysilane with stoichiometric tetrabutylammonium fluoride (TBAF). The structure was confirmed by ^{29}Si NMR and single crystal X-ray diffraction (XRD). The syntheses of $\text{F}^-@(\text{vinylSiO}_{1.5})_8$ and $\text{F}^-@(\textit{p}\text{-tolylSiO}_{1.5})_8$ were also reported.^{29b} The trapped fluoride ion results in only very slight changes in the Si-O distances and cage bond angles from structures where the central fluoride is absent.²⁹ ^{19}F NMR shows a single, sharp peak at $\delta = -26.4$ ppm, where F^- essentially behaves as a naked ion with very little coordination to the silicon atoms.²⁹

Building on this work, Bowers et al synthesized a new series of F^- encapsulated cubes (for reasons discussed further below), $\text{F}^-@(\text{RSiO}_{1.5})_8$, where R = vinyl, phenyl, styrenyl, trifluoropropyl, nonafluorohexyl, or tridecafluorooctyl by reaction of tetramethylammonium fluoride (TMAF) and the corresponding R_8T_8 cage (Scheme 6.1b).^{30a} While they report that the synthesis works well for electron withdrawing substituents, they find that it fails when R is an electron donating group (R = ethyl, cyclohexyl, and *i*-butyl).

Modeling studies of $(\text{RSiO}_{1.5})_8$ ($\text{R} = \text{H}, \text{F}, \text{HO}, \text{NH}_2, \text{alkyl}, \text{etc.}$) done by multiple groups³¹⁻³⁵ find that the $(\text{RSiO}_{1.5})_8$ HOMO involves the $2p$ lone pair states on the oxygen atoms and lies on the edges of the cubes (Figure 6.2a). These studies also find that the LUMO involves contributions from all Si, oxygen atoms, and the R substituents, is spherical and resides in the cube center (Figure 6.2b).³¹⁻³⁵ Bassindale has suggested that fluoride interaction with an electrophilic LUMO may account for the stability of F^- encapsulated silsesquioxanes.²⁹ Furthermore, the presence of an electronically accessible “core” state may also explain the unique red-shifted emission behavior of silsesquioxanes as discussed further below.

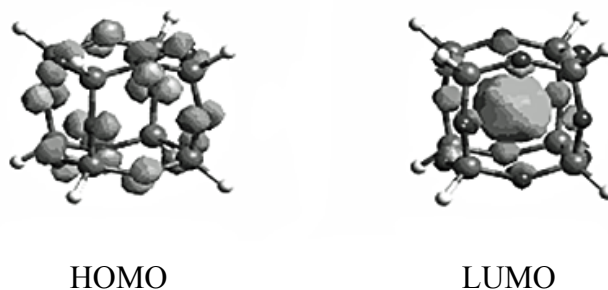


Figure 6.2. (a) HOMO and (b) LUMO of $[\text{XSiO}_{1.5}]_8$.³⁴

While the mechanism of fluoride inclusion is uncertain, it is clearly much more complicated than a simple insertion through the cube face. Figure 6.3a shows the ^{29}Si NMR spectrum of F^- encapsulated OPS and octavinylsilsesquioxane (OVS) after mixing with THF.^{30a} The sharp peaks at ~ -81 and ~ -83 ppm correlate to the eight equivalent silicon atoms in $\text{F}^-@OPS$ and $\text{F}^-@OVS$, respectively. The numerous small peaks between those of the pure starting materials suggest that many compounds with mixed phenyl and vinyl groups are generated in solution after mixing.

Similarly, Figure 6.3b shows a complex signal pattern when pure OPS and OVS are mixed in the presence of stoichiometric TMAF in THF. In this instance, no pure F^- encapsulated compounds are detected. However, Bowers et al suggest that the broad

multiplet between ~ -81 and ~ -83 ppm represents a complex mixture of compounds resulting from cage scrambling.^{30a}

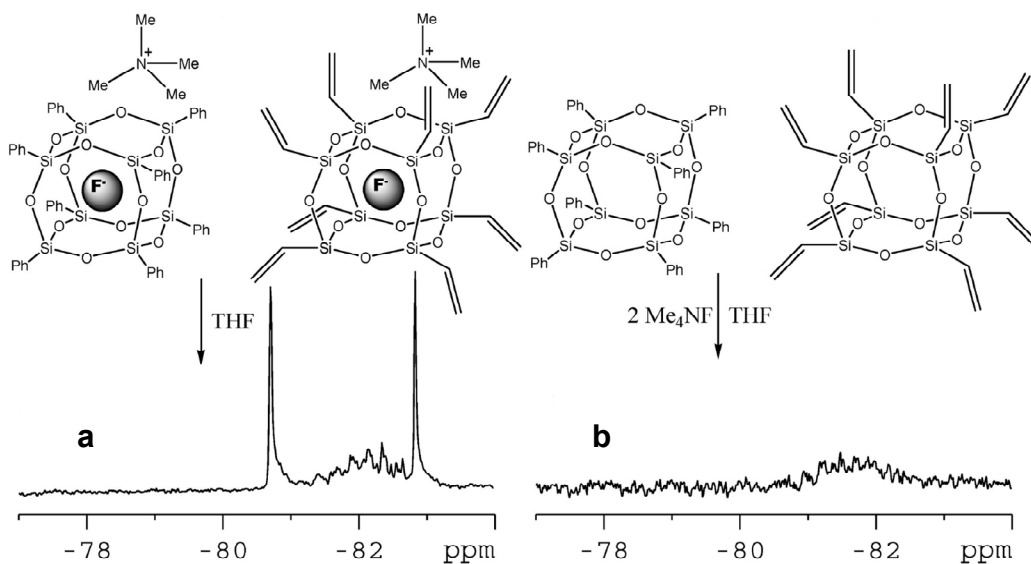


Figure 6.3. (a) ^{29}Si NMR spectrum obtained from mixing F⁻@OPS and F⁻@OVS in THF and the (b) spectrum obtained from mixing TMAF with equivalent amounts of OPS and OVS in THF. Adapted from Reference 30a.

The ESI mass spectrum (Figure 6.4) observed from the reaction of $(i\text{-Bu})_7(\text{C}_6\text{H}_5\text{CH}=\text{CH}_2)_1\text{T}_8$ and TMAF provides further evidence for F⁻-mediated cage rearrangement.^{30a} The spectrum shows peaks corresponding to F⁻@(*i*-Bu)₆Styrl₂, F⁻@(*i*-Bu)₅Styrl₃, and F⁻@(*i*-Bu)₄Styrl₄ T₈ side-products in addition to the structure of the target F⁻@(*i*-Bu)₇Styrl₁ T₈ cage. The presence of additional side products having mixed functionalities can only be reasonably explained by the complex scrambling of the original starting material catalyzed by F⁻.

The instability of F⁻@(RSiO_{1.5})₈ compounds as illustrated in Figures 6.3 and 6.4 suggests dynamic F⁻-mediated rearrangements of the silsesquioxanes in solution. It is likely that the fluoride ion catalyzes the exchange of RSiO- groups among cages, perhaps also assisted by traces of water. The authors report that scrambling is not observed when anhydrous THF is used.^{30a}

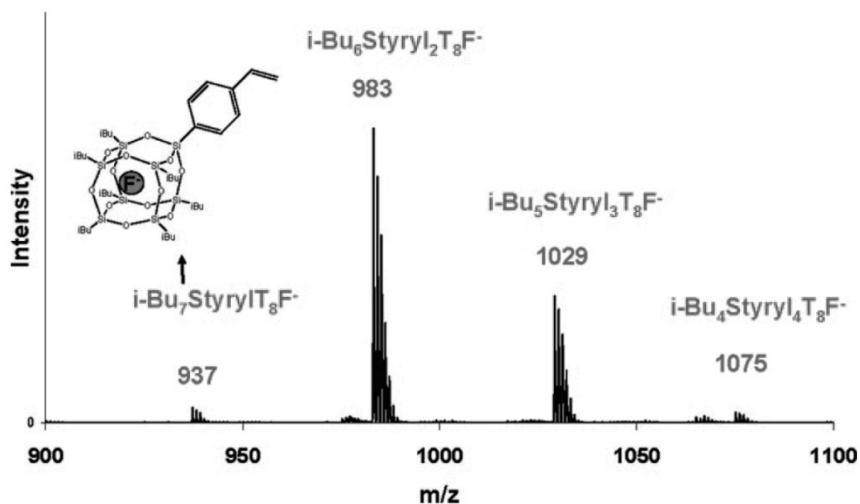


Figure 6.4. ESI mass spectrum of fluoride species derived from reaction of (*i*-Bu)₇(C₆H₅CH=CH₂)₁ T₈ and TMAF. Adapted from Reference 30a.

The work presented here seeks to take advantage of the phenomenon of F⁻-mediated silsesquioxane rearrangement in order to synthesize multifunctional cage compounds with controlled distribution of functionalities. Judging from the observations reported by Bowers et al.,^{30a} we anticipated that the number and type of functional groups on the target molecule could be controlled statistically by manipulating the ratio of silsesquioxanes prior to equilibration with F⁻. As we demonstrate below, success in our approach offers direct access to a potentially new class of multifunctional compounds with one, two (or more) distinct functionalities that may later be modified through chemical synthesis. These functional cages in turn can serve as possible platforms to: (1) thermally stable, linear, and soluble silsesquioxane polymers with the capability of being spin/spray/dip-coated, cast, drawn, etc.; (2) low T_m, alkylated silsesquioxane polymers for high temperature lubrication applications, as was previously demonstrated for OPS;^{11b} (3) silsesquioxane polymers functionalized with liquid crystalline (LC) mesogens for the fabrication of unique LC polymeric materials, etc.^{11c}

The synthesis of fluorescent silsesquioxane oligomers described below is meant to be representative of the unique and unlimited utility of these compounds. A further goal of the work initiated here is to explore the unusual luminescence behavior of these

materials. The exceptional red-shifted emission behavior associated with these compounds has significant scientific implications as discussed further in this chapter.

Silsesquioxane cages with two reactive functionalities are important because they are possible platforms to “string of beads” silsesquioxane polymers, where cages are directly incorporated along the backbone of the polymer chain. Reactive monofunctional silsesquioxanes, on the other hand, are typically used as co-polymerizable pendant groups for traditional polymer systems.^{36,37} They are readily prepared from “corner capping” reactions of partially condensed trisilanol cages and monofunctional trichlorosilanes. Relatively few polymers with cages along the chain backbone have been reported, however, because known routes to reactive difunctional cage compounds are rare and/or inefficient. For example, the polymerizable disilanol cage of Figure 6.5 is synthesized in only 15% yield after 12 weeks.³⁸

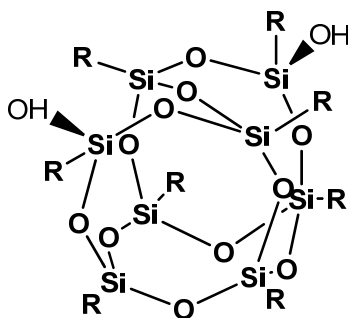
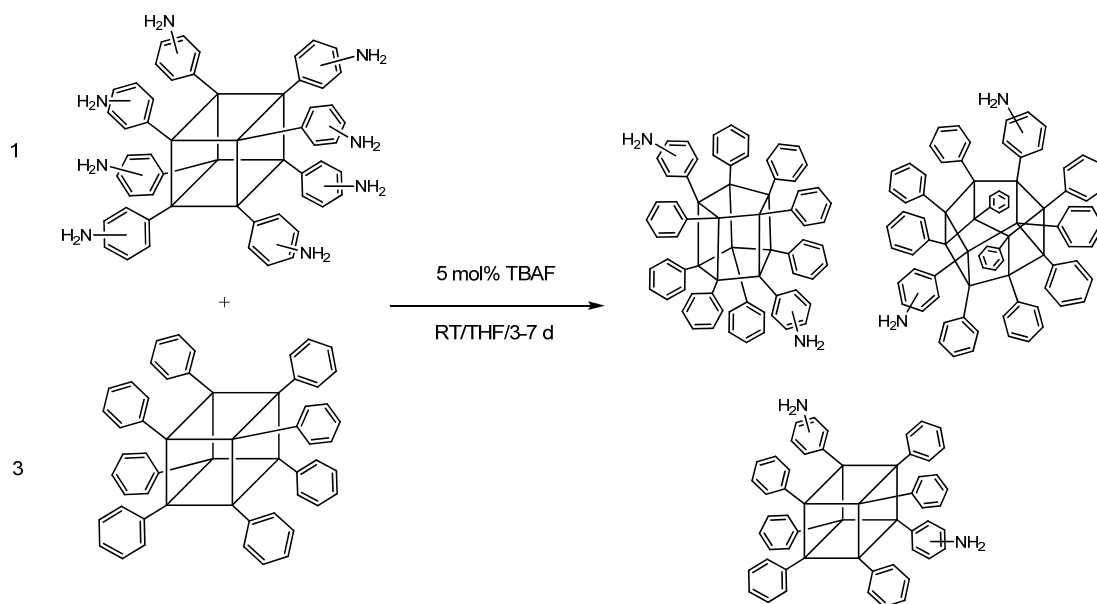


Figure 6.5. Disilanol silsesquioxane monomer ($R = c\text{-C}_6\text{H}_{11}$).³⁸

Currently, our group is investigating fluoride-catalyzed rearrangements to synthesize silsesquioxanes with mixed functional groups and controlled stoichiometries from OPS and octa(aminophenyl)silsesquioxane (OAPS; see Scheme 6.2).³⁹ Diamino cage compounds are potential platforms to thermally stable, soluble, and high molecular weight silsesquioxane polymers via reaction with dianhydrides or diepoxides. T_8 silsesquioxane nanocomposites based on imide^{11d,e} and amine/epoxy^{11a,f} chemistries have already been shown to demonstrate enhanced thermal and/or mechanical properties. We

have extended this work further by using the by-products of OPS and OVS syntheses as starting materials in a possible route to fluorescent cages and/or linear silsesquioxane oligomers as described further in **Section 6.3**.



Scheme 6.2. F⁻-mediated reaction of OPS and OAPS with TBAF.³⁹

Polyphenylsilsesquioxane (PPS) and polyvinylsilsesquioxane (PVS) are attractive precursors in fluoride-mediated rearrangement reactions, as they provide access to functionalized silsesquioxane *cages* originating from generally “useless” polymeric starting materials. PPS is a by-product in the synthesis of OPS, which is formed in 10-20% yield from the 60 h reaction of phenyltriethoxysilane, 7.5 wt% KOH, and 10 wt% H₂O in refluxing toluene.⁴⁰ It has the general formula (C₆H₅SiO_{1.5})_n and is reported to contain a mixture of linear chain, open-caged, and/or ladder-like structures.⁴¹ In these studies, “n” ≈ 15 for PPS (determined by GPC analysis).

Similarly, PVS is formed as a by-product in the synthesis of OVS, attained from the hydrolysis of vinyltriethoxysilane in ethanol/H₂O solution.⁴² PVS is formed as a methanol-soluble by-product in 60-70% yields. While the structure of PVS has not yet

been studied in detail, it has the fully condensed general formula $(C_2H_3SiO_{1.5})_n$. In these studies, “n” \approx 16 for PVS (determined by GPC analysis).

6.2 Experimental

6.2.1 Materials

Polyphenylsilsesquioxane (PPS) and polyvinylsilsesquioxane (PVS) were synthesized according to previously described methods.^{40,42} A first generation Grubbs catalyst $[RuCl_2(=CHPh)(PCy_3)_2]$, 1.0 M tetrabutylammonium fluoride (TBAF, \sim 5 wt% H_2O) in THF, and vinyltriethoxysilane were purchased from Aldrich and used as received. All other solvents were purchased from Fisher or Aldrich and used as received. All work was performed under nitrogen unless otherwise stated.

6.2.2 Synthetic Methods

6.2.2.1 Synthesis of Vinyl_xPh₁ (x = 9, 11) T₁₀ and T₁₂ Silsesquioxanes

PPS (1.00 g, 7.7 mmol) and PVS (7.0 g, 88.5 mmol) were placed in a dry 250 mL round bottom flask equipped with magnetic stirrer and condenser. The flask was evacuated and flushed three times with N_2 . THF (100 mL) and 0.96 mL (1.0 M in THF, 0.96 mmol) of 95% TBAF were added via syringe. The reaction mixture was stirred at room temperature for 48 h. $CaCl_2$ (0.8 g, 7.2 mmol) was added to the reaction mixture and stirred an additional 2 h. The insolubles (\sim 1 g) were then gravity filtered and the filtrate was removed under reduced pressure. The solid residue was dissolved in \sim 15 mL of THF and precipitated into 300 mL MeOH. The precipitated products were collected and dried *in vacuo* to give a white powder (7.05 g, 88% with respect to total initial mass of reactants). Characterization data: 1H NMR (400 MHz, CD_3Cl): 5.6-6.2 (br, - $CH=CH_2$), 6.9 (br, Ar-H); 7.4 (br, Ar-H); 7.6 (br, Ar-H). ^{13}C NMR: 126.9 (Ar-C), 130.2

(-Si-CH=CH₂), 130.7 (Ar-C), 139.8 (Ar-C), 136.0 (CH=CH₂) ppm. MALDI-TOF: *m/z* (Ag⁺ adduct) = 899 [AgSi₁₀O₁₅(C₂H₃)₁₀], 949 [AgSi₁₀O₁₅-(C₂H₃)₉(C₆H₅)₁], 999 [AgSi₁₀O₁₅(C₂H₃)₈(C₆H₅)₂], 1057 [AgSi₁₂O₁₈(C₂H₃)₁₂], 1107 [AgSi₁₂O₁₈(C₂H₃)₁₁(C₆H₅)₁], 1157 [AgSi₁₂O₁₈-(C₂H₃)₁₀(C₆H₅)₂] amu. GPC (found): M_n 1026; M_w 1077; PDI 1.05 (see also **Table 6.6**).

6.2.2.2 Synthesis of Vinyl₁Ph_x (x = 9, 11) T₁₀ and T₁₂ Silsesquioxanes

PPS (15.0 g, 116 mmol) and PVS (1.0 g, 12.6 mmol) were placed in a dry 250 mL round bottom flask equipped with magnetic stirrer and condenser. The flask was evacuated and flushed three times with N₂. THF (100 mL) and 1.29 mL (1.0 M in THF, 1.29 mmol) of 95% tetrabutylammonium fluoride were added via syringe. The reaction mixture was stirred at room temperature for 48 h. CaCl₂ (0.8 g, 7.2 mmol) was added to the reaction mixture and stirred an additional 2 h. The insolubles (~5 g) were then gravity filtered and the filtrate was removed under reduced pressure. The solid residue was dissolved in ~15 mL of THF and precipitated into 300 mL MeOH. The precipitated products were collected and dried *in vacuo* to give a white powder (11.52 g, 72% with respect to total initial mass of reactants). Characterization data: ¹H NMR (400 MHz, CD₃Cl): 5.8-6.1 (br, -CH=CH₂), 7.1-7.8 (br, Ar-H). ¹³C NMR: 127.0 (Ar-C), 130.0 (-Si-CH=CH₂), 130.6 (Ar-C), 134.0 (Ar-C), 136.1 (-CH=CH₂) ppm. MALDI-TOF: *m/z* (Ag⁺ adduct) = 1141 [AgSi₈O₁₂(C₆H₅)₈], 1299 [AgSi₁₀O₁₅-(C₂H₃)₂(C₆H₅)₈], 1349 [AgSi₁₀O₁₅(C₂H₃)₁(C₆H₅)₉], 1399 [AgSi₁₀O₁₅(C₆H₅)₁₀], 1557 [AgSi₁₂O₁₈(C₂H₃)₂(C₆H₅)₁₀], 1607 [AgSi₁₂O₁₈(C₂H₃)₁(C₆H₅)₁₁], 1658 [AgSi₁₂O₁₈-(C₆H₅)₁₂] amu. GPC (found): M_n 725; M_w 754; PDI 1.04 (see also **Table 6.6**).

6.2.2.3 Synthesis of Vinyl₂Ph_x (x = 8, 10) T₁₀ and T₁₂ Silsesquioxanes

PPS (7.24 g, 56.0 mmol) and PVS (1.0 g, 12.6 mmol) were placed in a dry 250 mL round bottom flask equipped with magnetic stirrer and condenser. The flask was evacuated and flushed three times with N₂. THF (100 mL) and 0.69 mL (1.0 M in THF, 0.69 mmol) of 95% tetrabutylammonium fluoride were added via syringe. The reaction

mixture was stirred at room temperature for 48 h. CaCl₂ (0.8 g, 7.2 mmol) was added to the reaction mixture and stirred an additional 2 h. The insolubles (~3 g) were then gravity filtered and the filtrate was removed under reduced pressure. The solid residue was dissolved in ~15 mL of THF and precipitated into 300 mL MeOH. The precipitated products were collected and dried *in vacuo* to give a white powder (6.67 g, 81% with respect to total initial mass of reactants). The products were further purified by column chromatography (silica, 1:10 THF:hexane) and followed by TLC. Characterization data: ¹H NMR (400 MHz, CD₃Cl): 5.2-6.3 (br, -CH=CH₂), 6.6-8.1 (br, Ar-H). ¹³C NMR: 127.0 (Ar-C), 130.0 (-Si-CH=CH₂), 130.7 (Ar-C), 133.8 (Ar-C), 136.3 (-CH=CH₂) ppm. IR: νC=H (3066-2917), νC=C (Ar ring, 1591), νC=C (Ar ring, 1429), νSi-O (1132), νSi-C (729) cm⁻¹. MALDI-TOF: *m/z* (Ag⁺ adduct) = 1199 [AgSi₁₀O₁₅(C₂H₃)₄(C₆H₅)₆], 1249 [AgSi₁₀O₁₅(C₂H₃)₃(C₆H₅)₇], 1299 [AgSi₁₀O₁₅-(C₂H₃)₂(C₆H₅)₈], 1349 [AgSi₁₀O₁₅-(C₂H₃)₁(C₆H₅)₉], 1399 [AgSi₁₀O₁₅(C₆H₅)₁₀], 1458 [AgSi₁₂O₁₈(C₂H₃)₄(C₆H₅)₈], 1507 [AgSi₁₂O₁₈(C₂H₃)₃(C₆H₅)₉], 1557 [AgSi₁₂O₁₈-(C₂H₃)₂(C₆H₅)₁₀] amu. GPC (found): M_n 986; M_w 1005; PDI 1.02 (see also **Table 6.6**). TGA (air, 1000 °C): found 49.4%; T_{d5%} = 459 °C (see also **Table 6.7**).

6.2.2.4 Metathesis Reaction of Vinyl₂Ph_x (x = 8, 10) T₁₀ and T₁₂ Silsesquioxanes and 4-Bromostyrene

Vinyl₂Ph_x (x = 8, 10) T₁₀ and T₁₂ silsesquioxanes (1.00 g) and 52 mg of first generation Grubb's catalyst⁴³ (0.13 mmol) were added to a dry 50 mL Schlenk flask under N₂. Dry CH₂Cl₂ (20 mL) was added by syringe followed by 4-bromostyrene (2.48 mL, 19.0 mmol). The mixture was stirred at room temperature for 72 h and then quenched by precipitation into 300 mL of MeOH. The solution was filtered and the products (0.98 g) were purified by column chromatography (silica, 1.5:8.5 THF:hexane) and followed by TLC. Characterization data: ¹H NMR (400 MHz, CD₃Cl): 5.2-6.1 (br, -CH=CH), 6.5-8.0 (br, Ar-H). ¹³C NMR: 121.9 (-C-Br), 126.5 (Ar-C), 127.0 (Ar-C), 130.8 (-Si-CH=CH-), 131.9 (Ar-C), 132.0 (Ar-C), 134.0 (Ar-C), 136.0 (-Si-CH=CH-) ppm. IR: νC=H (3079-2958), νC=C (Ar ring, 1593), νC=C (Ar ring, 1429), νSi-O (1132), νSi-C (731) cm⁻¹. MALDI-TOF: *m/z* (Ag⁺ adduct) = 1399 [AgSi₁₀O₁₅(C₆H₅)₁₀],

1505 [AgSi₁₀O₁₅(C₈H₆Br)₁(C₆H₅)₉], 1610 [AgSi₁₀O₁₅(C₈H₆Br)₂(C₆H₅)₈], 1763 [AgSi₁₂O₁₈(C₈H₆Br)₁(C₆H₅)₁₁], 1867 [AgSi₁₂O₁₈(C₈H₆Br)₂(C₆H₅)₁₀] amu. GPC (found): M_n 1383; M_w 1437; PDI 1.04 (see also **Table 6.6**). TGA (air, 1000 °C): found 40.1%; T_{d5%} = 303 °C (see also **Table 6.7**).

6.2.2.5 Self-Metathesis Reaction of Vinyl₂Ph_x (x = 8, 10) T₁₀ and T₁₂ Silsesquioxanes

Vinyl₂Ph_x (x = 8, 10) T₁₀ and T₁₂ silsesquioxanes (1.00 g) and 52 mg of first generation Grubb's catalyst⁴³ (0.13 mmol) were added to a dry 50 mL Schlenk flask under N₂. Dry CH₂Cl₂ (20 mL) was added by syringe. The mixture was stirred at room temperature for 72 h and then quenched by precipitation into 300 mL of MeOH. The solution was filtered and the recovered solid was analyzed by GPC, TGA, and MALDI, which confirmed only the presence of unreacted starting materials [vinyl₂Ph_x (x = 8, 10) T₁₀ and T₁₂ silsesquioxanes].

6.2.2.6 Heck Reaction of BrStyr₂Ph_x (x = 8, 10) T₁₀ and T₁₂ Silsesquioxanes and Vinyl₂Ph_x (x = 8, 10) T₁₀ and T₁₂ Silsesquioxanes

To a dry 50 mL Schlenk flask under N₂ was added 0.50 g of BrStyr₂Ph_x (x = 8, 10) T₁₀ and T₁₂, 19 mg (0.04 mmol) of Pd[P(*t*-Bu₃)]₂, and 18 mg (0.02 mmol) of Pd₂(dba)₃. 1,4-dioxane (10 mL) was then added by syringe, followed by NCy₂Me (2.11 mmol, 0.45 mL) and 0.40 g of vinyl₂Ph_x (x = 8, 10) T₁₀ and T₁₂. The mixture was stirred at room temperature for 72 h and then filtered through 1 cm celite, which was washed with 5 mL of THF. The solution was then quenched by precipitation into 300 mL of methanol and filtered and the solid redissolved in 10 mL of THF. This solution was then filtered again through a 1 cm celite column to remove any remaining Pd particles and reprecipitated into 200 mL of methanol. The products were further purified by column chromatography (silica, 1:10 THF:hexane) and followed by TLC, collected, and dried *in vacuo* to give a white powder (0.72 g). Characterization data: ¹H NMR (400 MHz, CD₃Cl): 5.1-6.3 (br, -CH=CH), 6.5-7.9 (br, Ar-H). ¹³C NMR: 127.3 (Ar-C), 129.0-132.0 (Ar-C), 134.0 (Ar-C) ppm. IR: νC=H (3077-2979), νC=C (Ar ring, 1591), νC=C (Ar ring, 1429), νSi-O

(1132), $\nu_{\text{Si-C}}$ (731) cm^{-1} . MALDI-TOF: m/z (Ag^+ adduct) = 1399 [$\text{AgSi}_{10}\text{O}_{15}(\text{C}_6\text{H}_5)_{10}$], 1505 [$\text{AgSi}_{10}\text{O}_{15}(\text{C}_8\text{H}_6\text{Br})_1(\text{C}_6\text{H}_5)_9$], 1763 [$\text{AgSi}_{12}\text{O}_{18}\text{C}_8\text{H}_6\text{Br})_2-(\text{C}_6\text{H}_5)_{10}$], 2593, 2697, 2797, 2849, 3003 amu. GPC (found): M_n 2973; M_w 3716; PDI 1.25 (see also **Table 6.6**). TGA (air, 1000 °C): found 45.0%; $T_{d5\%} = 325$ °C (see also **Table 6.7**).

6.2.2.7 Heck Reaction of $\text{BrStyr}_2\text{Ph}_x$ ($x = 8, 10$) T_{10} and T_{12} Silsesquioxanes and Vinyltriethoxysilane

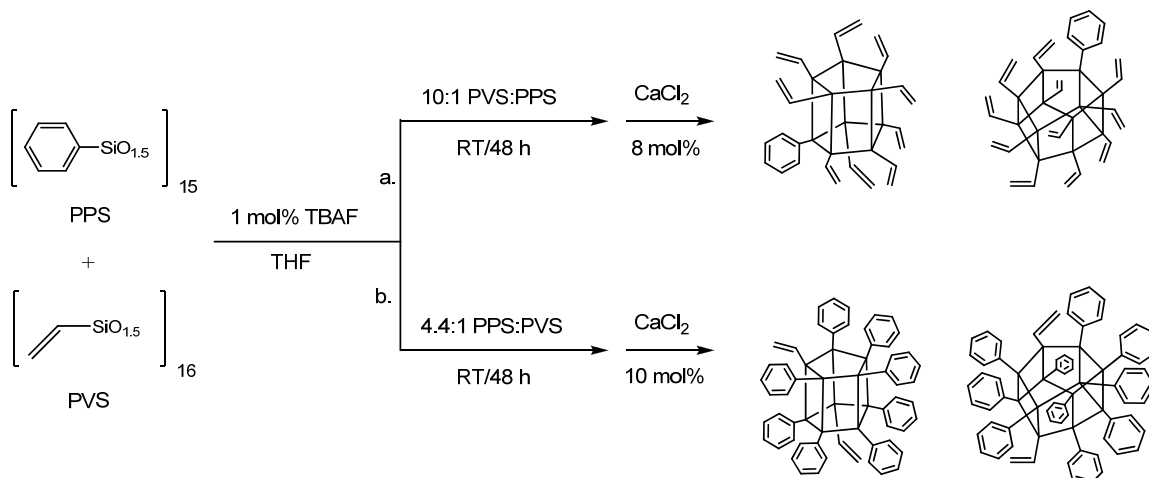
To a dry 50 mL Schlenk flask under N_2 was added 0.50 g of $\text{BrStyr}_2\text{Ph}_x$ ($x = 8, 10$) T_{10} and T_{12} , 19 mg (0.04 mmol) of $\text{Pd}[\text{P}(t\text{-Bu}_3)]_2$, and 18 mg (0.02 mmol) of $\text{Pd}_2(\text{dba})_3$. 1,4-dioxane (10 mL) was then added by syringe, followed by NCy_2Me (2.11 mmol, 0.45 mL) and 0.38 mL (2 mmol) of vinyltriethoxysilane. The mixture was stirred at room temperature for 72 h and then filtered through 1 cm celite, which was washed with 5 mL of THF. The solution was then quenched by precipitation into 300 mL of methanol and filtered and the solid redissolved in 10 mL of THF. This solution was then filtered again through a 1 cm celite column to remove any remaining Pd particles and reprecipitated into 200 mL of methanol. The products were further purified by column chromatography (silica, 1:10 THF:hexane) and followed by TLC, collected, and dried *in vacuo* to give a white powder (0.58 g). Characterization data: ^1H NMR (400 MHz, CD_3Cl): 1.2 (s, 3.6 H, $-\text{CH}_3$), 1.3 (s, 5.4 H, $-\text{CH}_3$), 3.8 (s, 2.4 H, $-\text{OCH}_2\text{CH}_3$), 3.9 (s, 3.6 H, $-\text{OCH}_2\text{CH}_3$), 5.1-6.3 (br, 4 H, $-\text{CH}=\text{CH}$), 6.4-7.9 (br, 68 H, Ar-H). ^{13}C NMR: 18.0 ($-\text{CH}_3$), 58.8 ($-\text{OCH}_2\text{CH}_3$), 127.3 (Ar-C), 129.0-132.0 (Ar-C), 134.1 (Ar-C), 136.1 ($-\text{CH}=\text{CH}$) ppm. IR: $\nu_{\text{C}=\text{H}}$ (3087-2985), $\nu_{\text{C}-\text{H}}$ (2981-2811), $\nu_{\text{C}=\text{C}}$ (Ar ring, 1591), $\nu_{\text{C}=\text{C}}$ (Ar ring, 1431), $\nu_{\text{Si}-\text{O}}$ (1132), $\nu_{\text{Si}-\text{C}}$ (737) cm^{-1} . MALDI-TOF: m/z (Ag^+ adduct) = 1399 [$\text{AgSi}_{10}\text{O}_{15}(\text{C}_6\text{H}_5)_{10}$], 1614 [$\text{AgSi}_{10}\text{O}_{15}(\text{C}_6\text{H}_5)_9(\text{C}_{16}\text{H}_{23}\text{O}_3\text{Si})_1$], 1828 [$\text{AgSi}_{10}\text{O}_{15}-(\text{C}_6\text{H}_5)_8(\text{C}_{16}\text{H}_{23}\text{O}_3\text{Si})_2$], 1872 [$\text{AgSi}_{10}\text{O}_{15}(\text{C}_6\text{H}_5)_{11}(\text{C}_{16}\text{H}_{23}\text{O}_3\text{Si})_1$], 2086 [$\text{AgSi}_{10}\text{O}_{15}-(\text{C}_6\text{H}_5)_{10}(\text{C}_{16}\text{H}_{23}\text{O}_3\text{Si})_2$] amu. GPC (found): M_n 1441; M_w 1527; PDI 1.06 (see also **Table 6.6**). TGA (air, 1000 °C): found 40.5%; $T_{d5\%} = 351$ °C (see also **Table 6.7**).

6.3 Results and Discussion

The unexpected discovery of a trapped fluoride ion in the center of silsesquioxane cages by Bassindale was initially motivated by efforts to improve silsesquioxane yields from alkoxy silanes.^{25,29a} Bowers' incorporation of F⁻ into cubes, however, targeted increasing the ionization efficiency of silsesquioxane-containing oligomers and polymers for study by mass spectrometry.^{30a} Though it is known that polyhedral silsesquioxanes are easily detected by MALDI-TOF MS, high molecular weight silsesquioxane-containing polymers are not readily ionizable.³⁰ Bowers previously reported the MALDI characterization of only two silsesquioxane oligomer systems (based on propylmethacrylates and siloxanes), having weakly detected systems with a maximum of only three cages.^{30b,c} We also observed similar difficulties detecting silsesquioxane oligomers by MALDI as described further in **Section 6.3.4**.

Bowers et al anticipated, therefore, that incorporation of fluoride ions into the cages of silsesquioxane-containing polymers would increase their ionization efficiencies (or reduce the mass to charge ratio of the ions), making the resulting samples easier to detect by MALDI-TOF MS. The scrambling of cages by F⁻ that they observed (see **Section 6.1**) serves as the inspiration for the work reported here.

Below we describe a simple and direct route to fluorescent silsesquioxane oligomers by reaction of TBAF with stoichiometrically-controlled amounts of PPS and PVS, followed by CaCl₂ workup to capture F⁻ (Scheme **6.3**). Failure to capture F⁻ after cage synthesis leads to further rearrangement and to resins of uncharacterizable products following solvent removal.³⁹ Subsequent chemical modification of the pendant organic tethers by olefin metathesis (Scheme **6.4**) and Heck coupling leads to a “string of beads” silsesquioxane oligomer (Scheme **6.6**). As depicted in Schemes **6.3**, **6.4**, and **6.6**, a single product from the fluoride ion-mediated rearrangement of PPS and PVS is not observed, but rather the result is a mixture of predominantly the T₁₀ and T₁₂ cages as described further below.



Scheme 6.3. Fluoride-mediated rearrangement of PPS and PVS to (a) vinyl_xPh₁ (x = 9, 11) T₁₀ and T₁₂ and (b) vinyl₂Ph_x (x = 8, 10) T₁₀ and T₁₂ silsesquioxanes.

6.3.1 Synthesis of Vinyl_xPh₁ (x = 9, 11) T₁₀ and T₁₂ Silsesquioxanes

In efforts to synthesize cages having ~2 phenyl groups (with vinyl groups as the remaining moieties), a 10:1 mole ratio of PVS:PPS was reacted with 1 mol% TBAF in THF (RT/48 h; Scheme 6.3a). A minimum amount of TBAF was used to reduce the chance of residual F⁻ catalyzing unwanted side products during workup (as previously described). An 8-10 mol% excess of CaCl₂ was used to trap F⁻ after completion of the reaction. Ca⁺² reacts with F⁻ to form the insoluble CaF₂ salt, allowing for easy removal of fluoride ion from the products. Similarly, Cl⁻ reacts to form insoluble tetrabutylammonium chloride. The successful trapping of fluoride ion by CaCl₂ workup was confirmed by an absence of peaks in the ¹⁹F NMR spectrum. The products were non-crystalline as XRD powder patterns exhibited only amorphous scattering.

The MALDI-TOF spectrum of the products of a 10:1 PVS:PPS reaction is shown in Figure 6.6 and the most common isotopes are listed in Table 6.1. Small discrepancies (<1 Da) between “found” and “calculated” values listed in Table 6.1 may be due to ionization potential differences in the experimental situation or possibly errors in calibration. The Figure 6.6 MALDI spectrum shows that the reaction does not give single cube products as anticipated, but rather a mixture of T₁₀ and T₁₂ cages with the

dominant ionizable species being the unsubstituted deca- and dodecavinylsilsesquioxanes and monophenyl compounds. While MALDI indicates the presence of the intended diphenyl T₁₀ and T₁₂ compounds, no T₈ cages are observed under these reaction conditions, perhaps indicating a preferential, thermodynamically-controlled reaction pathway to T₁₀ and T₁₂ cages. Unlabeled peaks in Figure 6.6 correspond to fragments generated by the MALDI laser, mainly from loss of 1-2 vinyl (-CH=CH₂) groups from the T₁₀ cages.

It is important to note that the *absolute* quantities of T₈, T₁₀, and T₁₂ in the product mixture cannot be determined by MALDI alone because the distribution patterns are not perfectly quantitative. It is well-known that the peak heights in MALDI-TOF MS correspond to the ionization efficiencies of the species and are not necessarily representative of the amounts of each in the sample. However, since silsesquioxane monomers are readily ionizable and many have been successfully characterized by MALDI techniques by us^{39,40,49} and others,³⁰ we can use the MALDI peak heights as a relative (qualitative) measure of the amounts of each species in the monomeric sample.

Mono- and diphenylvinyl T₁₀ and T₁₂ compounds are potentially useful as thermally stable, high density cross-linking agents or as platforms to 3-D “star” type materials.⁴⁹ Furthermore, the synthesis of such compounds demonstrates the ability to tailor the numbers and types of functional groups on the silsesquioxane cages by simply altering the ratio of the polymeric starting materials. This capability is further demonstrated below in the synthesis of the related divinylphenyl T₁₀ and T₁₂ cages, which serve as the starting materials for both cross metathesis (Scheme 6.4) and Heck coupling (Scheme 6.6) leading to the “string of beads” fluorescent oligomers described further in Section 6.3.4.

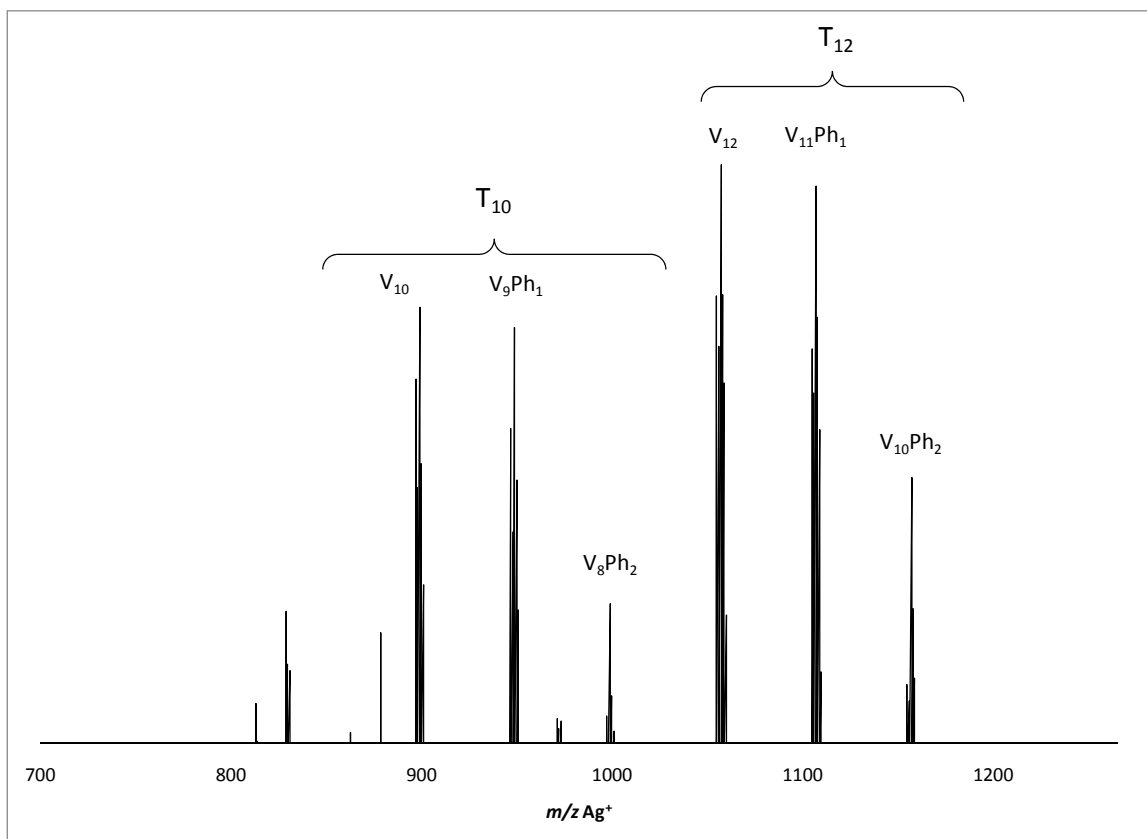


Figure 6.6. MALDI-TOF spectrum of 10:1 PVS:PPS reaction with TBAF (RT/48 h). The major products detected are the deca/dodecavinyl and monophenylvinyl T₁₀ and T₁₂ cages.

Table 6.1. MALDI-TOF data (Ag⁺ Adduct) for 10:1 PVS:PPS reaction with TBAF.

Most Common Isotope	Found (Da)	Calculated (Da)	Relative Peak Intensity (%)
(CH ₂ =CH) ₁₀ (SiO _{1.5}) ₁₀	898.8	899.2	77
(CH ₂ =CH) ₉ (C ₆ H ₅) ₁ (SiO _{1.5}) ₁₀	948.8	949.2	73
(CH ₂ =CH) ₈ (C ₆ H ₅) ₂ (SiO _{1.5}) ₁₀	998.8	999.3	28
(CH ₂ =CH) ₁₂ (SiO _{1.5}) ₁₂	1056.9	1057.4	100
(CH ₂ =CH) ₁₁ (C ₆ H ₅) ₁ (SiO _{1.5}) ₁₂	1106.9	1107.5	97
(CH ₂ =CH) ₁₀ (C ₆ H ₅) ₂ (SiO _{1.5}) ₁₂	1156.9	1157.5	49

6.3.2 Synthesis of Vinyl₂Ph_x (x = 8, 10) T₁₀ and T₁₂ Silsesquioxanes

A 10:1 mole ratio of PPS:PVS was reacted with 1 mol% TBAF in THF (RT/48 h) and gave results analogous to the 10:1 PVS:PPS reaction, with monovinyl compounds being the major products according to MALDI-TOF MS (see Figure 6.7 and Table 6.2). MALDI also detects the presence of T₈ cube in addition to the T₁₀ and T₁₂ species.

The MALDI spectrum of Figure 6.7 also shows the presence of OPS, decaphenyl- and dodecaphenylsilsesquioxane (DPS) species as by-products of the synthesis. Divinyl compounds of the T₁₀ and T₁₂ cages are also observed.

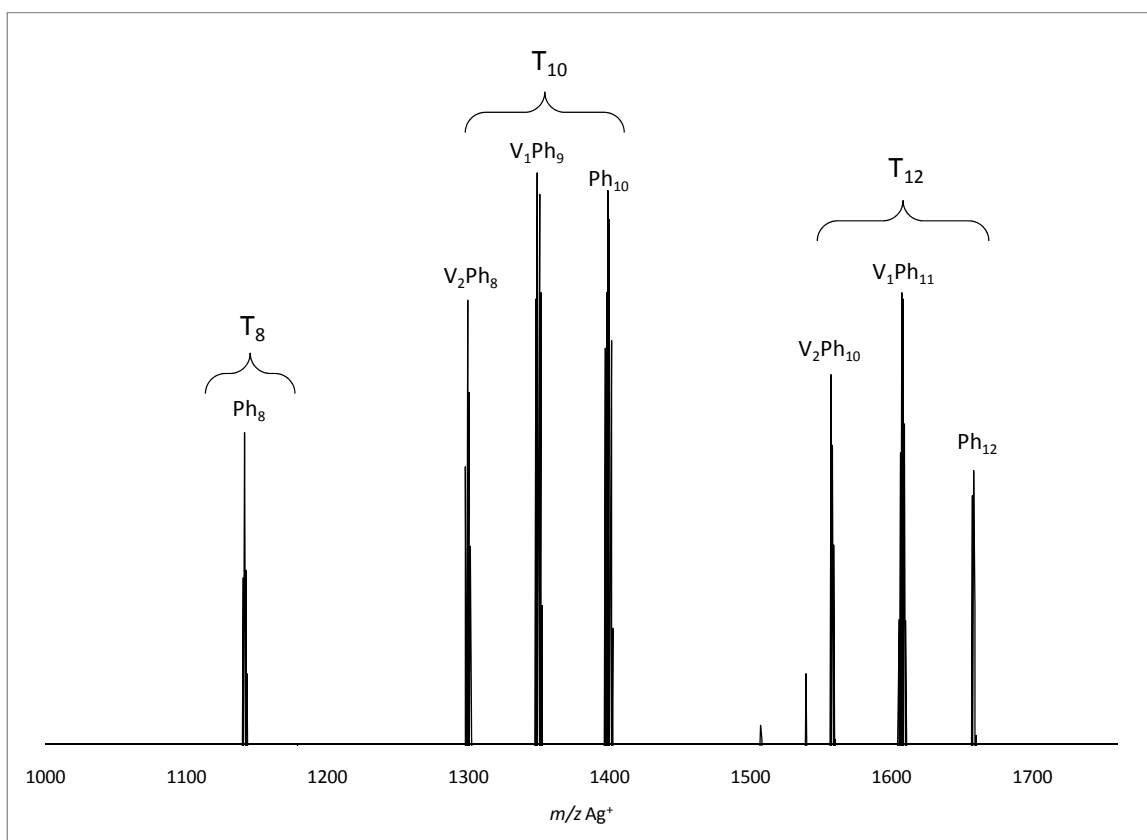


Figure 6.7. MALDI-TOF spectrum of 10:1 PPS:PVS reaction with TBAF (RT/48 h).

Table 6.2. MALDI-TOF data (Ag^+ Adduct) for 10:1 PPS:PVS reaction with TBAF.

Most Common Isotope	Found (Da)	Calculated (Da)	Relative Peak Intensity (%)
$(\text{C}_6\text{H}_5)_8(\text{SiO}_{1.5})_8$	1141.1	1141.4	60
$(\text{CH}_2=\text{CH})_2(\text{C}_6\text{H}_5)_8(\text{SiO}_{1.5})_{10}$	1299.2	1299.6	80
$(\text{CH}_2=\text{CH})_1(\text{C}_6\text{H}_5)_9(\text{SiO}_{1.5})_{10}$	1349.2	1349.7	100
$(\text{C}_6\text{H}_5)_{10}(\text{SiO}_{1.5})_{10}$	1399.2	1399.8	97
$(\text{CH}_2=\text{CH})_2(\text{C}_6\text{H}_5)_{10}(\text{SiO}_{1.5})_{12}$	1557.2	1558.0	68
$(\text{CH}_2=\text{CH})_1(\text{C}_6\text{H}_5)_{11}(\text{SiO}_{1.5})_{12}$	1607.3	1608.1	81
$(\text{C}_6\text{H}_5)_{12}(\text{SiO}_{1.5})_{12}$	1658.3	1658.1	55

Monovinyl silsesquioxane compounds offer potential use as organic-inorganic hybrid monomers for polymerization reactions and/or in the preparation of block copolymers, for example. They can be also used as pendant or end-cap groups in existing polymer systems. Polymer resins incorporating thermally robust silsesquioxane cages can exhibit improved thermal stabilities (increased degradation temperatures) suggested to be associated with the heat capacity of the cage components, which form a glassy layer of SiO_xC_y during pyrolysis that retards diffusion of O_2 through the surface char.^{44a}

Alternately, others suggest that increased thermal stability is achieved by retarding polymer chain motion, either by intermolecular interactions (between the cages and polymer chains) or by the tendency of the large cage molecules to restrict the mobility of the polymer segments at elevated temperatures.^{44b} Lee et al reported that pendant cubes also enhance the mechanical properties of polymers, such as the tensile strength of styrene-butadiene-styrene triblock copolymers near the T_g of styrene, for example.⁴⁵ The authors speculate that the pendant cubes act as “physical cross-linkers” in these systems and provide sites for physical constraint opposing the viscous flow of polymer chains at higher temperatures, which is responsible for the improved load carrying capacity over polymers that do not contain cubes.⁴⁵

After trial and error, we found that reaction of a 4.4:1 mole ratio of PPS:PVS with TBAF in THF (RT/48 h; Scheme **6.3b**) gave predominantly the T_{10} and T_{12} divinyl compounds as shown by the MALDI spectrum in Figure **6.8**. Divinyl compounds are

particularly important because further reaction of the two vinyl moieties can lead to “string of beads” oligomers/polymers as explained below.

The 4.4:1 PPS:PVS reaction MALDI-TOF spectrum shows reaction products corresponding to Ag^+ adducts of T_{10} and T_{12} cages; see **Table 6.3**. A small amount of phenyl T_8 cube formed as a by-product and is easily removed by column chromatography for reasons discussed below. MALDI indicates the presence of mono- and divinylphenyl T_{10} and T_{12} as well as small amounts of tri- and tetravinyl T_{10} and T_{12} . The structures of the T_{10} and T_{12} products are supported by FTIR, ^1H NMR, and ^{13}C NMR data as listed in **Section 6.2**. XRD powder patterns exhibit only amorphous scattering.

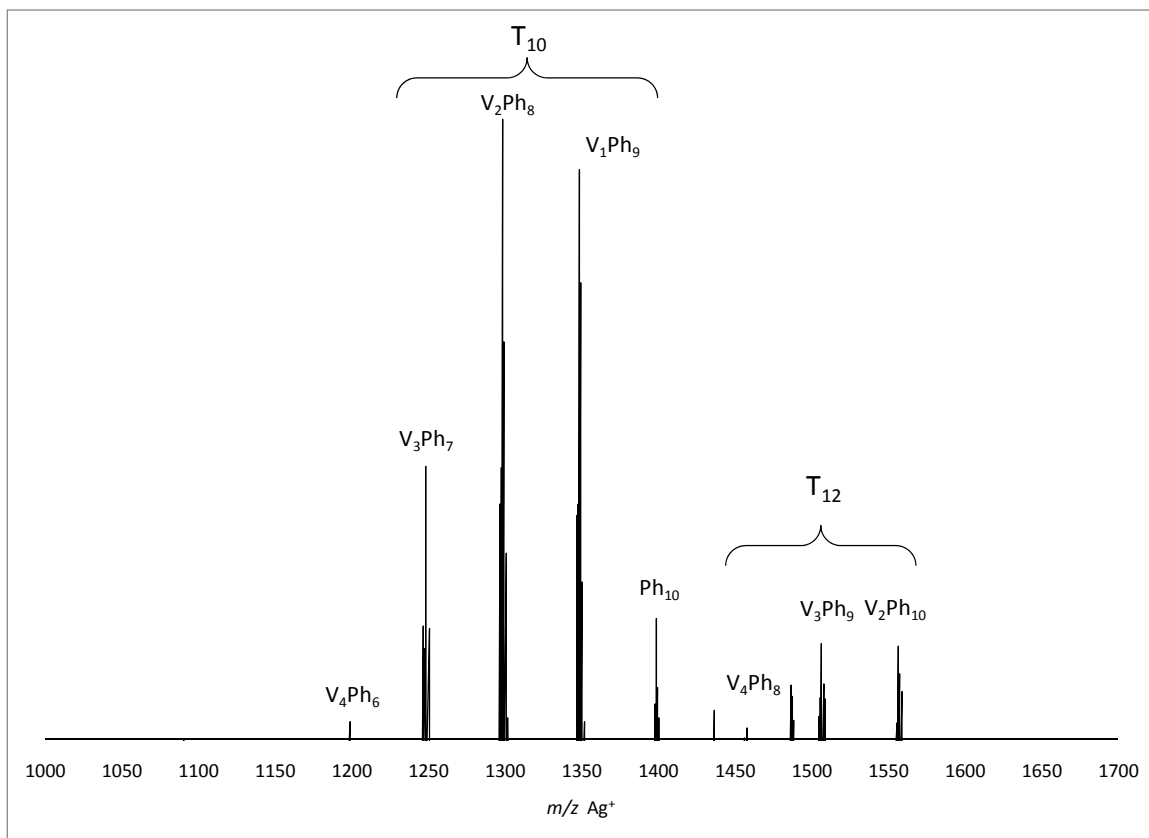


Figure 6.8. MALDI-TOF spectrum of 4.4:1 PPS:PVS reaction with TBAF (RT/48 h) after purification by column chromatography.

Table 6.3. MALDI-TOF data (Ag^+ Adduct) for 4.4:1 PPS:PVS reaction with TBAF.

Most Common Isotope	Found (Da)	Calculated (Da)	Relative Peak Intensity (%)
$(\text{CH}_2=\text{CH})_4(\text{C}_6\text{H}_5)_6(\text{SiO}_{1.5})_{10}$	1199.1	1199.5	12
$(\text{CH}_2=\text{CH})_3(\text{C}_6\text{H}_5)_7(\text{SiO}_{1.5})_{10}$	1249.4	1249.6	49
$(\text{CH}_2=\text{CH})_2(\text{C}_6\text{H}_5)_8(\text{SiO}_{1.5})_{10}$	1299.8	1299.6	100
$(\text{CH}_2=\text{CH})_1(\text{C}_6\text{H}_5)_9(\text{SiO}_{1.5})_{10}$	1349.3	1349.7	93
$(\text{C}_6\text{H}_5)_{10}(\text{SiO}_{1.5})_{10}$	1399.8	1399.8	27
$(\text{CH}_2=\text{CH})_4(\text{C}_6\text{H}_5)_8(\text{SiO}_{1.5})_{12}$	1458.0	1457.9	17
$(\text{CH}_2=\text{CH})_3(\text{C}_6\text{H}_5)_9(\text{SiO}_{1.5})_{12}$	1507.8	1508.0	23
$(\text{CH}_2=\text{CH})_2(\text{C}_6\text{H}_5)_{10}(\text{SiO}_{1.5})_{12}$	1557.9	1558.0	23

The dominant ionizable species according to the MALDI-TOF spectrum of Figure 6.8 is the vinyl₂Ph₈ T₁₀ species as anticipated. Separation (and thus quantification) of the cage species resulting from the reaction of 4.4:1 PPS:PVS by column chromatography is not trivial due to similarities in the chemical structures and properties (e.g. solubility, polarity, etc.) of the products. There are 9 distinct products from the reaction that differ only slightly in their chemical structures. The phenyl T₈ is the only compound readily separated by column chromatography. It is crystalline and highly insoluble in most solvents, and is the main insoluble by-product in the F⁻ rearrangement reactions of PPS and PVS. Furthermore, GPC analysis is not useful in determining the exact amounts of T₈, T₁₀, or T₁₂ in the product mixture due to similarities in their hydrodynamic volumes, as evidenced by a single peak in the GPC chromatogram of Figure 6.13 and narrow polydispersity [PDI = 1.02 (Table 6.6); see Section 6.3.4 for discussion of GPC data]. However, separation and purification of the products by column chromatography following metathesis with 4-bromostyrene makes separation of the resulting compounds easier due to more significant changes in the solubility of each species as described further below in Section 6.3.3.

The TGA curves of the vinyl₂Ph_x (x = 8, 10) T₁₀ and T₁₂ compounds in air and N₂ are shown in Figures 6.14 and 6.15, respectively. These compounds are very stable in air (T_{d5%} = 459 °C; Table 6.7), as is expected of silsesquioxane cages containing rigid,

thermally-stable phenyl groups. The ceramic yield of the products is 49.4%. An accurate theoretical ceramic yield could not be calculated because the products are a mixture of different cage structures of unknown quantities. However, a comparison of the ceramic yield to the theoretical ceramic yields of the individual compounds in the mixture (as detected by MALDI) corresponds closely ($\pm 4\%$, neglecting the amount of phenyl T₁₀) as evidenced in **Table 6.7**.

The amount of phenyl T₁₀ in the product mixture can be estimated to be $< 5\%$ by GPC (see Figure **6.13**). This is calculated by comparing the area of overlap between the divinyl T₁₀ and T₁₂ peak and phenyl T₈ peak. As previously suggested, GPC cannot adequately resolve phenyl T₈, T₁₀, or T₁₂ due to similarities in their hydrodynamic volumes. Comparing the area of overlap with phenyl T₈ gives a rough estimate of the amount of unreacted phenyl T₁₀ in the product mixture. This is also supported by the TGA of the divinyl compounds in N₂ (Figure **6.15**). The mass loss before 500 °C is likely due to sublimation of phenyl T₁₀ (~5 wt%).

The progress of the reaction of a 4.4:1 mole ratio of PPS:PVS with 1 mol% TBAF was monitored by GPC as shown in Figure **6.9**. At the beginning ($t=0$ h), only one broad peak appears for PPS and PVS [retention time (t_R) ≈ 31.5 mins]. After one hour, a large peak corresponding to the T₁₀ and T₁₂ cages appears ($t_R \approx 33$ mins; see also Figure **6.13**), indicating that the reaction proceeds rapidly on catalyst addition. At $t=2$ h, the PPS peak height drops to ~54% of the peak height at $t=1$ h, indicating further rearrangement. Unreacted PPS in the reaction solution is consumed slower as the reaction stirs longer than ~2 h. The unreacted PPS peak height drops an additional 22% over 5 d (from $t=48$ to 168 h), as opposed to 54% over one hour ($t=1$ to 2 h) at the beginning of the reaction. Thus from the behavior illustrated in Figure **6.17**, the yield of divinyl cage products (~81% with respect to mass of initial reactants) essentially reaches equilibrium after 48 h. We could not accurately determine a rate law because PPS is only sparingly soluble in THF.

Unreacted PPS is collected as insoluble material after CaCl₂ workup and/or separated from the products further by column chromatography (see Experimental, **Section 6.2.2**). While the rearrangement reactions work well using 1 mol% TBAF, it may be possible to improve the reaction times/yields by using more catalyst or raising the reaction

temperature. A detailed study of the effects of catalyst amounts (and/or temperature) on the reaction rate is needed and remains an area for further study.

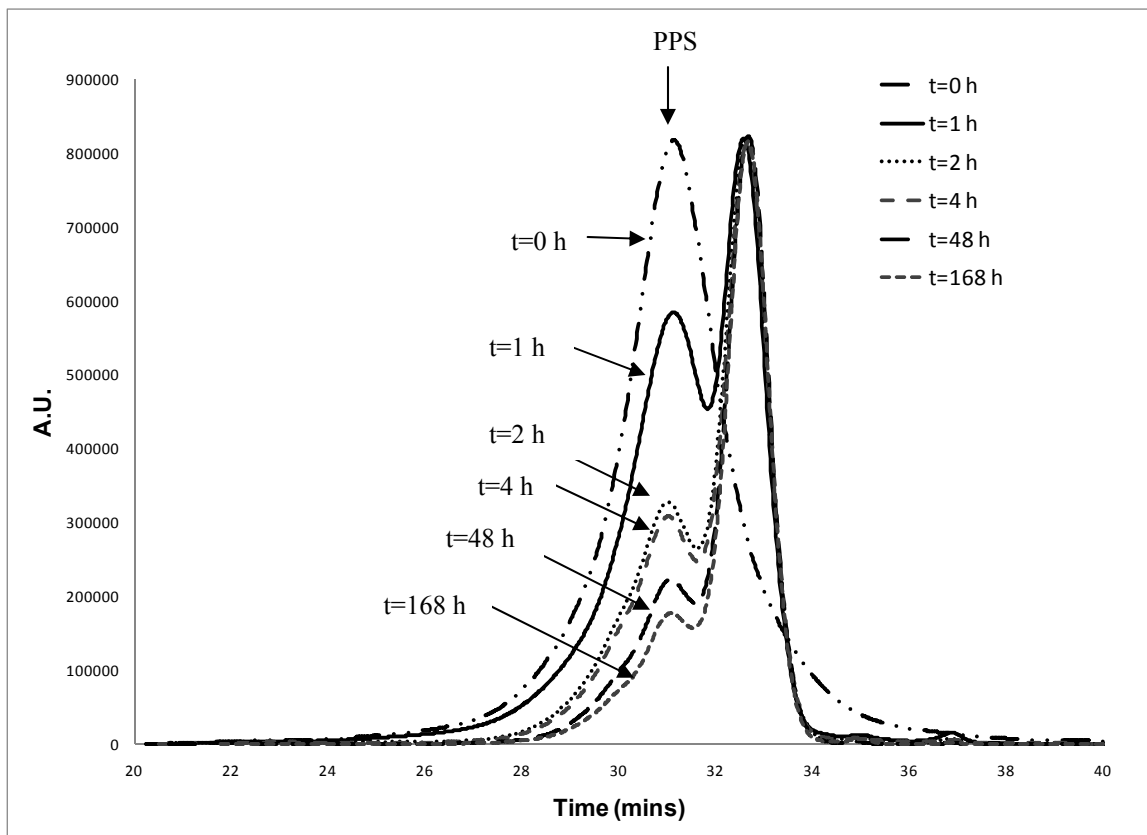


Figure 6.9. Progress of the reaction of a 4.4:1 mole ratio of PPS:PVS with 1 mol% TBAF as monitored by GPC.

6.3.3 Metathesis Reaction of Vinyl₂Ph_x (x = 8, 10) T₁₀ and T₁₂ Silsesquioxanes and 4-Bromostyrene

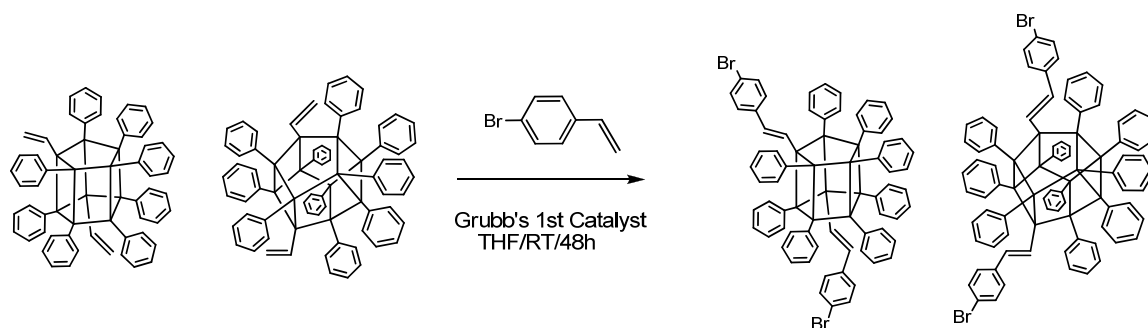
Vinyl₂Ph_x (x = 8, 10) T₁₀ and T₁₂ (from reaction of 4.4:1 PPS:PVS with TBAF) were reacted with 4-bromostyrene as shown in Scheme 6.4. All of the vinyl groups reacted to give ~2 aryl bromides per T₁₀ and T₁₂ as sites for further functionalization, as evidenced by MALDI of the purified products (Figure 6.10 and Table 6.4). Low intensity signals from the mono bromostyrenyl (BrStyr₁) T₁₀ and T₁₂ were also present in the spectrum.

MALDI MS of the crude metathesis products initially showed the presence of BrStyr₃ T₁₀ and T₁₂ as well as BrStyr₄ T₁₀ and T₁₂ compounds, indicating reaction of the trivinyl and tetravinyl cages present in the starting material as described in **Section 6.3.2**. However, the bromostyrenyl compounds are more easily purified by column chromatography (see **Section 6.2.2**) than their corresponding vinyl precursors, as the BrStyr₃ and BrStyr₄ derivatives are much more soluble than the BrStyr₁ and BrStyr₂ derivatives. It proved difficult to completely remove phenyl T₁₀ even after column chromatography.

The GPC chromatogram of the metathesis products (Figure **6.13**) shows a single, narrow peak (PDI=1.04; see **Table 6.6**) confirming the absence of polymeric side products and retention of intact silica cores. There is a small difference in the retention times of the peaks corresponding to the metathesis compounds and vinyl₂Ph T₁₀ and T₁₂, owing to only a slight increase in the hydrodynamic volumes after metathesis with 4-bromostyrene. We roughly estimate the amount of phenyl T₁₀ in the product mixture to be < 4% by measuring the area of overlap with the phenyl T₈ peak in the GPC of Figure **6.13**.

The ¹H NMR spectrum was complex and the broad peaks corresponding to the vinyl and phenyl protons from varying amounts of different compounds were not useful for determining the structures of the products. ¹³C NMR, however, shows distinct peaks for the vinyl carbons at ~130.8 (-Si-CH=CH-) and ~136.0 (-Si-CH=CH-) ppm. Peaks were assigned by comparison to ¹³C NMR spectra of vinyltriethoxysilane and phenyltriethoxysilane.⁴⁶ A peak at ~122 ppm is characteristic of bromine bonded to an aryl carbon, associated with the bromostyrenyl moieties of the expected product. The generally weak carbon-bromine bond stretch (~1028-1073 cm⁻¹) was not observed in the FTIR possibly due to overlap with the very intense and broad Si-O-Si stretching peak (~1130 cm⁻¹) characteristically associated with silsesquioxane cages.

The TGAs in air and N₂ are shown below in Figures **6.14** and **6.15**, respectively. T_{d5%} of the metathesis compounds is 303 °C (**Table 6.7**). The ceramic yield of the metathesis products (40.1%) corresponds closely to the range (39.9 - 43.6%) of theoretical ceramic yields of the compounds in the mixture.



Scheme 6.4. Olefin metathesis of vinyl₂Ph_x (x = 8, 10) T₁₀ and T₁₂ silsesquioxane with 4-bromostyrene.

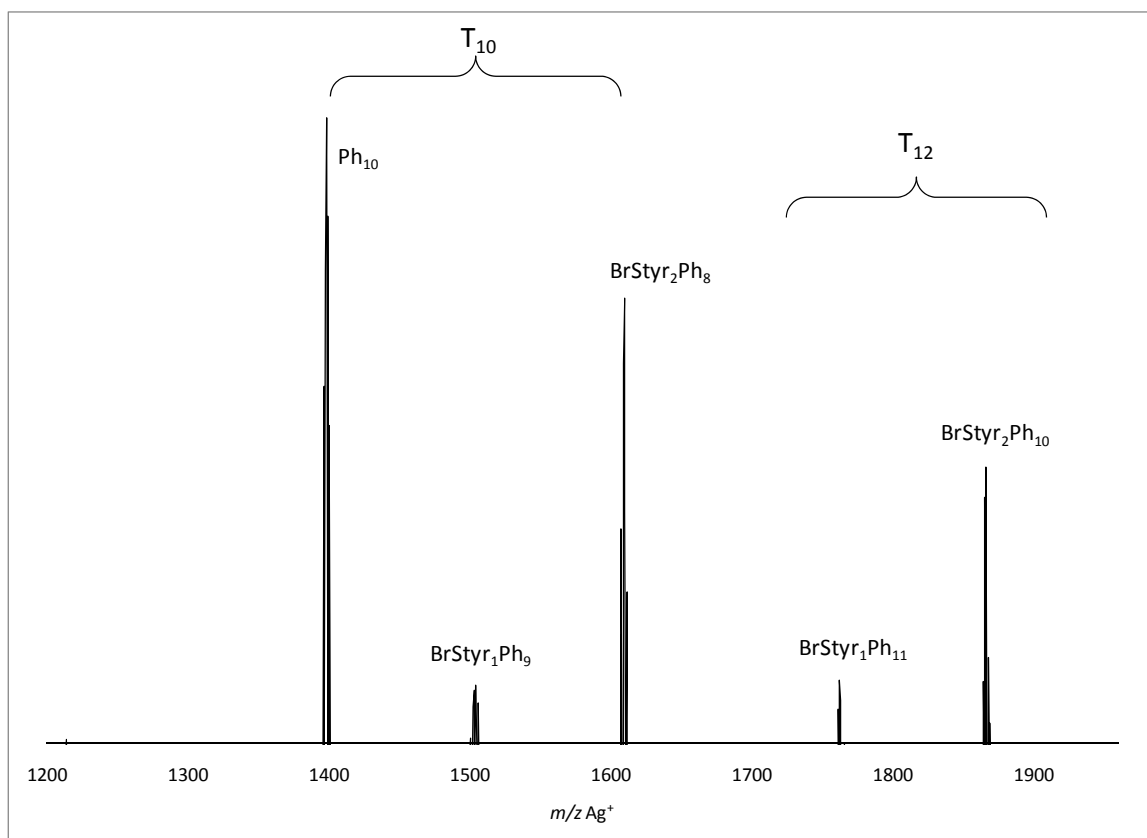
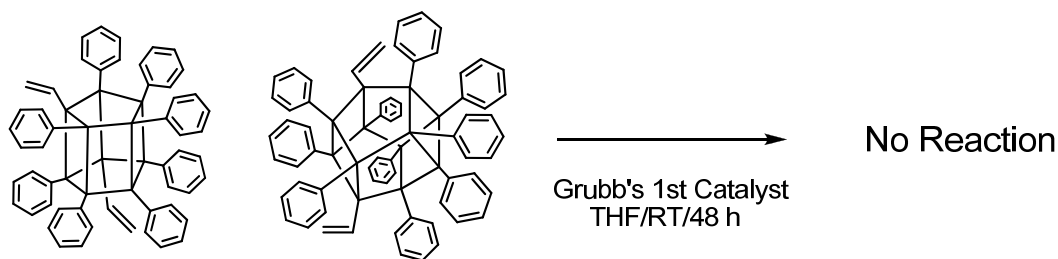


Figure 6.10. MALDI-TOF spectrum of metathesis reaction of vinyl₂Ph_x (x = 8, 10) T₁₀ and T₁₂ silsesquioxanes and 4-bromostyrene after column chromatography.

Table 6.4. MALDI-TOF data (Ag^+ Adduct) for metathesis reaction of $\text{vinyl}_2\text{Ph}_x$ ($x = 8, 10$) T_{10} and T_{12} and 4-bromostyrene.

Most Common Isotope	Found (Da)	Calculated (Da)	Relative Peak Intensity (%)
$(\text{C}_6\text{H}_5)_{10}(\text{SiO}_{1.5})_{10}$	1399.1	1399.8	100
$(\text{C}_8\text{H}_6\text{Br})_1(\text{C}_6\text{H}_5)_9(\text{SiO}_{1.5})_{10}$	1503.5	1504.7	18
$(\text{C}_8\text{H}_6\text{Br})_2(\text{C}_6\text{H}_5)_8(\text{SiO}_{1.5})_{10}$	1610.0	1609.6	74
$(\text{C}_8\text{H}_6\text{Br})_1(\text{C}_6\text{H}_5)_{11}(\text{SiO}_{1.5})_{12}$	1763.1	1763.1	19
$(\text{C}_8\text{H}_6\text{Br})_2(\text{C}_6\text{H}_5)_{10}(\text{SiO}_{1.5})_{12}$	1867.0	1868.0	50

A self-metathesis reaction of the divinyl cages using the same reaction conditions was attempted (Scheme 6.5) in efforts to directly synthesize cage oligomers/polymers. This resulted only in recovery of the starting materials (as determined by GPC, MALDI TOF, and TGA), likely due to the steric effects of the bulky phenyl groups and/or cages impeding formation of the intermediate four-member ring in the cross metathesis mechanism.⁴⁷ This suggests that cages with longer, more flexible vinyl-terminated tethers and/or less bulky non-reactive moieties may be more facile to self-metathesis. Furthermore, a molecular diluent with two reactive vinyl groups could be used to link the bulky cages together, for example. Reactions such as these remain an area for further study.

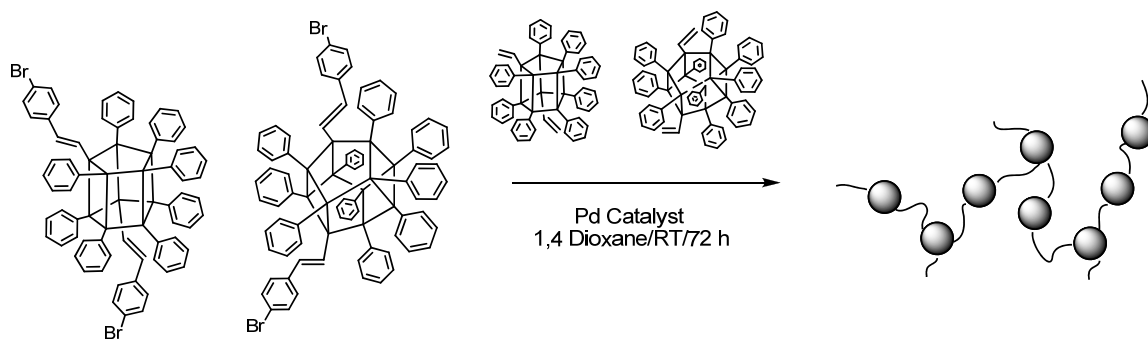


Scheme 6.5. Attempted olefin self-metathesis of $\text{vinyl}_2\text{Ph}_x$ ($x = 8, 10$) T_{10} and T_{12} silsesquioxanes.

6.3.4 Heck Reaction of BrStyr₂Ph_x (x = 8, 10) T₁₀ and T₁₂ Silsesquioxanes and Vinyl₂Ph_x (x = 8, 10) T₁₀ and T₁₂ Silsesquioxanes

BrStyr₂Ph_x (x = 8, 10) T₁₀ and T₁₂ silsesquioxanes were reacted with vinyl₂Ph_x (x = 8, 10) T₁₀ and T₁₂ under Heck coupling conditions (Scheme 6.6) in efforts to form linear oligomers. The isolated products are soluble in typical organic solvents (THF, ethyl acetate, and acetone) and its proposed structure is shown schematically in Figure 6.11. The unique photoluminescence properties of these compounds are discussed in more detail below.

Figure 6.12 shows the MALDI spectrum after Heck coupling (see also Table 6.5). Unreacted mono-bromostyrenyl species are present in the spectrum, as are unreactive phenyl T₁₀, which could not be completely separated from the starting materials by column chromatography. Higher molecular weight species (from dimers, trimers, etc.) are not readily detected by MALDI, for reasons previously discussed concerning the difficulties in ionizing silsesquioxane oligomers/polymers. ESI MS was also attempted, but gave results similar to MALDI and did not show the presence of high molecular weight species.



Scheme 6.6. Heck coupling of vinyl₂Ph_x (x = 8, 10) T₁₀ and T₁₂ silsesquioxanes with BrStyr₂Ph_x (x = 8, 10) T₁₀ and T₁₂ silsesquioxanes.

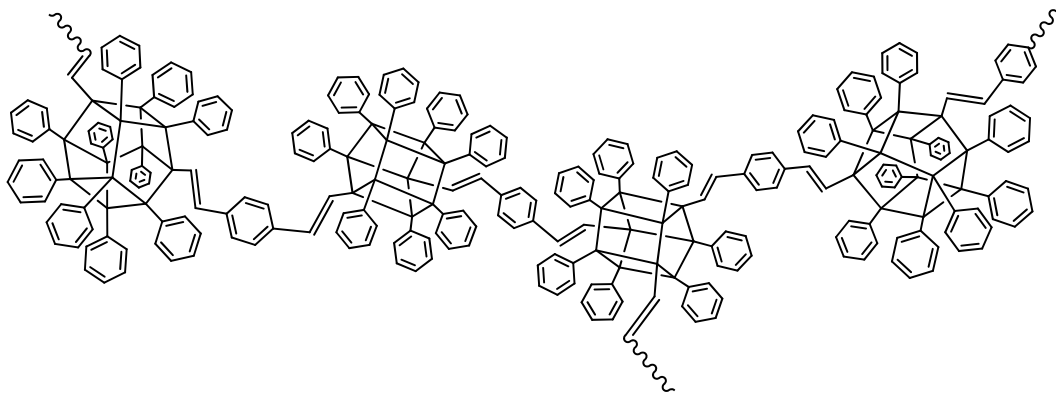


Figure 6.11. Schematic depiction of the proposed structure of the Heck coupling product.

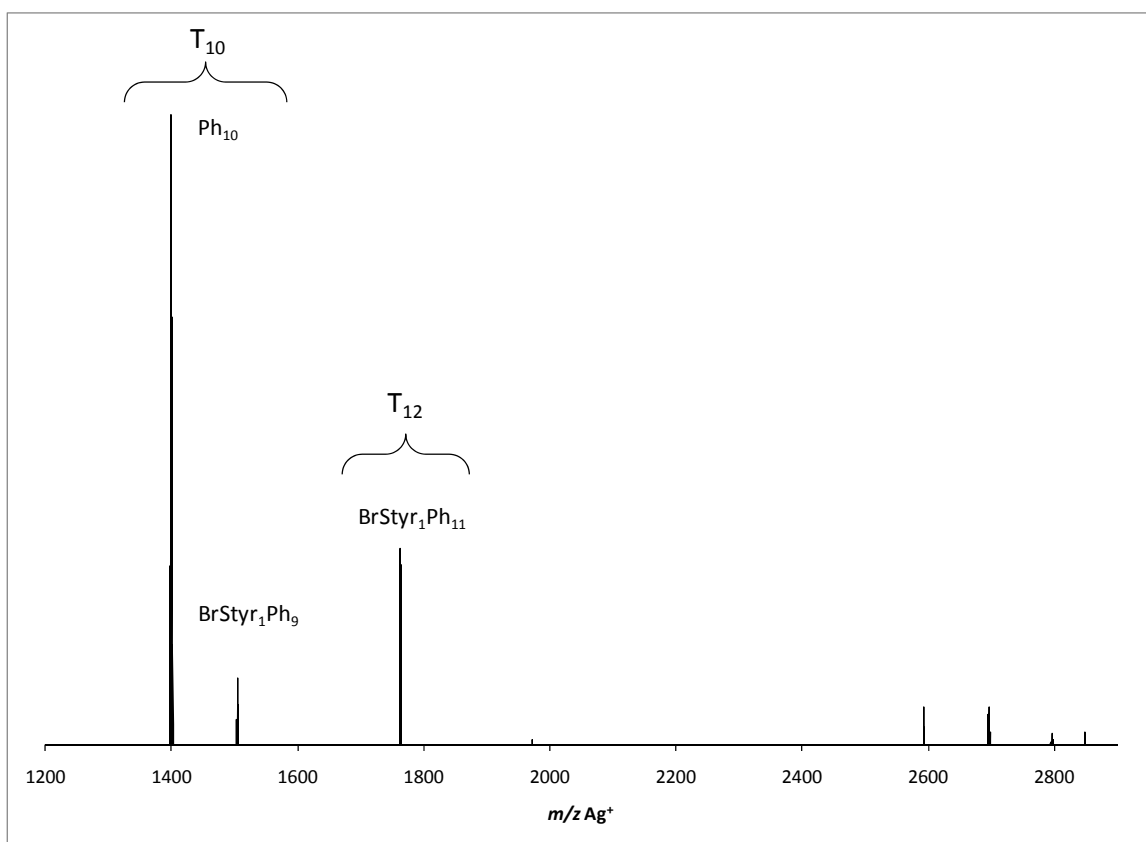


Figure 6.12. MALDI-TOF spectrum after Heck reaction of BrStyr₂Ph_x (x = 8, 10) T₁₀ and T₁₂ silsesquioxanes and vinyl₂Ph_x (x = 8, 10) T₁₀ and T₁₂ silsesquioxanes. (Purified by column chromatography).

Table 6.5. MALDI-TOF data (Ag^+ Adduct) for Heck reaction of $\text{BrStyr}_2\text{Ph}_x$ ($x = 8, 10$) T_{10} and T_{12} and $\text{vinyl}_2\text{Ph}_x$ ($x = 8, 10$) T_{10} and T_{12} .

Most Common Isotope	Found (Da)	Calculated (Da)	Relative Peak Intensity (%)
$(\text{C}_6\text{H}_5)_{10}(\text{SiO}_{1.5})_{10}$	1400.0	1399.8	100
$(\text{C}_8\text{H}_6\text{Br})_1(\text{C}_6\text{H}_5)_9(\text{SiO}_{1.5})_{10}$	1505.1	1504.7	20
$(\text{C}_8\text{H}_6\text{Br})_1(\text{C}_6\text{H}_5)_{11}(\text{SiO}_{1.5})_{12}$	1763.2	1763.1	39

The GPC chromatograms of the Heck oligomer, model compounds (see **Section 6.3.5** below), metathesis compounds, $\text{vinyl}_2\text{Ph}_8$ T_{10} , and $\text{vinyl}_2\text{Ph}_{10}$ T_{12} are shown in **Figure 6.13**. A mixture of OPS and OVS is also included for comparison of separation and retention times. Mass data as determined by GPC is listed in **Table 6.6**.

The GPC trace shows evidence of an increase in the molecular weight of the Heck products compared to the starting materials, thus confirming the formation of oligomer and the weakness of MALDI MS in detecting higher molecular weight silsesquioxane oligomers/polymers. A slight shoulder in the GPC at $t_R \approx 31$ min most likely indicates formation of dimer. Unreacted BrStyr_1 T_{10} and T_{12} also appears as a small peak ($t_R \approx 32$ min) and corresponds to the peak for metathesis products. The total amount of unreacted BrStyr_1 T_{10} and T_{12} and phenyl T_{10} is $\sim 10\%$ by GPC (see **Figure 6.13**).

The TGA curves of the Heck products are shown in **Figures 6.14** (air) and **6.15** (N_2) and pertinent thermal analysis data is given in **Table 6.7**. The 5% decomposition temperature for the Heck product is 325°C , making these oligomers very thermally stable in air yet highly soluble (and therefore processible). The ceramic yield of the compounds is 45.0%. An accurate determination of the theoretical ceramic yield is impossible since the products are an oligomeric mixture of different cage compounds.

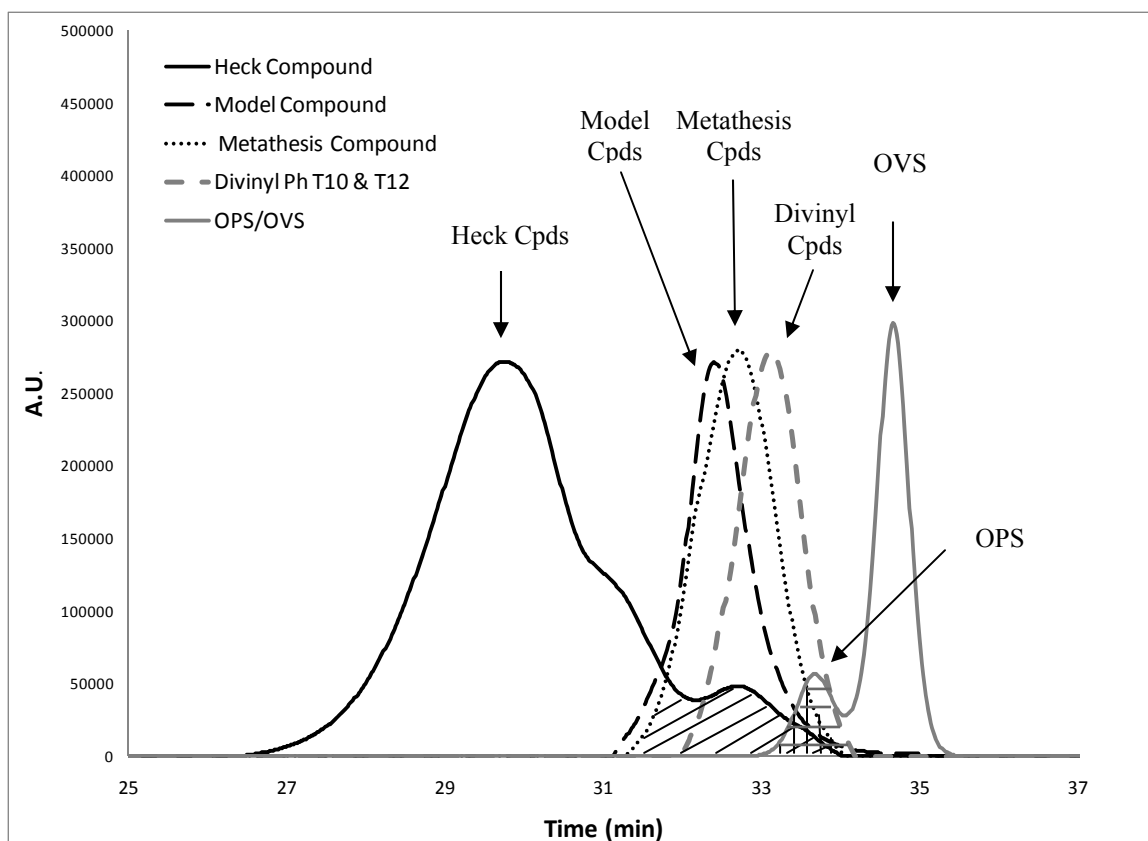


Figure 6.13. GPC chromatogram of Heck, model and metathesis compounds, vinyl₂Ph₈ T₁₀ and vinyl₂Ph₁₀ T₁₂, and OPS/OVS (for comparison). Shaded areas represent amounts of unreacted starting materials in divinyl, metathesis and Heck compounds (~5%, ~4%, and ~10%, respectively).

Table 6.6. GPC mass data for Heck, model and metathesis compounds, vinyl₂Ph₈ T₁₀ and vinyl₂Ph₁₀ T₁₂, and OPS/OVS (for comparison).

Compound Name	t _R (mins)	M _n	M _w	PDI
Heck Compounds [†]	29.7	2973	3716	1.25
Model Compounds	32.3	1441	1527	1.06
Metathesis Compounds	32.6	1383	1437	1.04
Divinyl Ph T ₁₀ & T ₁₂	33.1	986	1005	1.02
OPS	33.7	--	--	--
OVS	34.6	--	--	--

[†] Area under curve measured from t_R = 26.4 - 31.9 mins.

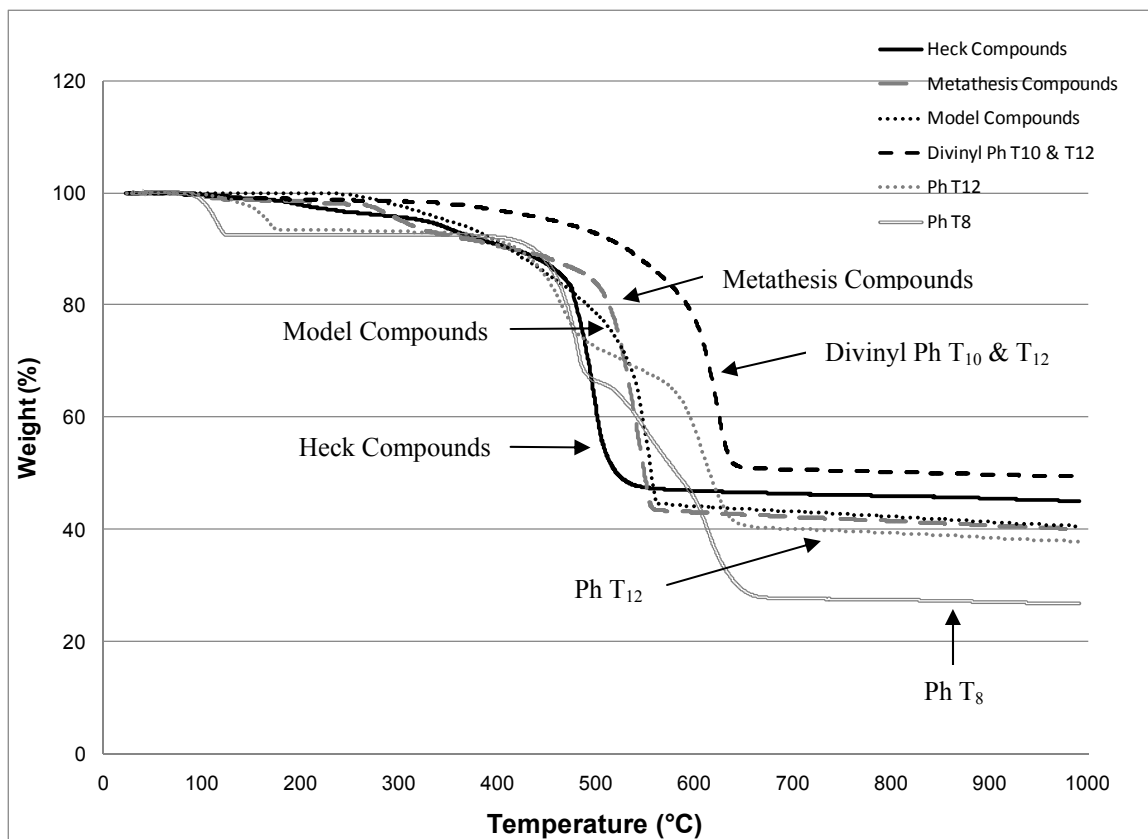


Figure 6.14. TGA of Heck, model and metathesis compounds, vinyl₂Ph₈ T₁₀ and vinyl₂Ph₁₀ T₁₂ silsesquioxanes (air, 10°C/min to 1000 °C). Ph T₈ and Ph T₁₂ are included for comparison.

Table 6.7. Decomposition temperatures ($T_{d5\%}$) and ceramic yields for Heck, model and metathesis compounds, vinyl₂Ph₈ T₁₀ and vinyl₂Ph₁₀ T₁₂ (air, 10°C/min to 1000°C). Theoretical ceramic yields for compounds detected by MALDI are given for reference.

Compound Name	T_{d5%} (°C)	Ceramic Yield (%)	Theoretical Ceramic Yield (%)
Heck Compounds	325	45.0	--
Model Compounds	351	40.5	--
(C ₈ H ₆ Br) ₁ (C ₆ H ₅) ₉ (SiO _{1.5}) ₁₀	--	--	39.9
(C ₈ H ₆ Br) ₂ (C ₆ H ₅) ₈ (SiO _{1.5}) ₁₀	--	--	35.0
(C ₈ H ₆ Br) ₁ (C ₆ H ₅) ₁₁ (SiO _{1.5}) ₁₂	--	--	40.9
(C ₈ H ₆ Br) ₂ (C ₆ H ₅) ₁₀ (SiO _{1.5}) ₁₂	--	--	36.5
(C ₆ H ₅) ₁₀ (SiO _{1.5}) ₁₀	--	--	30.3
Metathesis Compounds	303	40.1	--
(C ₈ H ₆ Br) ₁ (C ₆ H ₅) ₉ (SiO _{1.5}) ₁₀	--	--	43.0
(C ₈ H ₆ Br) ₂ (C ₆ H ₅) ₈ (SiO _{1.5}) ₁₀	--	--	39.9
(C ₈ H ₆ Br) ₁ (C ₆ H ₅) ₁₁ (SiO _{1.5}) ₁₂	--	--	43.6
(C ₈ H ₆ Br) ₂ (C ₆ H ₅) ₁₀ (SiO _{1.5}) ₁₂	--	--	41.0
(C ₆ H ₅) ₁₀ (SiO _{1.5}) ₁₀	--	--	30.3
Divinyl Ph T ₁₀ & T ₁₂	459	49.4	--
(CH ₂ =CH) ₃ (C ₆ H ₅) ₇ (SiO _{1.5}) ₁₀	--	--	52.7
(CH ₂ =CH) ₂ (C ₆ H ₅) ₈ (SiO _{1.5}) ₁₀	--	--	50.4
(CH ₂ =CH) ₁ (C ₆ H ₅) ₉ (SiO _{1.5}) ₁₀	--	--	48.4
(CH ₂ =CH) ₄ (C ₆ H ₅) ₈ (SiO _{1.5}) ₁₂	--	--	53.4
(CH ₂ =CH) ₃ (C ₆ H ₅) ₉ (SiO _{1.5}) ₁₂	--	--	51.5
(CH ₂ =CH) ₂ (C ₆ H ₅) ₁₀ (SiO _{1.5}) ₁₂	--	--	49.7
(C ₆ H ₅) ₁₀ (SiO _{1.5}) ₁₀	--	--	30.3

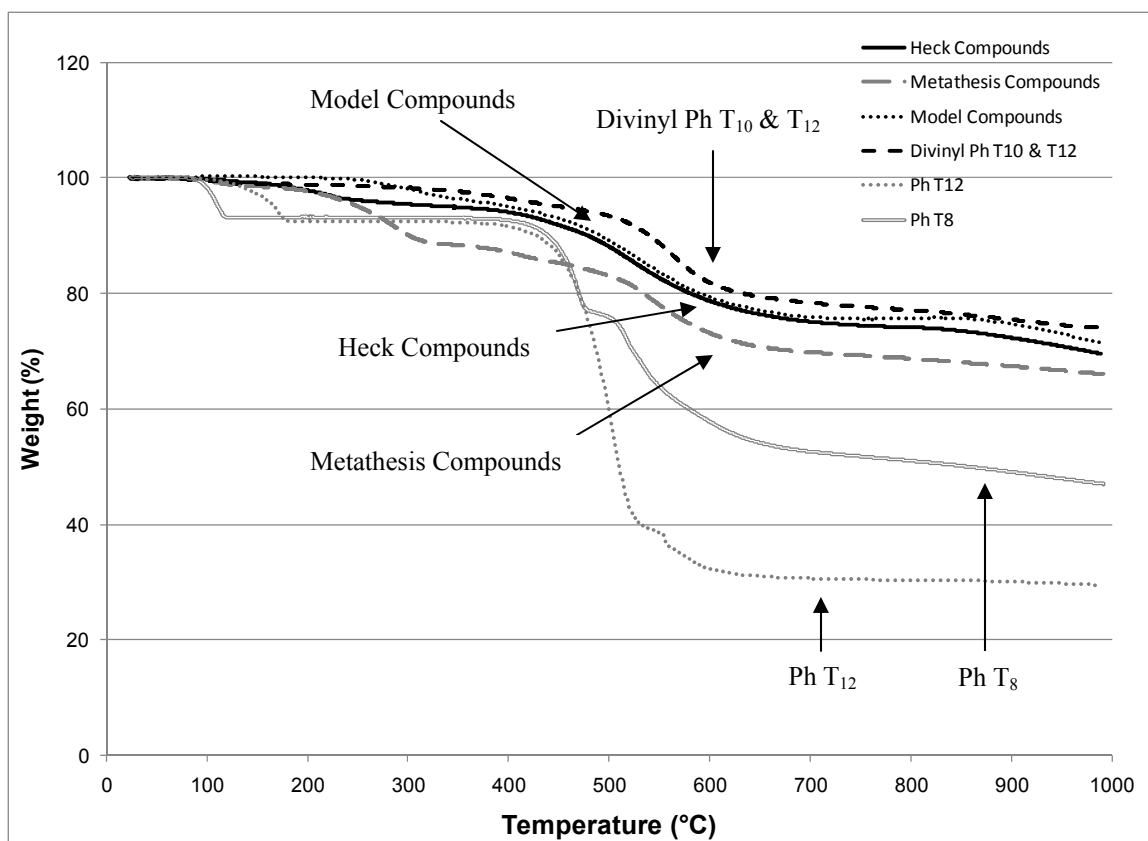


Figure 6.15. TGA of Heck, model and metathesis compounds, vinyl₂Ph₈ T₁₀ and vinyl₂Ph₁₀ T₁₂ silsesquioxanes (N₂, 10°C/min to 1000 °C). Ph T₈ and Ph T₁₂ are included for comparison.

6.3.5 Synthesis of Model Compounds by Heck Reaction of BrStyr₂Ph_x (x = 8, 10) T₁₀ and T₁₂ Silsesquioxanes and Vinyltriethoxysilane

We prepared the model compounds of Figure 6.16 via reaction of BrStyr₂Ph_x (x = 8, 10) T₁₀ and T₁₂ silsesquioxanes with vinyltriethoxysilane [CH₂=CH-Si(OEt)₃] under Heck conditions (see Section 6.2.2.7). The photoluminescence behavior of these compounds was compared to that of the Heck products (Figure 6.11) and is discussed further in Section 6.3.6 below.

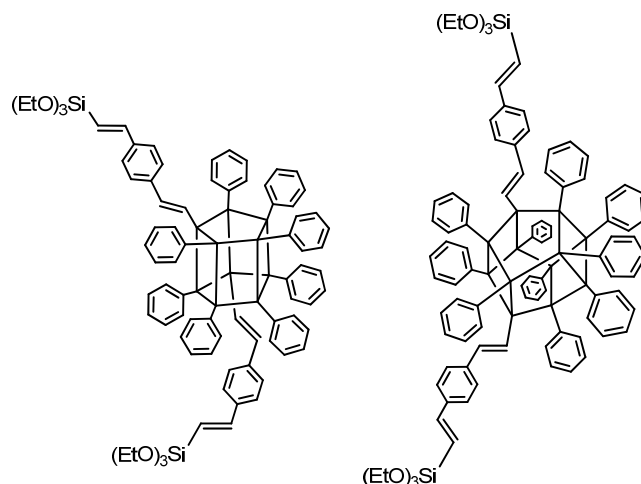


Figure 6.16. Structures of Heck model compounds from reaction of BrSty₂Ph_x ($x = 8, 10$) T₁₀ and T₁₂ silsesquioxanes with vinyltriethoxysilane.

The MALDI spectrum of the model compounds after purification by column chromatography is shown in Figure 6.17 and the correct masses for the disubstituted Ag⁺ adducts are observed at m/z 1828 [(C₁₆H₂₃O₃Si)₂Ph₈ T₁₀] and 2086 [(C₁₆H₂₃O₃Si)₂Ph₁₀ T₁₂] amu (see also Table 6.8). The MALDI spectrum also shows peaks corresponding to the monosubstituted T₁₀ and T₁₂ cages, as well as decaphenyl silsesquioxane present as an impurity in the starting materials. GPC shows a single, narrow peak at $t_R \sim 32.3$ mins (PDI = 1.06); see also Figure 6.13 and Table 6.6. The FTIR spectrum is also consistent with the structures associated with the model compounds (see characterization data in Section 6.2.2.7).

The T_{d5%} of the model compounds is 351 °C (Table 6.7). There is a small mass loss (~5 wt%) before 500 °C as the model compounds are heated in N₂ (Figure 6.15). This is attributed to sublimation of a small amount of phenyl T₁₀. The ceramic yield (40.5%) corresponds to the range (35.0 – 40.9%) of theoretical ceramic yields for compounds detected by MALDI in the product mixture.

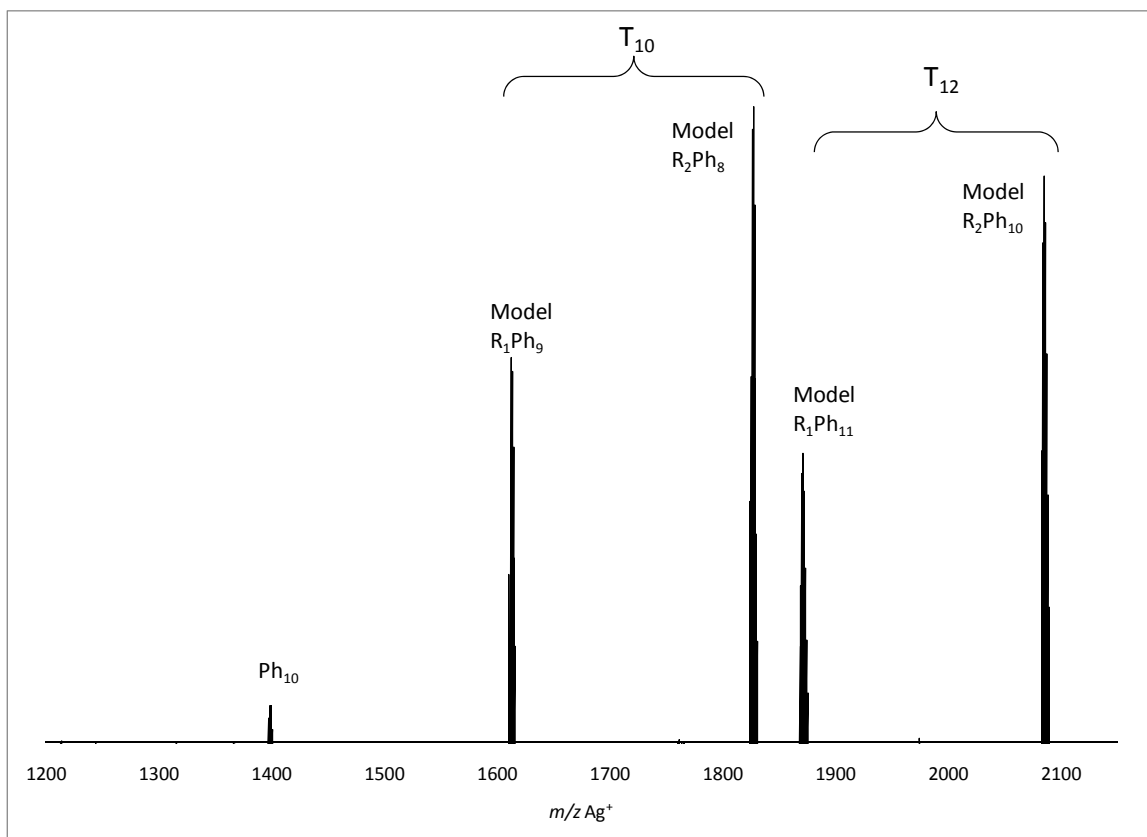


Figure 6.17. MALDI-TOF spectrum after Heck reaction of BrStyr₂Ph_x (x = 8, 10) T₁₀ and T₁₂ silsesquioxanes and vinyltriethoxysilane. Purified by column chromatography.

Table 6.8. MALDI-TOF data (Ag⁺ Adduct) for Heck reaction of model compound.

Most Common Isotope	Found (Da)	Calculated (Da)	Relative Peak Intensity (%)
(C ₆ H ₅) ₁₀ (SiO _{1.5}) ₁₀	1399.1	1399.8	7
(C ₆ H ₅) ₉ (C ₁₆ H ₂₃ O ₃ Si) ₁ (SiO _{1.5}) ₁₀	1614.0	1614.1	61
(C ₆ H ₅) ₈ (C ₁₆ H ₂₃ O ₃ Si) ₂ (SiO _{1.5}) ₁₀	1827.9	1828.4	100
(C ₆ H ₅) ₁₁ (C ₁₆ H ₂₃ O ₃ Si) ₁ (SiO _{1.5}) ₁₂	1872.1	1872.5	46
(C ₆ H ₅) ₁₀ (C ₁₆ H ₂₃ O ₃ Si) ₂ (SiO _{1.5}) ₁₂	2086.0	2086.8	89

Figure 6.18 shows the ¹H NMR spectrum of the model compounds with broad peaks in the aromatic (~6.4~7.9 ppm) and vinyl (~5.1~6.3 ppm; labeled peak “A” in Figure 6.18) proton regions that are typical for these compounds. The peaks ~3.8~3.9 (“B”) and

~1.2~1.3 ppm (“C”) correspond to the -OCH₂ and -CH₃ protons, respectively. The theoretical ratio of vinyl:methoxy:methyl protons (A:B:C = 1:1.5:2.3) matches the actual integration (1:1.4:2.3). Both “B” and “C” each exhibit two distinct signals, likely indicating protons in two magnetically different environments originating from the mono- and difunctional species and/or the T₁₀ and T₁₂ cages. Integration of the separate signals comprising “B” and “C” gives a ratio ≈ 1.5:1 for each. We can therefore assume that the T₁₀ and T₁₂ cages are present in similar proportion, though we cannot determine which cage species is present in greater amounts because the effect of the cage structure on the proton chemical shifts is unknown.

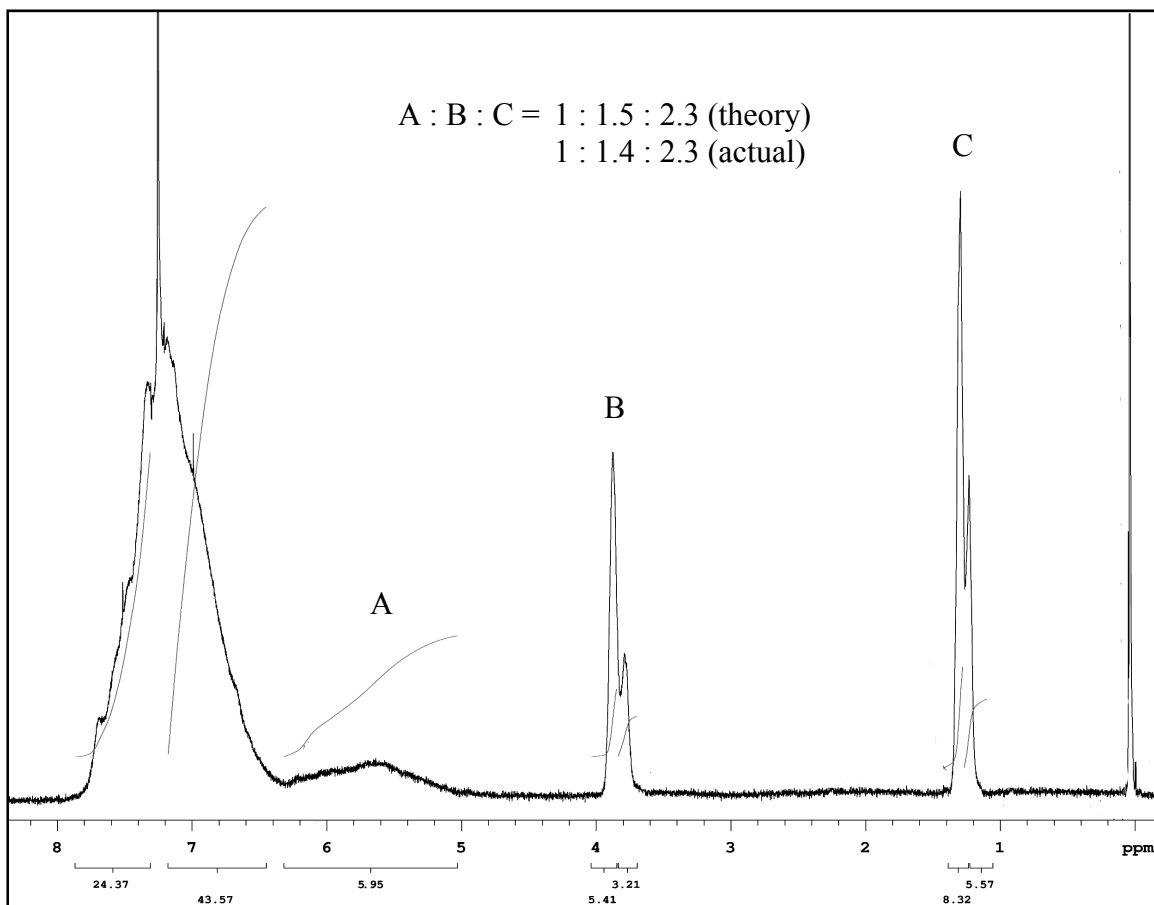


Figure 6.18. ¹H NMR spectrum (CDCl₃) after Heck reaction of BrSty_rPh_x (x = 8, 10) T₁₀ and T₁₂ silsesquioxanes and vinyltriethoxysilane. Purified by column chromatography.

The ^{13}C NMR spectrum of the model compounds (Figure 6.19) shows characteristic peaks for the methyl and methoxy carbons (~ 18 and ~ 59 ppm, respectively) and aryl carbons ($\sim 127\sim 134$ ppm). Vinyl carbons are attributed to the peak at ~ 136 ppm. Peaks were assigned by comparing with ^{13}C NMR spectra for vinyltriethoxysilane, phenyltriethoxysilane, and triphenylchlorosilane.⁴⁶

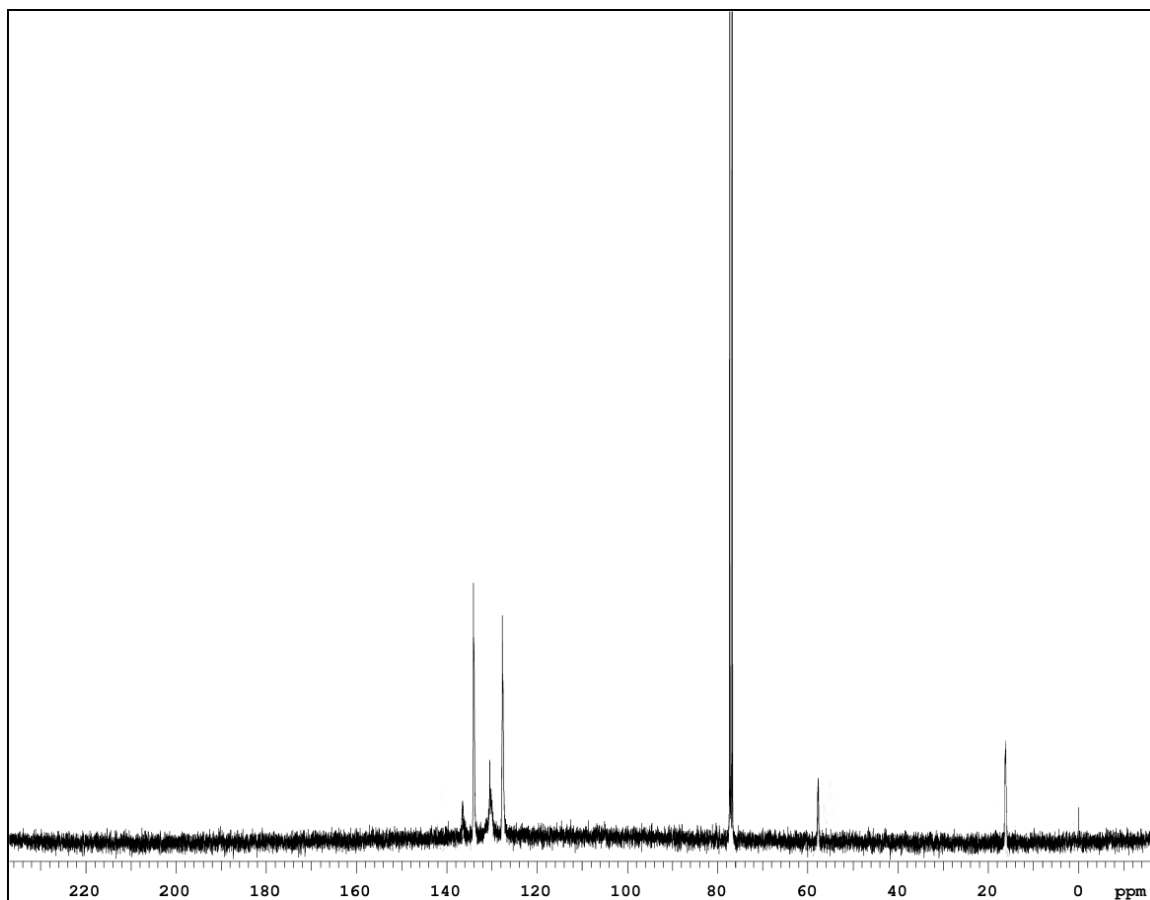


Figure 6.19. ^{13}C NMR spectrum (CDCl_3) after Heck reaction of $\text{BrStyr}_2\text{Ph}_x$ ($x = 8, 10$) T_{10} and T_{12} silsesquioxanes and vinyltriethoxysilane. Purified by column chromatography.

6.3.6 Photoluminescence Studies

Currently, our group is investigating the luminescence behavior of silsesquioxanes functionalized with conjugated organic moieties. Unusual red-shifted emission spectra

have been observed for octastilbene³⁵ and dodecastilbene⁵⁰ derivatives, and first and second generation “star” compounds derived from octavinylsilsesquioxane and functionalized styrenes.⁴⁹ These compounds exhibit highly red-shifted emissions typical of molecules with extensively delocalized electronic structures and is unexpected in compounds that to date are thought of as silica-like insulators.

As a result of our observations, we have long suspected that luminescent tethers in the periphery electronically interact with the predicted, spherical LUMO located within the cage cores (see **Section 6.1**). If this is indeed the case, then all eight (or twelve) tethers may “communicate” simultaneously through the cage.

The Heck oligomer formed in Scheme **6.6** exhibits unique photoluminescence properties at high dilution ($10^{-5} - 10^{-6}$ M) as shown below in Figure **6.20**. The emission spectrum has two maxima at 386 and 408 nm and is highly red-shifted compared to the corresponding UV absorption maximum at 265 nm. The magnitude of this red-shift seems inconsistent if one assumes the silsesquioxane cores to be solely insulating.

In an effort to explain this significant red-shift, the model compound was synthesized as previously discussed and its luminescence properties were measured. The model compound is red-shifted (≈ 70 -90 nm) compared to its UV absorption maximum. The shift to longer emission wavelength (Stokes shift) is typical and primarily due to energy lost as a consequence of collisions between the molecules of the excited species and those of the solvent. The Stokes shift of the oligomer, however, is considerably greater than the model compound (≈ 120 -140 nm). The Heck oligomer is shifted ≈ 60 nm from the model compound alone. The magnitude of the Heck oligomer red-shift cannot be adequately explained solely in terms of energy loss from solvent collisions. The spectra in Figure **6.20** imply that the addition of a cage to another cage increases conjugation and induces this shift.

The red-shift associated with the addition of cage structures joined to other T₁₀ and T₁₂ cages by conjugated tethers is indicative of extensive electron delocalization and far beyond the behavior of isolated conjugated molecules trapped between insulating cores. If there is indeed conjugation through the cage centers, the delocalization would lower the energy of the $\pi \rightarrow \pi^*$ transition and shift the emission maxima to longer wavelengths as a consequence. It is a compelling argument for the existence of 3-D excited state

interaction through the cage centers and seems to agree with previous results from our group and corroboration of recent modeling studies in this area.^{31-35,49} In any case, it seems reasonable to assume that the ease of fluoride encapsulation inside the cube core reflects the unique electronic characteristics of these molecules and thus may help explain their unexpected emission behavior. Further exploration of this phenomenon in detail is necessary and remains an area for further study.

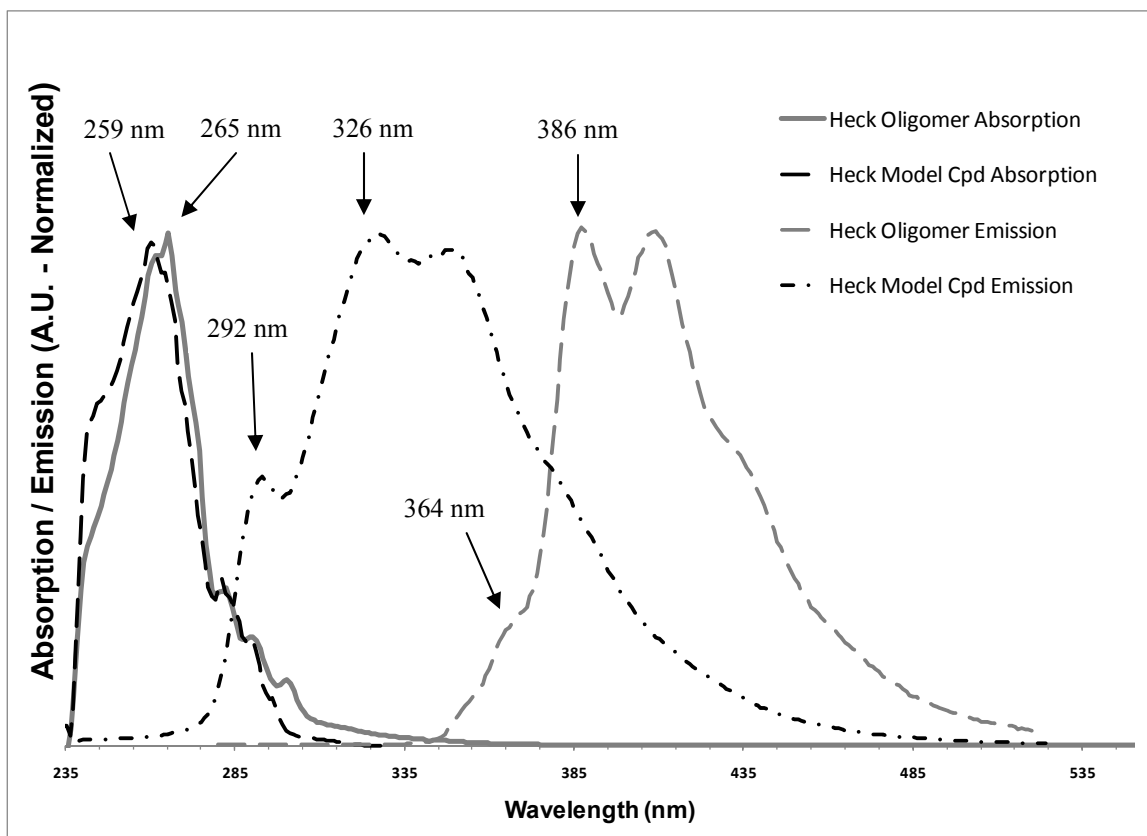


Figure 6.20. Solution (THF) absorption and emission spectra ($\lambda_{\text{excitation}} = 265 \text{ nm}$) of Heck compounds and corresponding Heck model $-\text{Si}(\text{OEt})_3$ compounds.

6.4 Conclusions

Fluoride-mediated rearrangement reactions of silsesquioxanes allow direct access to a potential new class of multifunctional cage compounds, offering unique and viable possibilities to build ordered, nanometer structures through simple control of the beginning materials ratio. The F^- rearrangement of polymeric phenyl- and vinylsilsesquioxanes, in particular, is exciting because the reactants are “useless” polymeric by-products in common silsesquioxane syntheses and lead opportunely to product mixtures of discreet polyhedral silsesquioxane cages. Silsesquioxane cages with ~ 2 reactive functionalities may be further modified and tailored to synthesize high molecular weight linear polymers with silsesquioxanes directly incorporated along the chain backbone. These polymers could offer unique and tunable properties, such as high thermal stability, improved mechanical properties, liquid crystalline behavior, etc. We illustrate the potential of these compounds here in the synthesis of novel, fluorescent “string of beads” oligomers with high solubility and thermal stability (up to 325 °C). The highly red-shifted (≈ 120 nm) luminescence behavior of these compounds is unique in its own right, as it suggests extensive electron delocalization and may involve conjugation through the silsesquioxane cores. The chemistries explored here are representative of many diverse structures of varying complexity that can be created using these simple cages as molecular scaffolds.

6.5 References

1. (a) *Organic/Inorganic Hybrid Materials*; Laine, R.M., Sanchez, C., Brinker, C.J., Giannelis, E., Eds.; MRS Symp. Ser. 519; Materials Research Society: Warrendale, PA, 1998. (b) *Organic/Inorganic Hybrid Materials II*; Klein, L. C., Francis, L., DeGuire, M. R., Mark, J. E., Eds.; MRS Symp. Ser. 576; Materials Research Society: Warrendale, PA, 1999. (c) *Organic/Inorganic Hybrid Materials*; Laine, R. M., Sanchez, C., Giannelis, E., Brinker, C. J., Eds.; MRS Symp. Ser. 628; Materials Research Society: Warrendale, PA, 2000. (d) *Organic/Inorganic Hybrid Materials*; Laine, R. M., Sanchez, C., Yang, S., Brinker, C. J., Eds.; MRS Symp. Ser. 726; Materials Research Society: Warrendale, PA, 2002. (e) Sanchez, C.; Soler-Illia, G. J. de A. A.; Ribot, F.; Lalot, T.; Mayer, C. R.; Cabuil, V. *Chem. Mater.* **2001**, *13*, 3061, and references therein.
2. Sellinger, A.; Laine, R. M. *Macromolecules* **1996**, *29*, 2327.
3. Sellinger, A.; Laine, R. M. *Chem. Mater.* **1996**, *8*, 1592.
4. Lichtenhan, J. D.; Otonari, Y. A.; Carr, M. J. *Macromolecules* **1995**, *28*, 8435.
5. Feher, F. J.; Budzichowski, T. A. *J. Organomet. Chem.* **1989**, *379*, 33.
6. Feher, F. J.; Soulivong, D.; Eklud, A. G.; Wyndham, K. D. *Chem. Commun.* **1997**, 1185.
7. Jeon, H. G.; Mather, P. T.; Haddad, T. S. *Polym. Int.* **2000**, *49*, 453.
8. (a) Gilman, J. W.; Schlitzere, D. S.; Lichtenhan, J. D. *J. Appl. Polym. Sci.* **1996**, *60*, 591. (b) Gonzalez, R. I.; Phillips, S. H.; Hoflund, G. B. *J. Spacecr. Rockets* **2000B**, *37*, 463.
9. Sellinger, A.; Laine, R. M.; Chu, V.; Viney, C. *J. Polym. Sci., Part A: Polym. Chem.* **1994**, *2*, 3069.
10. Zhang, C.; Babonneau, F.; Bonhomme, C.; Laine, R. M.; Soles, C. L.; Hristov, H. A.; Yee, A. F. *J. Am. Chem. Soc.* **1998**, *120* (33), 8380.
11. (a) Laine, R. M.; Choi, J.; Lee, I. *Adv. Mater.* **2001**, *13*, 800. (b) Brick, C.M.; Chan, E.R.; Glotzer, S.C.; Marchal, J.C.; Martin, D.C.; Laine, R.M. *Adv. Mater.* **2007**, *19*, 82. (c) Laine, R.M.; Zhang, C.; Sellinger, A.; Viculis, L. *Appl. Organometal. Chem.* **1998**, *12*, 715. (d) Tamaki, R.; Choi, J.; Laine, R.M. *Chem. Mater.* **2003**, *15*, 793. (e) Choi, J.; Kim, S.G.; Laine, R.M. *Macromolecules* **2004**, *37*, 99. (f) Sulaiman, S.; Brick, C.M.; De Sana, C.M.; Katzenstein, J.M.; Laine, R.M.; Basheer, R.A. *Macromolecules* **2006**, *39*, 5167.

12. Zhang, C.; Laine, R. M. *J. Am. Chem. Soc.* **2000**, *122* (29), 6979.
13. Feher, F.J.; Newman, D.A.; Walzer, J.F. *J. Am. Chem. Soc.* **1989**, *111*, 1741.
14. (a) Feher, F.J.; Budzichowski, T.A.; Blanski, R.L.; Weller, K.J.; Ziller, J.W. *Organometallics* **1991**, *10*, 2526. (b) Feher, F.J.; Soulivong, D.; Eklud, A.G.; Wyndham, K.D. *Chem. Commun.* **1997**, *13*, 1185.
15. (a) Feher, F.J.; Blanski, R.L. *J. Am. Chem. Soc.* **1992**, *114*, 5886. (b) Severn, J.R.; Duchateau, R.; van Santen, R.A.; Ellis, D.D.; Spek, A.L. *Organometallics* **2002**, *1*, 4. (c) Duchateau, R.; Abbenhuis, H.C.L.; van Santen, R.A.; Meetsma, A.; Thiele, S.K.-H.; van Tol, M.F.H. *Organometallics* **1998**, *26*, 5663. (d) Hanssen, R.W.J.M.; van Santen, R.A.; Abbenhuis, H.C.L. *Eur. J. Inorg. Chem.* **2004**, *4*, 675.
16. Maxim, N.; Magusin, P.C.M.M.; Kooyman, P.J.; van Wolput, J.H.M.C.; van Santen, R.A.; Abbenhuis, H.C.L. *Chem. Mater.* **2001**, *13*, 2958.
17. Bonhomme, C.; Toledano, P.; Maquet, J.; Livage, J.; Bohnomme-Coury, L. *J. Chem. Soc., Dalton Trans.* **1997**, *9*, 1617.
18. (a) Bassindale, A.R.; Pourny, M.; Taylor, P.G.; Hursthouse, M.B.; Light, M.E. *Angew. Chem., Int. Ed.* **2003**, *42*, 3488. (b) Bassindale, A.R.; Parker, D.J.; Pourny, M.; Taylor, P.G.; Horton, P.N.; Hursthouse, M.B. *Organometallics* **2004**, *23*, 4400.
19. (a) Pescarmona, P.P.; Maschmeyer, T. *J. Aust. Chem.* **2001**, *54*, 583. (b) Lickiss P.D.; Rataboul, F. In *Advances in Organometallic Chemistry Vol. 57*, Hill, A.F.; Fink, M.J.; Gordon, F. Eds.; Academic Press: United Kingdom, **2008**, pp. 1-116.
20. Voronkov, M.G.; Lavrent'yev, V.I. *Top. Curr. Chem.* **1982**, *102*, 199.
21. Scott, D.W. *J. Am. Chem. Soc.* **1946**, *68*, 356.
22. Brown, J.F. *J. Am. Chem. Soc.* **1965**, *87*, 4317.
23. Sprung, M.M.; Guenther, F.O. *J. Am. Chem. Soc.* **1955**, *77*, 3996.
24. Braunstein, P.; Galsworthy, J.R.; Hendan, B.J.; Marsmann, H.C. *J. Organomet. Chem.* **1998**, *551*, 125.
25. Bassindale, A.R.; Liu, Z.; MacKinnon, I.A.; Taylor, P.G.; Yang, Y.; Light, M.E.; Horton, P.N.; Hursthouse, M.B. *Dalton Trans.* **2003**, *14*, 2945.
26. Koželj, M.; Orel, B. *Dalton Trans.* **2008**, *37*, 5072.
27. Brook, M.A. In *Silicon in Organic, Organometallic, and Polymer Chemistry*, Wiley: New York, **2000**, p 29.

28. Pope, E. J. A.; Mackenzie, J.D. *J. Non-Cryst. Solids* **1986**, *87*,185.
29. (a) Bassindale, A.R.; Pourny, M.; Taylor, P.G.; Hursthouse, M.B.; Light, M.E. *Angew. Chem. Int. Ed.* **2003**, *42*, 3488. (b) Bassindale, A.R.; Parker, D.J.; Pourny, M.; Taylor, P.G.; Horton, P.N.; Hursthouse, M.B. *Organometallics* **2004**, *23*, 440.
30. (a) Anderson, S.E.; Bodzin, D.J.; Haddad, T.S.; Boatz, J.A.; Mabry, J.M.; Mitchell, C.; Bowers, M.T. *Chem. Mater.* **2008**, *20*, 4299. (b) Anderson, S.E.; Shammel Baker, E.; Mitchell, C.; Haddad, T.S.; Bowers, M.T. *Chem. Mater.* **2005**, *17*, 2537. (c) Anderson, S.E.; Mitchell, C.; Haddad, T.S.; Vij, A.; Schwab, J.J.; Bowers, M.T. *Chem. Mater.*, **2006**, *18*, 1490.
31. (a) Ossadnik, C.; Veprek, S.; Marsmann, H.C.; Rikowski, E. *Monat. Chem.* **1999**, *130*, 55. (b) Schneider, K.S.; Zhang, Z.; Banaszak-Holl, M.M.; Orr, B.G.; Pernisz, U.C. *Phys. Rev. Lett.* **2000**, *85*, 602.
32. (a) Ossadnik, C.; Veprek, S.; Marsmann, H. C.; Rikowski, E. *Monatsh.Chem.* **1999**, *130*, 55. (b) Azinovic, D.; Cai, J.; Eggs, C.; Konig, H.; Marsmann, H. C.; Veprek, S. *J. Lumin.* **2002**, *97*, 40.
33. (a) Xiang, K.-H.; Pandey, R.; Pernisz, U. C.; Freeman, C. *J. Phys. Chem. B* **1998**, *102*, 8704. (b) Cheng, W.-D.; Xiang, K.-H.; Pandey, R.; Pernisz, U. C. *J. Phys. Chem. B* **2000**, *104*, 6737.
34. Lin, T.; He, C.; Xiao, Y. *J. Phys. Chem. B* **2003**, *107*, 13788.
35. Neurock, M.; Filhol, J.-S.; Lee, C.-Y.; Laine, R.M.; Brick, C.M.; Roll, M.; Sulaiman, S. Unpublished work.
36. Lichtenhan, J.D. *Comments Inorg. Chem.* **1995**, *17*, 115.
37. Lichtenhan, J.D. In *Polymeric Material Encyclopedia Vol. 10*, Salamone, J.D., Ed.; CRC Press: New York, **1996**, pp. 7768-7778.
38. (a) Lichtenhan, J.D.; Vu, N.Q.; Carter, J.A.; Gilman, J.W.; Feher, F.J. *Macromolecules* **1993**, *26*, 2141. (b) Haddad, T.S.; Lichtenhan, J.D. *J. Inorg. Organometal. Polym.* **1995**, *5*, 237.
39. Sulaiman, S.; Ronchi, M.; Jung, J.H.; Laine, R.M. Unpublished work.
40. Kim, S.-G.; Sulaiman, S.; Fargier, D.; Laine, R.M. In *Materials Syntheses: A Practical Guide*, Shubert, U.; Hüsing, N.; Laine, R.M., Eds.; SpringerWien: New York, **2008**, pp. 179-191.
41. (a) Laine, R.M.; Youngdahl, K.A.; Babonneau, F.; Hoppe, M.L.; Zhang, Z.-F.; Harrod, J.F. *Chem. Mater.* **1990**, *2*, 464. (b) Laine, R.M.; Rahn, J.A.; Youngdahl,

- K.A.; Harrod, J.F. In *Homogeneous Transition Metal Catalyzed Reactions*, Moser, W.R.; Slocum, D.W. Eds.; ACS: Washington DC, **1992**, p 553. (c) Tsumura, M.; Kiyoshi, A.; Kotani, J.; Hiraishi, M.; Iwahara, T. *Macromolecules*, **1998**, *31*, 2716. (d) Lee, E.-C.; Kimura, Y. *Polym. J.* **1998**, *30*, 234. (e) Lee, E.-C.; Kimura, Y. *Polym. J.* **1998**, *30*, 730.
42. Harrison, P.G.; Hall, C. *Main Group Metal Chem.* **1997**, *20*, 515.
43. Grubbs, R. H. In *Handbook of Metathesis*, Wiley-VCH: New York, **2003**.
44. (a) Lichtenhan, J.D. *Comments Inorg. Chem.* **1995**, *17*, 115. (b) Liu, Y.R.; Huang, Y.D.; Liu, L. *Polym. Degradation and Stability* **2006**, *91*, 2731.
45. Fu, B.X.; Lee, A.; Haddad, T.S. *Macromolecules* **2004**, *37*, 5211.
46. SDBS Spectral Database. <http://riodb01.ibase.aist.go.jp/sdbs/cgi-bin/ENTRANCE.cgi> (accessed May 15, 2009).
47. Grubbs, R.H. *Prog. Inorg. Chem.* **1978**, *24*, 1.
48. (a) Sellinger, A.; Tamaki, R.; Laine, R. M.; Ueno, K.; Tanabe, H.; Williams, E.; Jabbour, G. E. *Chem. Commun.* **2005**, 3700. (b) Lo, M. Y.; Zhen, C.; Lauters, M.; Jabbour, G. E.; Sellinger, A. *J. Am. Chem. Soc.* **2007**, *129*, 5808.
49. Sulaiman, S.; Bhaskar, A.; Zhang, J.; Guda, R.; Goodson, T. III; Laine, R.M. *Chem. Mater.* **2008**, *20*, 5563.
50. Takahashi, K.; Brick, C.M.; Sulaiman, S.; Laine, R.M. Unpublished work.

Chapter 7

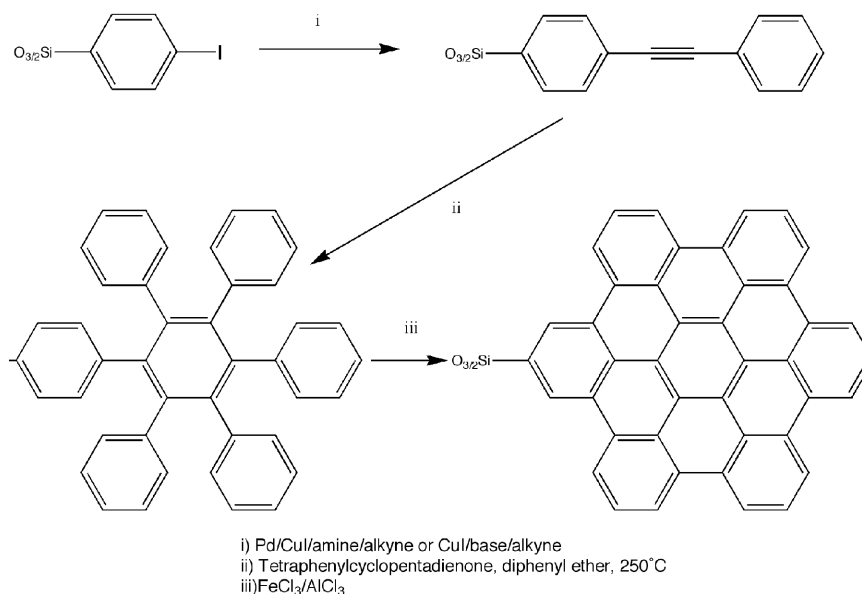
Future Work

7.1 Discussion

In this work, we demonstrated the novel syntheses and functionalization of octa-, deca-, and dodecameric silsesquioxanes and investigated their utility as nanoconstruction sites for a variety of applications. We have shown that films derived from cubic silsesquioxanes (**Chapter 3**) exhibit excellent barrier properties to oxygen ($< 1 \text{ cm}^3 \cdot 20 \text{ } \mu\text{m}^2 \cdot \text{day} \cdot \text{atm}$) that are competitive with high-performance commercial systems and require only a minimum amount of processing effort. These silsesquioxane films are thermally very robust, particularly the OAPS/imide films ($>500 \text{ }^\circ\text{C}$ when fully cured),¹ making them ideal for electronics packaging and encapsulation applications that require high use temperatures. The effect of moisture on the oxygen barrier properties and the barrier properties of silsesquioxane films to other gases, such as N_2 and CO_2 , remain an area for further investigation.

The self-polymerizable octaalkynes developed in **Chapter 4** offer considerable potential as high thermal stability matrices for advanced structural composites. While an in-depth study of the cross-linking process is warranted, the process must involve the interdigitation of the alkynes prior to polymerization. Octaalkynes are also currently being investigated by members of our group as platforms to supramolecular materials (Scheme 7.1).² The reaction of octa(phenylethyne) derivatives with tetraphenylcyclopentadienone to produce the hexaphenyl derivatives (Scheme 7.1-ii) has already been demonstrated. The octagraphene silsesquioxanes from Scheme 7.1-iii are

expected to exhibit unique electronic properties and/or gas adsorption properties, for example.



Scheme 7.1. Synthesis of 3-D octagraphene silsesquioxane structures starting from I₈OPS.

We demonstrated a facile route to [PhSiO(ONa)]₄ and [*p*-IPhSiO(ONa)]₄ half cube salts in **Chapter 5** by the reaction of OPS and I₈OPS with NaOH in *n*-butanol. These compounds have Ph- and I-Ph- groups entirely *cis* on one face of the half cube. We have also shown evidence for the syntheses of {PhSiO[OSi(OCH₃)₂R]}₄ (R = Me, vinyl, and cyclohexyl) compounds from reactions of the tetraphenyl salt with the corresponding functional trichlorosilanes. Optimization of the hydrolysis conditions to form Janus cubes in high yields is necessary. The hydrolysis of chloro- and alkoxy silanes to form cage silsesquioxanes is highly dependent on a number of factors³ as previously discussed and careful control and optimization of reaction conditions is required.

Chapter 6 detailed an innovative route to mixed-functionality silsesquioxane cages via fluoride-catalyzed rearrangement reactions. The ability to tailor the numbers and types of functional groups on the cages simply by controlling the amounts of starting

materials provides direct access to novel, hybrid nanoconstruction sites. The compounds of these reactions are a mixture of T_8 , T_{10} , and T_{12} cages with mixed vinyl and phenyl moieties. As a result they are modifiable via chemistry already demonstrated for phenyl and vinyl T_8 octamers. Our group has synthesized alkyl, nitro, amino, halo, aryl, and alkyne substituted phenyl T_8 and the related phenyl T_{12} silsesquioxanes.⁴⁻¹⁴ We also recently reported the synthesis of 3-D star materials elaborated from octavinylsilsesquioxane.¹⁵

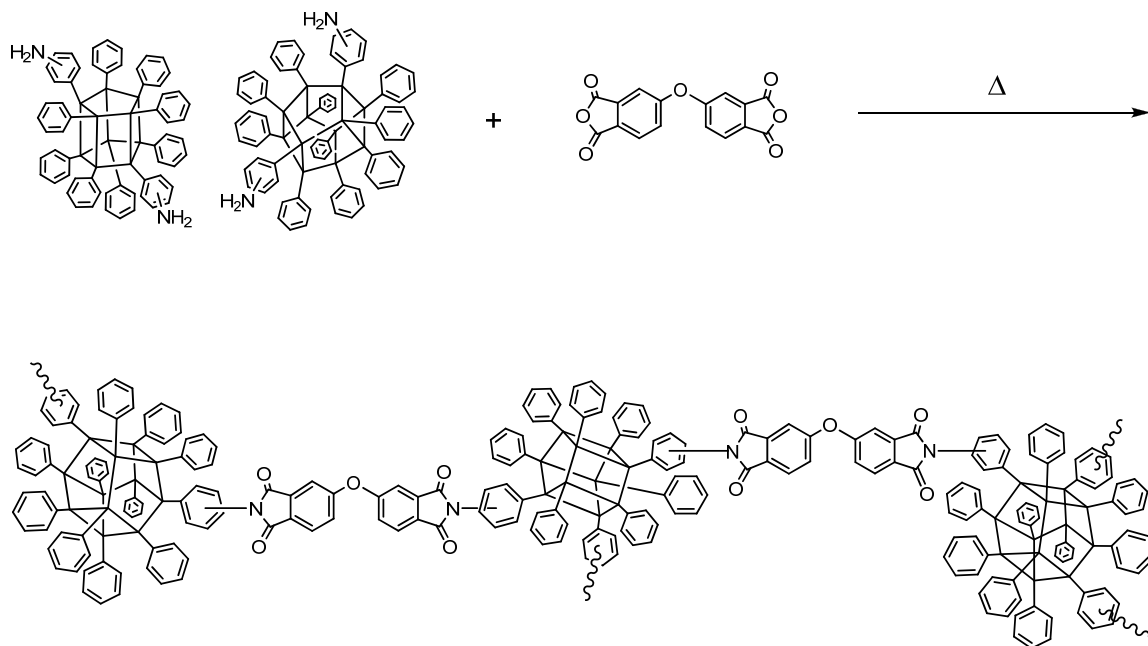
Further refinement of the reaction conditions described in **Chapter 6** to preferentially form the T_8 , T_{10} , or T_{12} cages exclusively could perhaps be achieved by careful control of reaction times, temperature, solvent, type of catalyst, amount of water/catalyst present, etc.³ Optimization of the oligomerization reaction via Heck coupling to form higher molecular weight, luminescent polymers is another area for future investigation.

The photoluminescence efficiencies of the Heck compound and model compound of **Chapter 6** (and/or similarly conjugated oligomers) warrant further exploration. In addition, past modeling studies of the HOMO-LUMO band gaps and core LUMO of the T_8 cube compounds should be extended to explain the unique photoluminescent properties of the T_{10} and T_{12} cage silsesquioxanes as well. If indeed there are electronic interactions through the cage cores, functionalized silsesquioxanes could come to represent a new class of 3-D semiconducting materials in the near future.

Currently, our group is exploring the synthesis of silsesquioxanes with mixed functional groups and controlled stoichiometries based on OPS and OAPS,¹⁶ similar to the experiments detailed in **Chapter 6**. The diamino cage compounds from the rearrangement reactions of OPS and OAPS are potential platforms to thermally stable, soluble, and high molecular weight silsesquioxane polymers via reaction with dianhydrides or diepoxides. T_8 silsesquioxane nanocomposites based on imide^{10,11} and amine/epoxy¹²⁻¹⁴ chemistries exhibit enhanced thermal and/or mechanical properties. In addition to these properties, we expect the analogous silsesquioxane oligomers/polymers to have superior solubility (due to statistical control of reactive sites) and thus possess similar processing advantages typically associated with soluble polymers.

Scheme 7.2 shows the reaction of diamino T_{10} and T_{12} compounds with oxydiphthalic anhydride (ODPA) to form cages connected by imide linkages, for example. We can

expect the polymer of Scheme 7.2 to have a thermal stability $>500\text{ }^{\circ}\text{C}^{10}$ with high solubility, making these compounds suitable for a variety of high temperature applications.



Scheme 7.2. Reaction of diamino(phenyl)₂ Ph₈ T₁₀ and T₁₂ silsesquioxanes with oxydiphthalic anhydride (ODPA) to form imide oligomers.

The approaches described in **Chapter 6** offer access to a potentially new class of multifunctional compounds with one, two (or more) distinct functionalities that may later be modified through chemical synthesis. In addition to the fluorescent oligomers synthesized in **Chapter 6**, these functional cages in turn can serve as possible platforms to: (1) thermally-stable and soluble silsesquioxane polymers with the capability of being spin/spray/dip-coated, cast, drawn, etc.; (2) low T_m , alkylated silsesquioxane polymers for high temperature lubrication applications, as was previously demonstrated in the Friedel-Crafts alkylation of OPS;⁴ (3) silsesquioxane polymers functionalized with liquid crystalline (LC) mesogens for the fabrication of unique LC polymeric materials, etc.¹⁷ The possibilities mentioned here are meant to be representative (and by no means

exhaustive) of the diverse utility of compounds derived from F⁻ rearrangement reactions of silsesquioxanes.

7.2 References

1. Choi, J.; Tamaki, R.; Kim, S.G.; Laine, R.M. *Chem. Mater.* **2003**, *15*, 3365.
2. Roll, M.F.; Laine, R.M. Unpublished work.
3. Pescarmona, P.P.; Maschmeyer, T. *J. Aust. Chem.* **2001**, *54*, 583.
4. Brick, C.M.; Chan, E.R.; Glotzer, S.C.; Marchal, J.C.; Martin, D.C.; Laine, R.M. *Adv. Mater.* **2007**, *19*, 82.
5. Tamaki, R.; Tanaka, Y.; Asuncion, M.Z.; Choi, J.; Laine, R.M. *J. Am. Chem. Soc.* **2001**, *123*, 12416.
6. Brick, C.M.; Tamaki, R.; Kim, S.G.; Asuncion, M.Z.; Roll, M.; Nemoto, T.; Laine, R.M. *Macromolecules* **2005**, *38*, 4655.
7. Brick, C.M.; Ouchi, Y.; Chujo, Y.; Laine, R.M. *Macromolecules* **2005**, *38*, 4661.
8. Roll, M.F.; Asuncion, M.Z.; Kampf, J.; Laine, R.M. *ACS Nano* **2008**, *2*, 320.
9. Asuncion, M.Z.; Roll, M.; Laine, R.M. *Macromolecules* **2008**, *41*, 8047.
10. (a) Tamaki, R.; Choi, J.; Laine, R.M. *Chem. Mater.* **2003**, *15*, 793. (b) Choi, J.; Tamaki, R.; Laine, R.M. *Chem. Mater.* **2003**, *15*, 3365.
11. Choi, J.; Kim, S.G.; Laine, R.M. *Macromolecules* **2004**, *37*, 99.
12. Takahashi, K.; Sulaiman, S.; Katzenstein, J.M.; Snoblen, S.; Laine, R.M. *Aust. J. Chem.* **2006**, *59*, 564.
13. Laine, R. M.; Choi, J.; Lee, I. *Adv. Mater.* **2001**, *13*, 800.
14. Sulaiman, S.; Brick, C.M.; De Sana, C.M.; Katzenstein, J.M.; Laine, R.M.; Basheer, R.A. *Macromolecules* **2006**, *39*, 5167.
15. Sulaiman, S.; Bhaskar, A.; Zhang, J.; Guda, R.; Goodson, T. III; Laine, R.M. *Chem. Mater.* **2008**, *20*, 5563.
16. Jung, J.H.; Sulaiman, S.; Laine, R.M. Unpublished work.
17. Laine, R.M.; Zhang, C.; Sellinger, A.; Viculis, L. *Appl. Organometal. Chem.* **1998**, *12*, 715.